



University of Kentucky  
UKnowledge

---

Theses and Dissertations--Mechanical  
Engineering

Mechanical Engineering

---


2020

## FILTERED-DYNAMIC-INVERSION CONTROL FOR UNKNOWN MINIMUM-PHASE SYSTEMS WITH UNKNOWN RELATIVE DEGREE

Sumit Suryakant Kamat

*University of Kentucky*, [sumitkmt@gmail.com](mailto:sumitkmt@gmail.com)

Author ORCID Identifier:

 <https://orcid.org/0000-0002-3368-6403>

Digital Object Identifier: <https://doi.org/10.13023/etd.2020.087>

[Right click to open a feedback form in a new tab to let us know how this document benefits you.](#)

### Recommended Citation

Kamat, Sumit Suryakant, "FILTERED-DYNAMIC-INVERSION CONTROL FOR UNKNOWN MINIMUM-PHASE SYSTEMS WITH UNKNOWN RELATIVE DEGREE" (2020). *Theses and Dissertations--Mechanical Engineering*. 149.

[https://uknowledge.uky.edu/me\\_etds/149](https://uknowledge.uky.edu/me_etds/149)

This Master's Thesis is brought to you for free and open access by the Mechanical Engineering at UKnowledge. It has been accepted for inclusion in Theses and Dissertations--Mechanical Engineering by an authorized administrator of UKnowledge. For more information, please contact [UKnowledge@lsv.uky.edu](mailto:UKnowledge@lsv.uky.edu).

## **STUDENT AGREEMENT:**

I represent that my thesis or dissertation and abstract are my original work. Proper attribution has been given to all outside sources. I understand that I am solely responsible for obtaining any needed copyright permissions. I have obtained needed written permission statement(s) from the owner(s) of each third-party copyrighted matter to be included in my work, allowing electronic distribution (if such use is not permitted by the fair use doctrine) which will be submitted to UKnowledge as Additional File.

I hereby grant to The University of Kentucky and its agents the irrevocable, non-exclusive, and royalty-free license to archive and make accessible my work in whole or in part in all forms of media, now or hereafter known. I agree that the document mentioned above may be made available immediately for worldwide access unless an embargo applies.

I retain all other ownership rights to the copyright of my work. I also retain the right to use in future works (such as articles or books) all or part of my work. I understand that I am free to register the copyright to my work.

## **REVIEW, APPROVAL AND ACCEPTANCE**

The document mentioned above has been reviewed and accepted by the student's advisor, on behalf of the advisory committee, and by the Director of Graduate Studies (DGS), on behalf of the program; we verify that this is the final, approved version of the student's thesis including all changes required by the advisory committee. The undersigned agree to abide by the statements above.

Sumit Suryakant Kamat, Student

Dr. Jesse B. Hoagg, Major Professor

Dr. Alexandre Martin, Director of Graduate Studies

FILTERED-DYNAMIC-INVERSION CONTROL FOR UNKNOWN  
MINIMUM-PHASE SYSTEMS WITH UNKNOWN RELATIVE DEGREE

---

THESIS

---

A thesis submitted in partial fulfillment of the requirements for the  
degree of Master of Science in Mechanical Engineering in the  
College of Engineering at the University of Kentucky

By

Sumit Suryakant Kamat

Lexington, Kentucky

Director: Dr. Jesse B. Hoagg, Professor of Mechanical Engineering

Lexington, Kentucky

2020

Copyright© Sumit Suryakant Kamat 2020

<https://orcid.org/0000-0002-3368-6403>

## ABSTRACT OF THESIS

### FILTERED-DYNAMIC-INVERSION CONTROL FOR UNKNOWN MINIMUM-PHASE SYSTEMS WITH UNKNOWN RELATIVE DEGREE

We present filtered-dynamic-inversion (FDI) control for unknown linear time-invariant systems that are multi-input multi-output and minimum phase with unknown-but-bounded relative degree. This FDI controller requires limited model information, specifically, knowledge of an upper bound on the relative degree and knowledge of the first nonzero Markov parameter. The FDI controller is a single-parameter high-parameter-stabilizing controller that is robust to uncertainty in the relative degree. We characterize the stability of the closed-loop system. We present numerical examples, where the FDI controller is implemented in feedback with mathematical and physical systems. The numerical examples demonstrate that the FDI controller for unknown relative degree is effective for stabilization, command following, and disturbance rejection. We demonstrate that for a sufficiently large parameter, the average power of the closed-loop performance is arbitrarily small.

KEYWORDS: dynamic inversion; high-parameter stabilization; high-gain control; unknown relative degree; control with model uncertainty

Author's signature: Sumit Suryakant Kamat

Date: March 30, 2020

FILTERED-DYNAMIC-INVERSION CONTROL FOR UNKNOWN  
MINIMUM-PHASE SYSTEMS WITH UNKNOWN RELATIVE DEGREE

By

Sumit Suryakant Kamat

Director of Thesis: Prof. Jesse B. Hoagg

Director of Graduate Studies: Prof. Alexandre Martin

Date: March 30, 2020

*To my parents and my brother,  
for their love and sacrifice.*

## ACKNOWLEDGMENTS

First, I would like to thank my advisor Dr. Hoagg for his guidance and support throughout the past couple of years. Under his tutelage, I learned how to become an efficient researcher and technical writer, which I am grateful for. He spent an immense amount of time and effort to bring my thesis to completion. Also, I would like to thank him for imparting his knowledge through his courses. They were challenging and it was a pleasure to learn and work on the course material.

Second, I would like to thank my parents and my brother for their immense support. They have always motivated me to achieve my goals.

Third, I would like to thank my friends and colleagues notably, Roshan Chavan, Zachary Lippay, Grayson Woods, Mohammadreza Kamaldar, Chris Heintz, Alireza Moosavi, Zahra Abbasi, Shaoqian Wang, and Pedram Rabiee.

Finally, I would like to thank Dr. Seigler and Dr. Poonawala for serving on my committee.

# CONTENTS

<b>Acknowledgments</b> . . . . .	<b>iii</b>
<b>Contents</b> . . . . .	<b>iv</b>
<b>List of Figures</b> . . . . .	<b>vi</b>
<b>Chapter 1 — Introduction and Motivation</b> . . . . .	<b>1</b>
1.1 Motivation . . . . .	1
1.2 Literature Review . . . . .	2
1.3 Contributions of this Thesis . . . . .	5
<b>Chapter 2 — Review of Filtered Dynamic Inversion</b> . . . . .	<b>7</b>
2.1 Problem Formulation . . . . .	7
2.2 Ideal Dynamic Inversion . . . . .	9
2.3 Filtered Dynamic Inversion . . . . .	11
2.4 Motivating Example . . . . .	15
<b>Chapter 3 — Filtered Dynamic Inversion with Unknown Relative De- gree</b> . . . . .	<b>20</b>
3.1 Problem Formulation . . . . .	20
3.2 Ideal Dynamic Inversion . . . . .	22
3.3 Filtered Dynamic Inversion . . . . .	30
<b>Chapter 4 — Numerical Simulations</b> . . . . .	<b>37</b>
4.1 Numerical Simulations of Mathematical Examples . . . . .	37
4.1.1 Single Integrator, Double Integrator and Triple Integrator . . . . .	37
4.1.2 Multi-Input Multi-Output Example . . . . .	48



4.2	Numerical Simulations of Physical Examples . . . . .	56
4.2.1	Serially Connected Mass-Spring-Damper System (SISO) . . .	56
4.2.2	Serially Connected Mass-Spring-Damper System (MIMO) . .	80
4.2.3	Two-Mass Servo System with Flexible Shaft . . . . .	93
<b>Chapter 5 — Conclusions and Future Work . . . . .</b>		<b>101</b>
5.1	Future Work . . . . .	102
<b>Bibliography . . . . .</b>		<b>104</b>
<b>Vita . . . . .</b>		<b>108</b>

## LIST OF FIGURES

2.1	Locus of the eigenvalues of $\tilde{A}$ of the closed-loop system (2.31)–(2.35), which consists of the triple integrator (2.1), (2.2), (2.37), and (2.38); and the FDI controller (2.24)–(2.30). For all $k > 45$ , the origin of the closed-loop system is asymptotically stable. Note that two eigenvalues of $\tilde{A}$ diverge along the asymptote towards $-\infty$ . . . . .	18
2.2	Locus of the eigenvalues of $\tilde{A}$ of the closed-loop system (2.31)–(2.35), which consists of the double integrator (2.1), (2.2), (2.42), and (2.43); and the FDI controller (2.24)–(2.30), which is designed for the triple integrator. For all $k > 0$ , the closed-loop system is unstable. . . . .	19
4.1	The FDI controller (3.53)–(3.59), where $k \in \{2.9, 3.1, 5\}$ , is implemented in feedback with the single integrator (4.1)–(4.3). By increasing $k$ , the time it takes $y$ to converge to the origin decreases. . . . .	41
4.2	The FDI controller (3.53)–(3.59), where $k \in \{9, 10, 14\}$ , is implemented in feedback with the double integrator (4.4)–(4.6). By increasing $k$ , the time it takes $y$ to converge to the origin decreases. . . . .	41
4.3	The FDI controller (3.53)–(3.59), where $k \in \{47, 50, 55\}$ , is implemented in feedback with the triple integrator (4.7)–(4.9). By increasing $k$ , the time it takes $y$ to converge to the origin decreases. . . . .	42
4.4	The FDI controller (3.53)–(3.59), where $k \in \{3, 4, 9\}$ , is implemented in feedback with the single integrator (4.1)–(4.3). The command $r$ is a series of steps passed through a filter $G_r(s) = 10^3/(s + 10)^3$ . The average power of performance $z$ decreases with increase of $k$ . . . . .	44

4.5	The FDI controller (3.53)–(3.59), where $k \in \{10, 15, 30\}$ , is implemented in feedback with the double integrator (4.4)–(4.6). The command $r$ is a series of steps passed through a filter $G_r(s) = 10^3/(s + 10)^3$ . The average power of performance $z$ decreases with increase of $k$ . . . . .	44
4.6	The FDI controller (3.53)–(3.59), where $k \in \{50, 70, 100\}$ , is implemented in feedback with the triple integrator (4.7)–(4.9). The command $r$ is a series of steps passed through a filter $G_r(s) = 10^3/(s + 10)^3$ . The average power of performance $z$ decreases with increase of $k$ . . . . .	45
4.7	The FDI controller (3.53)–(3.59), where $k \in \{3, 4, 9, 30\}$ , is implemented in feedback with the single integrator (4.1)–(4.3) with white-noise disturbance. The command $r$ is a series of steps passed through the filter $G_r(s) = 10^3/(s + 10)^3$ . The performance $z$ degrades with the introduction of disturbance in comparison to the performance in Figure 4.4. By increasing $k$ to 30, the performance improves. . . . .	46
4.8	The FDI controller (3.53)–(3.59), where $k \in \{10, 15, 30, 80\}$ , is implemented in feedback with the double integrator (4.4)–(4.6) with white-noise disturbance. The command $r$ is a series of steps passed through the filter $G_r(s) = 10^3/(s + 10)^3$ . The performance $z$ degrades with the introduction of disturbance in comparison to the performance in Figure 4.5. By increasing $k$ to 80, the performance improves. . . . .	47
4.9	The FDI controller (3.53)–(3.59), where $k \in \{50, 70, 100, 200\}$ , is implemented in feedback with the triple integrator (4.7)–(4.9) with white-noise disturbance. The command $r$ is a series of steps passed through the filter $G_r(s) = 10^3/(s + 10)^3$ . The performance $z$ degrades with the introduction of disturbance in comparison to the performance in Figure 4.6. By increasing $k$ to 200, the performance improves. . . . .	47

4.10	The FDI controller (3.53)–(3.59), where $k \in \{5, 6, 8\}$ , is implemented in feedback with the MIMO system (4.14)–(4.16). In this case, $d = 1$ . There is a noticeable error between $y$ and $y_m$ . By increasing $k$ , the average power of the performance is reduced. . . . .	51
4.11	The FDI controller (3.53)–(3.59), where $k \in \{15, 20, 30\}$ , is implemented in feedback with the MIMO system (4.14), (4.15), and (4.17). In this case, $d = 2$ . There is a noticeable error between $y$ and $y_m$ . By increasing $k$ , the average power of the performance is reduced. . . . .	52
4.12	The FDI controller (3.53)–(3.59), where $k \in \{5, 6, 8, 20\}$ , is implemented in feedback with the MIMO system (4.14)–(4.16). In this case, $d = 1$ . The performance $z$ degrades slightly in comparison to the disturbance free case, which is shown in Figure 4.10. By increasing $k$ to 20, the performance $z$ improves. . . . .	54
4.13	The FDI controller (3.53)–(3.59), where $k \in \{15, 20, 30, 100\}$ , is implemented in feedback with the MIMO system (4.14), (4.15), and (4.17). In this case, $d = 2$ . The performance $z$ degrades slightly in comparison to the disturbance free case, which is shown in Figure 4.11. By increasing $k$ to 100, the performance $z$ improves. . . . .	55
4.14	A serially connected four-mass structure. . . . .	56
4.15	The FDI controller (3.53)–(3.59), where $k \in \{3, 4, 6\}$ , is implemented in feedback with the mass-spring-damper system (4.25)–(4.27). In this case, $d = 2$ . By increasing $k$ , the average power of the performance $z$ decreases. . . . .	61
4.16	The FDI controller (3.53)–(3.59), where $k \in \{8, 12, 20\}$ , is implemented in feedback with the mass-spring-damper system (4.25), (4.26), and (4.28). In this case, $d = 3$ . By increasing $k$ , the average power of the performance $z$ decreases. . . . .	62

4.17	The FDI controller (3.53)–(3.59), where $k \in \{20, 30, 50\}$ , is implemented in feedback with the mass-spring-damper system (4.25), (4.26), and (4.29). In this case, $d = 4$ . By increasing $k$ , the average power of the performance $z$ decreases. . . . .	63
4.18	The FDI controller (3.53)–(3.59), where $k \in \{65, 80, 110\}$ , is implemented in feedback with the mass-spring-damper system (4.25), (4.26), and (4.30). In this case, $d = 5$ . By increasing $k$ , the average power of the performance $z$ decreases. . . . .	64
4.19	The FDI controller (3.53)–(3.59), where $k \in \{3, 4, 6, 10\}$ , is implemented in feedback with the mass-spring-damper system (4.25)–(4.27). In this case, $d = 2$ . In comparison to Figure 4.15, the performance $z$ degrades slightly. By increasing $k$ to 10, the performance $z$ improves. . . . .	66
4.20	The FDI controller (3.53)–(3.59), where $k \in \{8, 12, 20, 40\}$ , is implemented in feedback with the mass-spring-damper system (4.25), (4.26), and (4.28). In this case, $d = 3$ . In comparison to Figure 4.16, the performance $z$ degrades slightly. By increasing $k$ to 40, the performance $z$ improves. . . . .	67
4.21	The FDI controller (3.53)–(3.59), where $k \in \{20, 30, 50, 90\}$ , is implemented in feedback with the mass-spring-damper system (4.25), (4.26), and (4.29). In this case, $d = 4$ . In comparison to Figure 4.17, the performance $z$ degrades slightly. By increasing $k$ to 90, the performance $z$ improves. . . . .	68
4.22	The FDI controller (3.53)–(3.59), where $k \in \{65, 80, 110, 160\}$ , is implemented in feedback with the mass-spring-damper system (4.25), (4.26), and (4.30). In this case, $d = 5$ . In comparison to Figure 4.18, we observe that the performance $z$ degrades slightly. By increasing $k$ to 160, the performance $z$ improves. . . . .	69

4.23	FDI control with $k \in \{3, 4, 6\}$ for the disturbance free and unstable mass-spring-damper system shown in Figure 4.14. The FDI controller (3.53)–(3.59), where $k \in \{3, 4, 6\}$ , is implemented in feedback with the mass-spring-damper system (4.25)–(4.27). In this case, $d = 2$ . By increasing $k$ , the average power of the performance $z$ decreases. . . . .	71
4.24	FDI control with $k \in \{10, 15, 25\}$ for the disturbance free and unstable mass-spring-damper system shown in Figure 4.14. The FDI controller (3.53)–(3.59), where $k \in \{10, 15, 25\}$ , is implemented in feedback with the mass-spring-damper system (4.25), (4.26), and (4.28). In this case, $d = 3$ . By increasing $k$ , the average power of the performance $z$ decreases. . . .	72
4.25	FDI control with $k \in \{35, 55, 85\}$ for the disturbance free and unstable mass-spring-damper system shown in Figure 4.14. The FDI controller (3.53)–(3.59), where $k \in \{35, 55, 85\}$ , is implemented in feedback with the mass-spring-damper system (4.25), (4.26), and (4.29). In this case, $d = 4$ . By increasing $k$ , the average power of the performance $z$ decreases. . . .	73
4.26	FDI control with $k \in \{100, 115, 140\}$ for the disturbance free and unstable mass-spring-damper system shown in Figure 4.14. The FDI controller (3.53)–(3.59), where $k \in \{100, 115, 140\}$ , is implemented in feedback with the mass-spring-damper system (4.25), (4.26), and (4.30). In this case, $d = 5$ . By increasing $k$ , the average power of the performance $z$ decreases.	74
4.27	FDI control with $k \in \{3, 4, 6, 10\}$ for the unstable mass-spring-damper system shown in Figure 4.14, with white-noise disturbance. The FDI controller (3.53)–(3.59), where $k \in \{3, 4, 6, 10\}$ , is implemented in feedback with the mass-spring-damper system (4.25)–(4.27). In this case, $d = 2$ . The performance $z$ degrades slightly in comparison to the disturbance free case which is shown in Figure 4.23. By increasing $k$ to 10, the average power of the performance $z$ decreases. . . . .	76

4.28	FDI control with $k \in \{10, 15, 25, 40\}$ for the unstable mass-spring-damper system shown in Figure 4.14, with white-noise disturbance. The FDI controller (3.53)–(3.59), where $k \in \{10, 15, 25, 40\}$ , is implemented in feedback with the mass-spring-damper system (4.25), (4.26), and (4.28). In this case, $d = 3$ . The performance $z$ degrades slightly in comparison to the disturbance free case which is shown in Figure 4.24. By increasing $k$ to 40, the average power of the performance $z$ decreases. . . . .	77
4.29	FDI control with $k \in \{35, 55, 85, 200\}$ for the unstable mass-spring-damper system shown in Figure 4.14, with white-noise disturbance. The FDI controller (3.53)–(3.59), where $k \in \{35, 55, 85, 200\}$ , is implemented in feedback with the mass-spring-damper system (4.25), (4.26), and (4.29). In this case, $d = 4$ . The performance $z$ degrades slightly in comparison to the disturbance free case which is shown in Figure 4.25. By increasing $k$ to 200, the average power of the performance $z$ decreases. . . . .	78
4.30	FDI control with $k \in \{100, 115, 140, 245\}$ for the unstable mass-spring-damper system shown in Figure 4.14, with white-noise disturbance. The FDI controller (3.53)–(3.59), where $k \in \{100, 115, 140, 245\}$ , is implemented in feedback with the mass-spring-damper system (4.25), (4.26), and (4.30). In this case, $d = 5$ . The performance $z$ degrades slightly in comparison to the disturbance free case which is shown in Figure 4.26. By increasing $k$ to 245, the average power of the performance $z$ decreases. . . . .	79
4.31	The FDI controller (3.53)–(3.59), where $k \in \{15, 20, 30\}$ , is implemented in feedback with the mass-spring-damper system (3.1), (3.2), and (4.21)–(4.26). $B$ and $C$ are given by (4.33). In this case, $d = 2$ . By increasing $k$ , the performance $z$ improves. . . . .	82

4.32	The FDI controller (3.53)–(3.59), where $k \in \{45, 60, 80\}$ , is implemented in feedback with the mass-spring-damper system (3.1), (3.2), and (4.21)–(4.26). $B$ and $C$ are given by (4.34). In this case, $d = 3$ . By increasing $k$ , the performance $z$ improves. . . . .	83
4.33	FDI control with $k \in \{15, 20, 30, 50\}$ for the MIMO mass-spring-damper system with white-noise disturbance. The FDI controller (3.53)–(3.59), where $k \in \{15, 20, 30, 50\}$ , is implemented in feedback with the mass-spring-damper system (3.1), (3.2), and (4.21)–(4.26). $B$ and $C$ are given by (4.33). In this case, $d = 2$ . The performance $z$ degrades slightly in comparison to the disturbance free case which is shown in Figure 4.31. By increasing $k$ to 50, the performance $z$ improves. . . . .	85
4.34	FDI control with $k \in \{45, 60, 80, 250\}$ for the MIMO mass-spring-damper system with white-noise disturbance. The FDI controller (3.53)–(3.59), where $k \in \{45, 60, 80, 250\}$ , is implemented in feedback with the mass-spring-damper system (3.1), (3.2), and (4.21)–(4.26). $B$ and $C$ are given by (4.34). In this case, $d = 3$ . The performance $z$ degrades slightly in comparison to the disturbance free case which is shown in Figure 4.32. By increasing $k$ to 250, the performance $z$ improves. . . . .	86
4.35	FDI control with $k \in \{20, 30, 50\}$ for the unstable MIMO mass-spring-damper system (disturbance free). The FDI controller (3.53)–(3.59), where $k \in \{20, 30, 50\}$ , is implemented in feedback with the mass-spring-damper system (3.1), (3.2), and (4.21)–(4.26). $B$ and $C$ are given by (4.33). In this case, $d = 2$ . By increasing $k$ , the performance $z$ improves. . . . .	88



4.36	FDI control with $k \in \{65, 80, 120\}$ for the unstable MIMO mass-spring-damper system (disturbance free). The FDI controller (3.53)–(3.59), where $k \in \{65, 80, 120\}$ , is implemented in feedback with the mass-spring-damper system (3.1), (3.2), and (4.21)–(4.26). $B$ and $C$ are given by (4.34). In this case, $d = 3$ . By increasing $k$ , the performance $z$ improves. . . . .	89
4.37	FDI control with $k \in \{20, 30, 50, 80\}$ for the unstable MIMO mass-spring-damper system with white-noise disturbance. The FDI controller (3.53)–(3.59), where $k \in \{20, 30, 50, 80\}$ , is implemented in feedback with the mass-spring-damper system (3.1), (3.2), and (4.21)–(4.26). $B$ and $C$ are given by (4.33). In this case, $d = 2$ . By comparing with Figure 4.35, we observe that the performance $z$ degrades slightly in comparison to the disturbance free case. By increasing $k$ to 80, the performance $z$ improves. . . . .	91
4.38	FDI control with $k \in \{65, 80, 120, 300\}$ for the unstable MIMO mass-spring-damper system with white-noise disturbance. The FDI controller (3.53)–(3.59), where $k \in \{65, 80, 120, 300\}$ , is implemented in feedback with the mass-spring-damper system (3.1), (3.2), and (4.21)–(4.26). $B$ and $C$ are given by (4.34). In this case, $d = 3$ . By comparing with Figure 4.36, we observe that the performance $z$ degrades slightly in comparison to the disturbance free case. By increasing $k$ to 300, the performance $z$ improves. . . . .	92
4.39	Two-mass servo system with flexible shaft. . . . .	93
4.40	The FDI controller (3.53)–(3.59), where $k \in \{5, 10, 20\}$ , is implemented in feedback with the two-mass servo system with flexible shaft (4.40)–(4.42). In this case, $d = 1$ . The angular velocity of the electric drive $\omega_E$ is measured at output. By increasing $k$ , the performance $z$ improves. . . . .	96

4.41	The FDI controller (3.53)–(3.59), where $k \in \{480, 650, 900\}$ , is implemented in feedback with the two-mass servo system with flexible shaft (4.40), (4.41), and (4.43). In this case, $d = 2$ . The angular velocity of the load $\omega_L$ is measured at output. By increasing $k$ , the performance $z$ improves. . . . .	97
4.42	The FDI controller (3.53)–(3.59), where $k \in \{5, 10, 20, 100\}$ , is implemented in feedback with the two-mass servo system with flexible shaft (4.40)–(4.42). In this case, $d = 1$ . The angular velocity of the electric drive $\omega_E$ is measured at output. The performance $z$ decreases slightly in comparison to the disturbance free case as shown in Figure 4.40. By increasing $k$ to 100, the performance $z$ improves. . . . .	99
4.43	The FDI controller (3.53)–(3.59), where $k \in \{480, 650, 900, 2500\}$ , is implemented in feedback with the two-mass servo system with flexible shaft (4.40), (4.41), and (4.43). In this case, $d = 2$ . The angular velocity of the load $\omega_L$ is measured at output. The performance $z$ decreases slightly in comparison to the disturbance free case as shown in Figure 4.41. By increasing $k$ to 2500, the performance $z$ improves. . . . .	100

# Chapter 1

---

## Introduction and Motivation

### 1.1 Motivation

Developing an accurate mathematical model of a physical dynamic system can be challenging, time-intensive, and expensive. In particular, developing such models can require construction or use of expensive test systems. For example, wind tunnels are used to obtain model parameters for aircraft and automobiles. However, these experimental tests can be prone to systematic errors (e.g., calibration, instrument drift, lag time), which result in inaccurate models. In addition, specialized computer software packages (e.g., COMSOL, Vensim, Magnolia) are often used to determine mathematical models. However, computational models can include approximations and might not accurately represent the dynamics of the physical system. Also, obtaining high-fidelity computational models can require considerable resources (e.g., processing power, memory), which lead to higher costs. Furthermore, multiple evaluations might be required to obtain the accurate model, which might not be possible due to time constraints.

If a feedback controller is designed with an inaccurate model, then the controller may not achieve the desired performance. It also might not be able to stabilize the

system if the uncertainties of the system are not considered or are not modeled accurately.

In real-world applications, it is important to consider the effect of disturbances, which are often unknown and unmeasured because of limitations in the sensors and their placements. Thus, accurately modeling and estimating the disturbances might not be possible. For example, in [1], wind is considered as an unknown and unmeasured disturbance as the anemometer's signal from the unmanned aerial vehicle is not available for feedback.

The relative degree of the input-to-output transfer function of a physical system can vary depending on the locations of the inputs and outputs, and the structure of the physical system. For example, [2] presents an expression for the relative degree of single-input single-output (SISO) force-to-motion transfer function for collinear lumped-parameter structures (consisting of springs, masses and dashpots) that depends on the positions of the springs and dashpots.

Thus, we are motivated to develop a controller for unknown minimum phase systems with unknown-and-unmeasured disturbances and uncertain relative degree.

## 1.2 Literature Review

Plant uncertainty can be classified as structured uncertainty or unstructured uncertainty. In the case of structured uncertainty, the structure of the plant is known but the plant parameters are uncertain. Unstructured uncertainty arises because the plant model might have unmodeled dynamics (e.g., sensor and actuator dynamics, high frequency flexible modes).

Robust control techniques are effective for the stabilization of uncertain systems. However, they function efficiently when the uncertainties in the plant parameters and the disturbances are bounded. In [3], a robust controller for minimum-phase linear time-invariant (LTI) systems is presented. However, disturbance rejection is

not addressed. A model reference robust control for minimum-phase LTI systems is presented in [4], where the disturbances are bounded and the transfer function matrix is diagonal and strictly positive real. In [5], robust control for uncertain constrained linear systems is presented; however, disturbance rejection is not addressed. In [6],  $H_\infty$  control for uncertain multi-input multi-output (MIMO) linear systems with time-varying delayed control input is presented. In [7], a nonlinear robust control method for nonlinear uncertain systems is presented.

Adaptive control methods can also accommodate uncertainties in plant parameters. Adaptive control systems measure the signal systems and change the control accordingly. Stabilization of linear systems with unknown plant parameters is presented in [8], but disturbance rejection is not addressed. In [9], an adaptive controller is presented for uncertain SISO systems in the presence of unknown Preisach-type hysteresis in input, bounded unknown time-varying parameters, and bounded unknown time-varying disturbances. In [10], a direct adaptive controller for nonlinear uncertain systems with exogenous disturbances is presented, where the disturbances are assumed to be bounded.

High-gain adaptive stabilization methods can be effective for minimum-phase systems since zeros attract closed-loop poles under high gain. In [11], [12], and [13], adaptive high-gain proportional feedback is used to stabilize square MIMO systems that are minimum phase and relative degree one. In [14], [15], [16], and [17], high-gain proportional feedback is used to stabilize MIMO nonlinear systems that are minimum phase and relative degree one.

As discussed in Section 1.1, the problem of developing controllers for unknown/uncertain relative degree is of interest. For example, [18] presents an active disturbance rejection control for uncertain LTI systems that are SISO and minimum phase with unknown relative degree. The controller requires limited model information, specifically, knowledge of an upper bound on the relative degree, knowledge of the sign

of the high-frequency gain, and knowledge of an upper bound on the magnitude of the high-frequency gain. However, the control method is effective for plants that are open-loop stable. Also, command following is not addressed. In [19], a model reference adaptive controller is presented for uncertain minimum phase SISO systems with unknown-but-bounded relative degree. The controller in [19] is effective with disturbances, which are bounded and piecewise continuous. In [20], a robust model reference adaptive control is presented for uncertain SISO LTI systems that are minimum phase with unknown relative degree. The controller in [20] requires knowledge of an upper bound on the degree of the denominator of the plant transfer function, knowledge of a lower bound and an upper bound on the relative degree, and knowledge of the sign of the high-frequency gain. In [21], a model reference adaptive control is presented for uncertain LTI systems that are minimum phase and open-loop stable with unknown relative degree and subject to unknown disturbances. The controller in [21] requires the knowledge of the plant order, knowledge of an upper bound on the relative degree, and knowledge of an upper bound on the plant parameters. The controller is effective for rejection of disturbances that are bounded. In [22], an adaptive pole assignment control scheme is presented for a class of unknown LTI systems that are nonminimum phase and SISO with unknown relative degree. The controller in [22] requires the knowledge of the sign of the high-frequency gain. However [22] does not address disturbance rejection. A high-parameter-stabilizing controller is presented in [23] for uncertain SISO minimum-phase systems with unknown-but-bounded relative degree. In [24], the controller in [23] is extended to address adaptive command following and disturbance rejection. However, the controller in [24] is effective with command and disturbances, which consists of steps and sinusoids. It also requires the knowledge of the frequencies of the command and disturbance sinusoids. In [25], global output-feedback stabilization for SISO uncertain nonlinear systems with unknown relative degree is presented. However, command following and disturbance

rejection is not addressed.

Filtered dynamic inversion (FDI), presented in [26], is a high-parameter-stabilizing controller for unknown MIMO LTI minimum-phase systems. The FDI controller only requires the knowledge of the relative degree of the system and the first nonzero Markov parameter to achieve stabilization, command following, and disturbance rejection. The disturbances are unknown-and-unmeasured. In [27], the FDI control in [26] is extended to address decentralized control. In [28, 29], FDI is examined for vibration control of uncertain structures that are minimum phase and where the sensors and actuators are colocated. In [1], FDI is used for altitude control of fixed-wing unmanned air vehicles. In [30, 31], a single-parameter high-parameter-stabilizing controller for MIMO uncertain nonlinear systems is presented, where the equilibrium of the zero dynamics is locally asymptotically stable. The controller in [30, 31] is an extension of the control method in [26, 27]. The controller in [30, 31] only requires the knowledge of the vector relative degree and knowledge of the dynamic-inversion matrix, which is the nonlinear extension of the first nonzero Markov parameter of linear systems. Note that none of these control methods mentioned in this paragraph address uncertainty in the relative degree.

### **1.3 Contributions of this Thesis**

In Chapter 2, we review the FDI control presented in [26, 27] and provide an example where the FDI controller is not necessarily robust to uncertainty in the relative degree. This provides the motivation for the work in this thesis.

In Chapter 3, we extend the FDI control presented in [26, 27] to accommodate unknown relative degree. This extended FDI control is a method for unknown LTI systems that are MIMO and minimum phase with unknown-but-bounded relative degree. This extended FDI controller requires limited model information, specifically, knowledge of an upper bound on the relative degree and knowledge of the

first nonzero Markov parameter. This FDI controller is a single-parameter high-parameter-stabilizing controller that is robust to uncertainty in the relative degree. We also characterize the stability of the closed-loop system.

In Chapter 4, we present simulation results of examples of mathematical systems and physical systems with the FDI control for unknown relative degree implemented in feedback. We design a single FDI controller that can control a single integrator, double integrator, and triple integrator. We also design an FDI controller to be implemented in feedback with a MIMO system. We consider several different choices of input and output matrices, which result in different relative degrees. Next, we design an FDI controller to be implemented in feedback with a serially connected four mass-spring-damper system. We consider different choices of sensor and actuator placements, which result in different relative degrees. Finally, we design an FDI controller to be implemented in feedback with a two-mass servo system with a flexible shaft. We consider different choices of sensor placements, which result in different relative degrees. We show that the FDI controller for unknown relative degree is effective for stabilization, command following, and disturbance rejection.



# Chapter 2

---

## Review of Filtered Dynamic Inversion

In this chapter, we review filtered-dynamic-inversion (FDI) control, which is presented in [26, 27]. FDI is a control method for linear time-invariant (LTI) systems that are multi-input multi-output (MIMO) and minimum phase. FDI requires limited model information, specifically, knowledge of the relative degree and knowledge of the first nonzero Markov parameter. The FDI controller is effective for stabilization, command following, and rejection of disturbances, which need not be known or measured. For sufficiently large choice of a single control parameter, FDI yields an asymptotically stable closed-loop system and makes the average power of the performance arbitrarily small. However, in Section 2.4, we provide an example demonstrating that FDI is not necessarily robust to uncertainty in the relative degree.

### 2.1 Problem Formulation

Consider the MIMO LTI system

$$\dot{x}(t) = Ax(t) + Bu(t) + w(t), \tag{2.1}$$

$$y(t) = Cx(t), \quad (2.2)$$

where  $t \geq 0$ ,  $x(0) \in \mathbb{R}^n$  is the initial condition,  $A \in \mathbb{R}^{n \times n}$ ,  $B \in \mathbb{R}^{n \times m}$ ,  $C \in \mathbb{R}^{m \times n}$ ,  $u(t) \in \mathbb{R}^m$  is the control,  $y(t) \in \mathbb{R}^m$  is the measurement, and  $w(t) \in \mathbb{R}^n$  is the unknown and unmeasured disturbance. Define the relative degree  $d$  to be the smallest positive integer  $i$  such that the  $i$ th Markov parameter  $H_i \triangleq CA^{i-1}B$  is nonzero. Let  $\mathbf{p} = d/dt$  denote the differential operator. We make the following assumptions:

(A2.1) The triple  $(A, B, C)$  is controllable and observable.

(A2.2) If  $\lambda \in \mathbb{C}$  and  $\det \begin{bmatrix} \lambda I_n - A & B \\ C & 0_{m \times m} \end{bmatrix} = 0$ , then  $\text{Re } \lambda < 0$ .

(A2.3)  $d$  is known.

(A2.4)  $H_d$  is nonsingular and known.

(A2.5)  $w$  is  $d$  times differentiable, and  $w, \mathbf{p}w, \dots, \mathbf{p}^d w$  are bounded.

Assumption (A2.2) states that  $(A, B, C)$  is minimum phase, that is, the invariant zeros of  $(A, B, C)$  are contained in the open-left-half complex plane. Assumption (A2.3) requires that the relative degree  $d$  is known, and (A2.4) requires that the first nonzero Markov parameter  $H_d$  is known. Note that the FDI approach presented in this chapter can be extended to accommodate uncertainty in  $H_d$  (see [26, 27]). However, we invoke (A2.4) for clarity of presentation. Assumption (A2.5) is a technical condition required for analysis. This assumption requires that  $w$  is sufficiently smooth. The plant (2.1) and (2.2) is otherwise unknown, that is,  $A, B, C$  and  $x(0)$  are unknown, and  $w$  and  $x$  are unmeasured.

Consider the  $m \times m$  polynomial matrices

$$\alpha_m(\mathbf{p}) = \mathbf{p}^d \alpha_d + \mathbf{p}^{d-1} \alpha_{d-1} + \dots + \mathbf{p} \alpha_1 + \alpha_0, \quad (2.3)$$

$$\beta_m(\mathbf{p}) = \mathbf{p}^{d-1}\beta_{d-1} + \dots + \mathbf{p}\beta_1 + \beta_0, \quad (2.4)$$

where  $\alpha_d = I_m$ ;  $\alpha_0, \dots, \alpha_{d-1} \in \mathbb{R}^{m \times m}$ ;  $\beta_0, \dots, \beta_{d-1} \in \mathbb{R}^{m \times m}$ ; and if  $\lambda \in \mathbb{C}$  and  $\det \alpha_m(\lambda) = 0$ , then  $\text{Re } \lambda < 0$ . Now, consider the reference model

$$\alpha_m(\mathbf{p})y_m(t) = \beta_m(\mathbf{p})r(t), \quad (2.5)$$

where  $t \geq 0$ ;  $r(t) \in \mathbb{R}^m$  is the reference-model command, which is  $d$ -times differentiable and  $r, \mathbf{p}r, \dots, \mathbf{p}^d r$  are bounded;  $y_m(t) \in \mathbb{R}^m$  is the reference-model output; and the initial condition is given by  $y_m(0), \dots, \mathbf{p}^{d-1}y_m(0)$ , and  $r(0), \dots, \mathbf{p}^{d-2}r(0)$ . The performance is defined as

$$z(t) \triangleq y(t) - y_m(t), \quad (2.6)$$

which is the command-following error. The aim is to design a high parameter-stabilizing output-feedback controller such that for sufficiently large parameter, the average power of the performance

$$\lim_{T \rightarrow \infty} \frac{1}{T} \int_0^T z^T(t)z(t) dt$$

is arbitrary small despite the unknown and unmeasured disturbance  $w$ .

## 2.2 Ideal Dynamic Inversion

To construct the ideal dynamic-inversion (IDI) control, we assume that the plant (2.1) and (2.2) is known, the disturbance  $w$  is measured, and the full state  $x$  is available for feedback. Note that the IDI control is not implementable.

Taking the  $d$ th derivative of (2.2) and using (2.1) yields

$$\mathbf{p}^d y(t) = H_d u(t) + CA^d x(t) + \sum_{i=0}^{d-1} CA^{d-1-i} \mathbf{p}^i w(t). \quad (2.7)$$

Next, define the IDI control

$$u_* \triangleq -H_d^{-1} \left[ CA^d x + \sum_{i=0}^{d-1} \left( CA^{d-1-i} \mathbf{p}^i w - \beta_i \mathbf{p}^i r + \alpha_i \mathbf{p}^i y \right) \right]. \quad (2.8)$$

Since  $H_1 = \dots = H_{d-1} = 0$ , substituting (2.1) and (2.2) into (2.8) for  $\mathbf{p}^i y$  yields

$$\begin{aligned} u_*(x, \Phi) &= -H_d^{-1} \left[ CA^d x + \sum_{i=0}^{d-1} \left( CA^{d-1-i} \mathbf{p}^i w - \beta_i \mathbf{p}^i r + \alpha_i CA^i x + \sum_{j=0}^{i-1} \alpha_i CA^{i-1-j} \mathbf{p}^j w \right) \right] \\ &= H_d^{-1} K_x x + H_d^{-1} \Phi, \end{aligned} \quad (2.9)$$

where

$$K_x \triangleq - \sum_{i=0}^d \alpha_i CA^i \in \mathbb{R}^{m \times n}, \quad (2.10)$$

$$\Phi(t) \triangleq \sum_{i=0}^{d-1} \left( \beta_i \mathbf{p}^i r(t) - CA^{d-1-i} \mathbf{p}^i w(t) - \sum_{j=0}^{i-1} \alpha_i CA^{i-1-j} \mathbf{p}^j w(t) \right). \quad (2.11)$$

Let  $x_*$  and  $y_*$  denote the solution to (2.1) and (2.2) with  $u = u_*(x_*, \Phi)$  and  $x_*(0) = x(0)$ . Thus, the ideal closed-loop system (2.1), (2.2), and (2.9)–(2.11) is given by

$$\dot{x}_*(t) = \tilde{A}_* x_*(t) + BH_d^{-1} \Phi(t) + w(t), \quad (2.12)$$

$$y_*(t) = Cx_*(t), \quad (2.13)$$

where

$$\tilde{A}_* \triangleq A + BH_d^{-1} K_x. \quad (2.14)$$

Define the ideal performance  $z_* \triangleq y_* - y_m$ . The following result characterizes the stability and performance of the ideal closed-loop system (2.12)–(2.14). This result is from [26, Lemma 1].

**Lemma 2.1.** Consider the ideal closed-loop system (2.12)–(2.14), which consists of (2.1), (2.2), and (2.9)–(2.11), and satisfies (A2.1), (A2.2), and (A2.4). Then, the following statements hold:

(i) Let  $\lambda \in \mathbb{C}$ . Then,  $\det(\lambda I_n - \tilde{A}_*) = 0$  if and only if  $\det \alpha_m(\lambda) = 0$  or

$$\det \begin{bmatrix} \lambda I_n - A & B \\ C & 0_{m \times m} \end{bmatrix} = 0.$$

(ii)  $\tilde{A}_*$  is Hurwitz.

(iii) For all initial conditions  $x_*(0) \in \mathbb{R}^n$ ,  $\alpha_m(\mathbf{p})y_*(t) = \beta_m(\mathbf{p})r(t)$ .

(iv) For all initial conditions  $x_*(0) \in \mathbb{R}^n$ ,  $\lim_{t \rightarrow \infty} z_*(t) = 0$  and  $\int_0^\infty z_*^T(t)z_*(t) dt$  exists.

Part (i) of Lemma 2.1 states that the eigenvalues of  $\tilde{A}_*$  consists of the roots of  $\alpha_m$  and the invariant zeros of  $(A, B, C)$ , which are in the open-left-half complex plane. Part (iii) states that the closed-loop input-output relationship from  $r$  to  $y_*$  matches the reference model (2.5). Part (iv) implies that for all initial conditions  $x_*(0)$ , performance  $z_*$  tends to zero asymptotically.

### 2.3 Filtered Dynamic Inversion

In this section, we review the FDI controller presented in [26]. The IDI control (2.9)–(2.11) is not implementable because it relies on knowledge of the plant parameters  $A$  and  $C$  as well as measurements of  $x$  and  $w$ . Since this information is not assumed to be known, the IDI control cannot be implemented. Thus, we use a linear filter to construct the FDI control, which is implementable and approximates the IDI control.

Let  $\eta_k(s)$  be a parameter-dependent polynomial, that is, a polynomial in  $s$  over the reals whose coefficients are functions of a real parameter  $k$ . Furthermore, let  $\eta_k$

be monic with degree  $\rho \geq d$ . Thus,  $\eta_k$  can be written as

$$\eta_k(s) \triangleq s^\rho + \eta_{\rho-1,k}s^{\rho-1} + \dots + \eta_{1,k}s + \eta_{0,k}, \quad (2.15)$$

where for all  $k \in [0, \infty)$ ,  $\eta_{0,k}, \dots, \eta_{\rho-1,k} \in \mathbb{R}$ . Define the transfer function

$$\Delta_k(s) \triangleq \frac{\bar{\eta}_k(s)}{\eta_k(s)}, \quad (2.16)$$

where

$$\bar{\eta}_k(s) \triangleq s^{\rho-1} + \eta_{\rho-1,k}s^{\rho-2} + \dots + \eta_{2,k}s + \eta_{1,k}. \quad (2.17)$$

Note that for all  $k \geq 0$ ,  $\Delta_k$  is well defined, that is,  $\eta_k(s) \neq 0$ . Next, consider the following conditions:

(C2.1) There exists  $k_0 > 0$  such that for all  $k > k_0$ ,  $\eta_k$  is Hurwitz.

(C2.2) For all  $\varepsilon > 0$ , there exists  $k_\varepsilon > k_0$  such that for all  $k > k_\varepsilon$ ,

$$\gamma_k \triangleq \sup_{\omega \in \mathbb{R}} |\Delta_k(j\omega)| < \varepsilon. \quad (2.18)$$

Condition (C2.2) states that for sufficiently large  $k$ , the  $\mathcal{H}_\infty$  norm of  $\Delta_k$  is arbitrarily small. Note that  $\eta_k(s) = (s + k)^\rho$  is an example of a parameter-dependent polynomial that satisfies (C2.1) and (C2.2). Other examples that satisfy (C2.1) and (C2.2) are given in [26, 27].

Consider the control  $u$  that satisfies

$$\eta_k(\mathbf{p})u = \eta_k(0)u_*(x, \Phi), \quad (2.19)$$

where  $u_*(x, \Phi)$  is given by (2.9)–(2.11). The transfer function from  $u_*$  to  $u$  is given

by

$$\zeta_k(s) \triangleq \frac{\eta_k(0)}{\eta_k(s)} I_m = (I - s\Delta_k(s))I_m, \quad (2.20)$$

which is a low-pass filter. It follows from (C2.2) that as  $k$  tends to infinity, the cutoff frequency of  $\zeta_k$  tends to infinity, suggesting that  $u$  approximates  $u_*(x, \Phi)$  for sufficiently large  $k$ .

To express (2.19) as an implementable control, it follows from (2.7) and (2.8) that

$$\begin{aligned} u_* &= -H_d^{-1} \left[ \mathbf{p}^d y - H_d u + \sum_{i=0}^{d-1} (\alpha_i \mathbf{p}^i y - \beta_i \mathbf{p}^i r) \right] \\ &= u - H_d^{-1} [\alpha_m(\mathbf{p})y - \beta_m(\mathbf{p})r]. \end{aligned} \quad (2.21)$$

Substituting (2.21) into (2.19) yields the FDI controller

$$\mathbf{p}\bar{\eta}_k(\mathbf{p})u(t) = \eta_{0,k}H_d^{-1}[\beta_m(\mathbf{p})r(t) - \alpha_m(\mathbf{p})y(t)]. \quad (2.22)$$

The controller (2.22) is a dynamic output-feedback controller, which uses  $y$  for feedback,  $r$  for feedforward, and can be implemented for  $k > k_0$  using knowledge of only  $H_d$  and the design parameters  $\alpha_m, \beta_m$ , and  $\eta_k$ .

The transfer function from  $\begin{bmatrix} y^T & r^T \end{bmatrix}^T$  to  $u$  is given by

$$G_c(s) \triangleq \frac{\eta_{0,k}}{s\bar{\eta}_k(s)} H_d^{-1} \begin{bmatrix} -\alpha_m(s) & \beta_m(s) \end{bmatrix}, \quad (2.23)$$

which characterizes the forced response of (2.22). Next, for all  $k > k_0$ , let  $G_c$  have the  $\rho m$ -order state-space realization

$$\dot{x}_c(t) = A_c x_c(t) + B_c y(t) + E_c r(t), \quad (2.24)$$

$$u(t) = C_c x_c(t) + D_c y(t), \quad (2.25)$$

where  $x_c(t) \in \mathbb{R}^{\rho m}$ , and for all  $k > k_0$ ,  $A_c \in \mathbb{R}^{\rho m \times \rho m}$ ,  $B_c \in \mathbb{R}^{\rho m \times m}$ ,  $C_c \in \mathbb{R}^{m \times \rho m}$ ,  $D_c \in \mathbb{R}^{m \times m}$ , and  $E_c \in \mathbb{R}^{\rho m \times m}$ . To see that such a realization exists, consider the block-observable realization

$$A_c = \begin{bmatrix} -\eta_{\rho-1,k} & 1 & 0 & \dots & 0 \\ -\eta_{\rho-2,k} & 0 & 1 & & 0 \\ \vdots & \vdots & \ddots & & \\ -\eta_{1,k} & 0 & 0 & & 1 \\ 0 & 0 & 0 & \dots & 0 \end{bmatrix} \otimes I_m \in \mathbb{R}^{\rho m \times \rho m}, \quad (2.26)$$

$$B_c = \begin{bmatrix} -\eta_{0,k} H_d^{-1} \alpha_{\rho-1} - \eta_{\rho-1,k} D_c \\ \vdots \\ -\eta_{0,k} H_d^{-1} \alpha_1 - \eta_{1,k} D_c \\ -\eta_{0,k} H_d^{-1} \alpha_0 \end{bmatrix} \in \mathbb{R}^{\rho m \times m}, \quad (2.27)$$

$$E_c = \begin{bmatrix} 0_{(\rho-d)m \times m} \\ -\eta_{0,k} H_d^{-1} \beta_{d-1} \\ \vdots \\ -\eta_{0,k} H_d^{-1} \beta_0 \end{bmatrix} \in \mathbb{R}^{\rho m \times m}, \quad (2.28)$$

$$C_c = \begin{bmatrix} 1 & 0_{1 \times \rho-1} \end{bmatrix} \otimes I_m \in \mathbb{R}^{m \times \rho m}, \quad (2.29)$$

$$D_c = -\eta_{0,k} H_d^{-1} \alpha_\rho \in \mathbb{R}^{m \times m}, \quad (2.30)$$

where  $\otimes$  is the Kronecker product and  $\alpha_{d+1} = \alpha_{d+2} = \dots = 0_{m \times m}$ .

The closed-loop system (2.1), (2.2), and (2.24)–(2.30) is given by

$$\dot{\tilde{x}}(t) = \tilde{A}\tilde{x}(t) + \tilde{B}w(t) + \tilde{E}r(t), \quad (2.31)$$

$$y(t) = \tilde{C}\tilde{x}(t), \quad (2.32)$$



where

$$\tilde{x}(t) \triangleq \begin{bmatrix} x(t) \\ x_c(t) \end{bmatrix} \in \mathbb{R}^{n+\rho m}, \quad (2.33)$$

and

$$\tilde{A} \triangleq \begin{bmatrix} A + BD_c C & BC_c \\ B_c C & A_c \end{bmatrix} \in \mathbb{R}^{(n+\rho m) \times (n+\rho m)}, \quad \tilde{B} \triangleq \begin{bmatrix} I_n \\ 0_{\rho m \times n} \end{bmatrix} \in \mathbb{R}^{(n+\rho m) \times n}, \quad (2.34)$$

$$\tilde{E} \triangleq \begin{bmatrix} 0_{n \times m} \\ E_c \end{bmatrix} \in \mathbb{R}^{(n+\rho m) \times m}, \quad \tilde{C} \triangleq \begin{bmatrix} C & 0_{m \times \rho m} \end{bmatrix} \in \mathbb{R}^{m \times (n+\rho m)}. \quad (2.35)$$

The following result characterizes the stability and performance of the closed-loop system (2.31)–(2.35). This result is from [26, Theorem 1].

**Theorem 2.1.** Consider the closed-loop system (2.31)–(2.35), which consists of (2.1), (2.2), and (2.24)–(2.30), where (A2.1)–(A2.5) are satisfied and  $\eta_k$  satisfies (C2.1) and (C2.2). Then, the following statements hold:

- (i) There exists  $k_s > k_0$  such that for all  $k > k_s$ ,  $\tilde{A}$  is Hurwitz.
- (ii) For all  $\delta > 0$ , there exists  $k_\delta > k_s$  such that for all  $k > k_\delta$ ,

$$\lim_{T \rightarrow \infty} \frac{1}{T} \int_0^T z^\top(t) z(t) dt < \delta.$$

Part (i) of Theorem 2.1 states that for sufficiently large  $k$ , the origin is an asymptotically stable equilibrium of closed-loop system (2.31)–(2.35). Part (ii) states that for sufficiently large  $k$ , the average power of performance  $z$  is arbitrarily small.

## 2.4 Motivating Example

In this section, we present an example that demonstrates that the FDI controller (2.22) is not necessarily robust to uncertainty in the relative degree  $d$ . This example

motivates the work in this thesis, which extends the FDI approach to systems with unknown-but-bounded relative degree.

Consider the triple integrator

$$\ddot{y}(t) = u(t), \quad (2.36)$$

where  $t \geq 0$ ,  $y(t) \in \mathbb{R}$  is the measured output, and  $u(t) \in \mathbb{R}$  is the control. It follows that (2.36) can be expressed as (2.1) and (2.2), where

$$x(t) \triangleq \begin{bmatrix} y(t) \\ \dot{y}(t) \\ \ddot{y}(t) \end{bmatrix}, \quad w(t) \equiv 0, \quad (2.37)$$

and

$$A \triangleq \begin{bmatrix} 0 & 1 & 0 \\ 0 & 0 & 1 \\ 0 & 0 & 0 \end{bmatrix}, \quad B \triangleq \begin{bmatrix} 0 \\ 0 \\ 1 \end{bmatrix}, \quad C \triangleq \begin{bmatrix} 1 & 0 & 0 \end{bmatrix}. \quad (2.38)$$

Note that the relative degree is  $d = 3$ , and the first nonzero Markov parameter is given by  $H_d = CA^2B = 1$ .

To design an FDI controller to stabilize the triple integrator (2.36), we select the reference-model polynomials as

$$\alpha_m(\mathbf{p}) = (\mathbf{p} + 5)^3, \quad \beta_m(\mathbf{p}) = 125, \quad (2.39)$$

and we let  $r = 0$ . Note that we focus on stabilization only rather than command following and/or disturbance rejection for clarity of presentation. Next, let  $\rho = 4 \geq$

$d = 3$ , and let

$$\eta_k(s) = (s + k)^4, \quad (2.40)$$

which satisfies (C2.1) and (C2.2). Since (A2.1)–(A2.5) are satisfied, and  $\eta_k$  satisfies (C2.1) and (C2.2), it follows from Theorem 2.1 that for sufficiently large  $k$ , the origin is an asymptotically stable equilibrium of the closed-loop system consisting of the triple integrator (2.1), (2.2), (2.37), and (2.38); and the FDI controller (2.24)–(2.30). Note that the closed-loop dynamics matrix  $\tilde{A}$ , given by (2.34), has 7 eigenvalues. Figure 2.1 shows the locus of the closed-loop eigenvalues (i.e., the eigenvalues of  $\tilde{A}$ ) for different  $k > 0$ . As  $k$  is increased, 3 eigenvalues of  $\tilde{A}$  approach  $-5$  (the roots of  $\alpha_m$ ) and the remaining eigenvalues of  $\tilde{A}$  diverge to infinity through the open-left-half complex plane. In fact, for all  $k > 45$ , all eigenvalues of  $\tilde{A}$  are in the open-left-half complex plane. Thus, for all  $k > 45$ , the FDI controller stabilizes the triple integrator.

Next, consider the double integrator

$$\ddot{y}(t) = u(t), \quad (2.41)$$

where  $t \geq 0$ ,  $y(t) \in \mathbb{R}$  is the measured output, and  $u(t) \in \mathbb{R}$  is the control. It follows that (2.41) can be expressed as (2.1) and (2.2), where

$$x(t) \triangleq \begin{bmatrix} y(t) \\ \dot{y}(t) \end{bmatrix}, \quad w(t) \equiv 0, \quad (2.42)$$

and

$$A \triangleq \begin{bmatrix} 0 & 1 \\ 0 & 0 \end{bmatrix}, \quad B \triangleq \begin{bmatrix} 0 \\ 1 \end{bmatrix}, \quad C \triangleq \begin{bmatrix} 1 & 0 \end{bmatrix}. \quad (2.43)$$

Note that the relative degree is  $d = 2$ , and the first nonzero Markov parameter is given by  $H_d = CAB = 1$ .

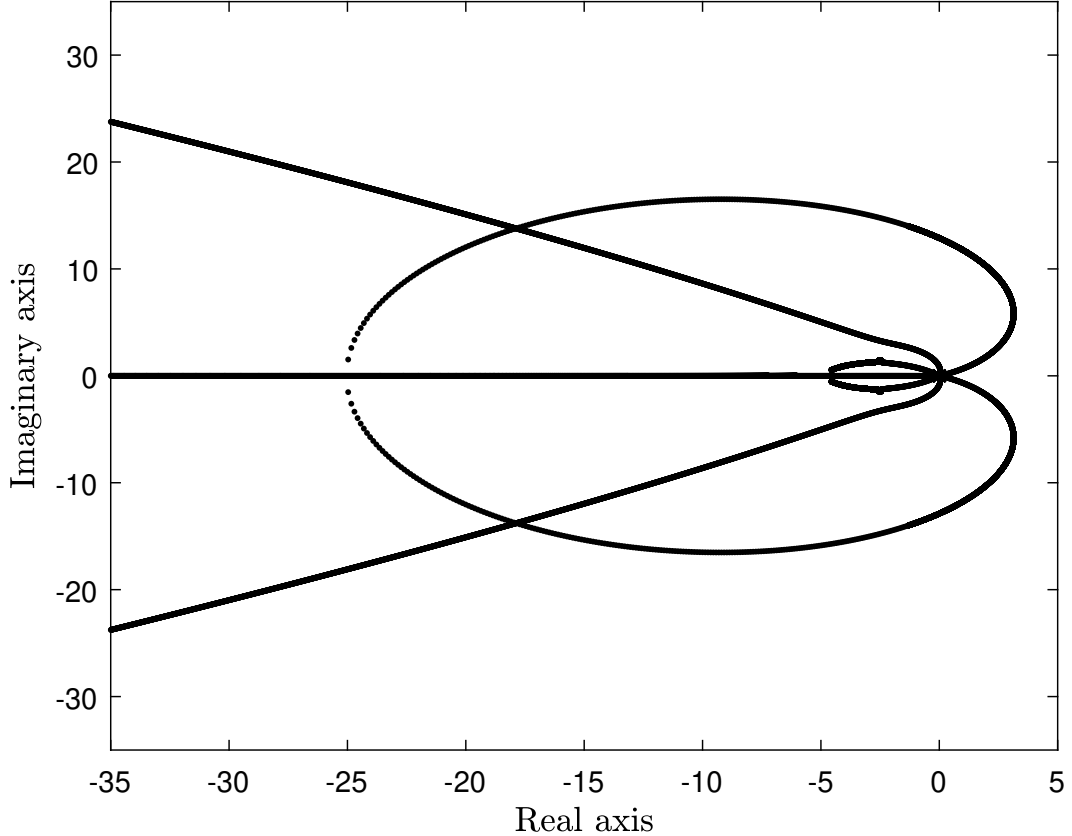


Figure 2.1: Locus of the eigenvalues of  $\tilde{A}$  of the closed-loop system (2.31)–(2.35), which consists of the triple integrator (2.1), (2.2), (2.37), and (2.38); and the FDI controller (2.24)–(2.30). For all  $k > 45$ , the origin of the closed-loop system is asymptotically stable. Note that two eigenvalues of  $\tilde{A}$  diverge along the asymptote towards  $-\infty$ .

Now, we use the FDI control designed for the triple integrator (2.36) to control the double integrator (2.41). The closed-loop system consists of the double integrator (2.1), (2.2), (2.42), and (2.43); and the FDI controller (2.24)–(2.30). Note that the closed-loop dynamics matrix  $\tilde{A}$ , given by (2.34), has 6 eigenvalues. Figure 2.2 shows the locus of the closed-loop eigenvalues (i.e., the eigenvalues of  $\tilde{A}$ ) for different  $k > 0$ . As  $k$  is increased, 3 eigenvalues of  $\tilde{A}$  approach  $-5$  (the roots of  $\alpha_m$ ) and one eigenvalue diverges to minus infinity. For all  $k > 0$ , the remaining 2 eigenvalues of  $\tilde{A}$  lie in the open-right-half complex plane. Thus, the FDI controller does not stabilize the double integrator.

This example shows that the FDI controller is not necessarily robust to uncertainty

in the relative degree  $d$ . This example motivates the work in the thesis, which extends the FDI approach to unknown minimum-phase systems with unknown relative degree.

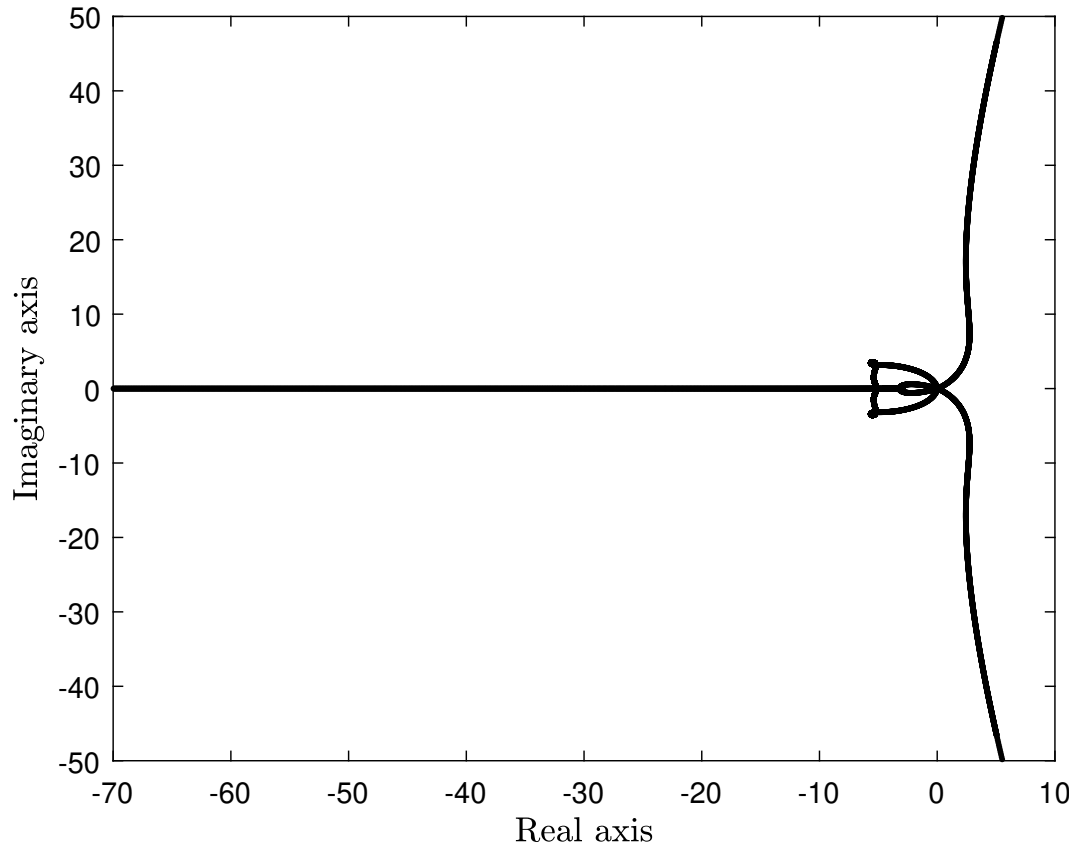


Figure 2.2: Locus of the eigenvalues of  $\tilde{A}$  of the closed-loop system (2.31)–(2.35), which consists of the double integrator (2.1), (2.2), (2.42), and (2.43); and the FDI controller (2.24)–(2.30), which is designed for the triple integrator. For all  $k > 0$ , the closed-loop system is unstable.

# Chapter 3

---

## Filtered Dynamic Inversion with Unknown Relative Degree

In this chapter, we extend filtered-dynamic-inversion (FDI) control to accommodate unknown relative degree. This extended FDI control is a method for unknown linear time-invariant (LTI) systems that are multi-input multi-output (MIMO) and minimum phase with unknown-but-bounded relative degree. This FDI controller requires limited model information, specifically, knowledge of an upper bound on the relative degree and knowledge of the first nonzero Markov parameter. This FDI controller is a single-parameter high-parameter-stabilizing controller that is robust to uncertainty in the relative degree. The main analytic result in this chapter shows that the origin of the closed-loop system, consisting of the FDI controller for unknown relative degree connected in feedback with a single-input single-output (SISO) open-loop system, is an asymptotically stable equilibrium.

### 3.1 Problem Formulation

Consider the MIMO LTI system

$$\dot{x}(t) = Ax(t) + Bu(t) + w(t), \tag{3.1}$$

$$y(t) = Cx(t), \quad (3.2)$$

where  $t \geq 0$ ,  $x(0) \in \mathbb{R}^n$  is the initial condition,  $A \in \mathbb{R}^{n \times n}$ ,  $B \in \mathbb{R}^{n \times m}$ ,  $C \in \mathbb{R}^{m \times n}$ ,  $u(t) \in \mathbb{R}^m$  is the control,  $y(t) \in \mathbb{R}^m$  is the measurement, and  $w(t) \in \mathbb{R}^n$  is the unknown and unmeasured disturbance. Define the relative degree  $d$  to be the smallest positive integer  $i$  such that the  $i$ th Markov parameter  $H_i \triangleq CA^{i-1}B$  is nonzero. Let  $\mathbf{p} = d/dt$  denote the differential operator. We make the following assumptions:

(A3.1) The triple  $(A, B, C)$  is controllable and observable.

(A3.2) If  $\lambda \in \mathbb{C}$  and  $\det \begin{bmatrix} \lambda I_n - A & B \\ C & 0_{m \times m} \end{bmatrix} = 0$ , then  $\text{Re } \lambda < 0$ .

(A3.3) There is a known integer  $\bar{d}$  such that  $\bar{d} \geq d$ .

(A3.4)  $H_d$  is nonsingular and known.

(A3.5)  $w$  is  $\bar{d}$  times differentiable, and  $w, \mathbf{p}w, \dots, \mathbf{p}^{\bar{d}}w$  are bounded.

Assumption (A3.2) states that  $(A, B, C)$  is minimum phase, that is, the invariant zeros of  $(A, B, C)$  are contained in the open-left-half complex plane. Assumption (A3.3) requires that an upper bound  $\bar{d}$  on the relative degree  $d$  is known. Note that (A3.3) replaces the more restrictive standard FDI assumption (A2.3), which requires that  $d$  is known. Assumption (A3.4) requires that the first nonzero Markov parameter  $H_d$  is known. Assumption (A3.5) is a technical condition required for analysis. This assumption requires that  $w$  is sufficiently smooth. The plant (3.1) and (3.2) is otherwise unknown, that is,  $A, B, C$  and  $x(0)$  are unknown, and  $w$  and  $x$  are unmeasured.

Consider the  $m \times m$  polynomial matrices

$$\alpha_m(\mathbf{p}) = \mathbf{p}^{\bar{d}}\alpha_{\bar{d}} + \mathbf{p}^{\bar{d}-1}\alpha_{\bar{d}-1} + \dots + \mathbf{p}\alpha_1 + \alpha_0, \quad (3.3)$$

$$\beta_m(\mathbf{p}) = \mathbf{p}^{\bar{d}-1}\beta_{\bar{d}-1} + \dots + \mathbf{p}\beta_1 + \beta_0, \quad (3.4)$$

where  $\alpha_{\bar{d}} = I_m$ ;  $\alpha_0, \dots, \alpha_{\bar{d}-1} \in \mathbb{R}^{m \times m}$ ;  $\beta_0, \dots, \beta_{\bar{d}-1} \in \mathbb{R}^{m \times m}$ ; and if  $\lambda \in \mathbb{C}$  and  $\det \alpha_m(\lambda) = 0$ , then  $\text{Re } \lambda < 0$ . Now, consider the reference model

$$\alpha_m(\mathbf{p})y_m(t) = \beta_m(\mathbf{p})r(t), \quad (3.5)$$

where  $t \geq 0$ ;  $r(t) \in \mathbb{R}^m$  is the reference-model command, which is  $\bar{d}$ -times differentiable and  $r, \mathbf{p}r, \dots, \mathbf{p}^{\bar{d}}r$  are bounded;  $y_m(t) \in \mathbb{R}^m$  is the reference-model output; and the initial condition is given by  $y_m(0), \dots, \mathbf{p}^{\bar{d}-1}y_m(0)$ , and  $r(0), \dots, \mathbf{p}^{\bar{d}-2}r(0)$ . The performance is defined as

$$z(t) \triangleq y(t) - y_m(t), \quad (3.6)$$

which is the command-following error. The aim is to design a high parameter-stabilizing output-feedback controller such that for sufficiently large parameter, the average power of the performance

$$\lim_{T \rightarrow \infty} \frac{1}{T} \int_0^T z^T(t)z(t) dt$$

is arbitrary small despite the unknown and unmeasured disturbance  $w$ .

### 3.2 Ideal Dynamic Inversion

To construct the ideal dynamic-inversion (IDI) control, we assume that the plant (3.1) and (3.2) is known, the disturbance  $w$  is measured, and the full state  $x$  is available for feedback. Note that the IDI control is not implementable.

Taking the  $d$ th derivative of (3.2) and using (3.1) yields

$$\mathbf{p}^d y(t) = H_d u(t) + CA^d x(t) + \sum_{i=0}^{d-1} CA^{d-1-i} \mathbf{p}^i w(t). \quad (3.7)$$



Next, define the IDI control

$$u_* \triangleq -H_d^{-1} \left[ CA^d x + \alpha_{\bar{d}} \mathbf{p}^{\bar{d}} y - \mathbf{p}^d y + \sum_{i=0}^{d-1} CA^{d-1-i} \mathbf{p}^i w + \sum_{i=0}^{\bar{d}-1} \left( \alpha_i \mathbf{p}^i y - \beta_i \mathbf{p}^i r \right) \right], \quad (3.8)$$

and note that if  $\bar{d} = d$ , then the IDI control (3.8) is equivalent to the IDI control (2.8) for known relative degree. Substituting (3.7) into (3.8) yields

$$\begin{aligned} u_* &= -H_d^{-1} \left[ \alpha_{\bar{d}} \mathbf{p}^{\bar{d}} y - H_d u + \sum_{i=0}^{\bar{d}-1} \left( \alpha_i \mathbf{p}^i y - \beta_i \mathbf{p}^i r \right) \right] \\ &= u - H_d^{-1} \left[ \sum_{i=0}^{\bar{d}} \alpha_i \mathbf{p}^i y - \sum_{i=0}^{\bar{d}-1} \beta_i \mathbf{p}^i r \right] \\ &= u - H_d^{-1} \left[ \sum_{i=0}^{d-1} \alpha_i \mathbf{p}^i y + \sum_{i=d}^{\bar{d}} \alpha_i \mathbf{p}^i y - \sum_{i=0}^{\bar{d}-1} \beta_i \mathbf{p}^i r \right]. \end{aligned} \quad (3.9)$$

Since  $H_1 = \dots = H_{d-1} = 0$ , substituting (3.1) and (3.2) into (3.9) for  $\mathbf{p}^i y$  yields

$$\begin{aligned} u_*(x, u, \dots, \mathbf{p}^{\bar{d}-d} u, \Phi) &= u - H_d^{-1} \left[ \sum_{i=0}^{d-1} \left( \alpha_i CA^i x + \sum_{j=0}^{i-1} \alpha_i CA^{i-1-j} \mathbf{p}^j w \right) \right. \\ &\quad \left. + \sum_{i=d}^{\bar{d}} \left( \alpha_i CA^i x + \sum_{j=0}^{i-d} \alpha_i H_{i-j} \mathbf{p}^j u + \sum_{j=0}^{i-1} \alpha_i CA^{i-1-j} \mathbf{p}^j w \right) \right. \\ &\quad \left. - \sum_{i=0}^{\bar{d}-1} \beta_i \mathbf{p}^i r \right] \\ &= u - H_d^{-1} \left[ \sum_{i=0}^{d-1} \alpha_i CA^i x + \sum_{i=d}^{\bar{d}} \alpha_i CA^i x + \sum_{i=d}^{\bar{d}} \sum_{j=0}^{i-d} \alpha_i H_{i-j} \mathbf{p}^j u \right. \\ &\quad \left. + \sum_{i=0}^{d-1} \sum_{j=0}^{i-1} \alpha_i CA^{i-1-j} \mathbf{p}^j w + \sum_{i=d}^{\bar{d}} \sum_{j=0}^{i-1} \alpha_i CA^{i-1-j} \mathbf{p}^j w \right. \\ &\quad \left. - \sum_{i=0}^{\bar{d}-1} \beta_i \mathbf{p}^i r \right] \\ &= u - H_d^{-1} \left[ \sum_{i=0}^{\bar{d}} \alpha_i CA^i x + \sum_{i=0}^{\bar{d}-d} \sum_{j=d+i}^{\bar{d}} \alpha_j H_{j-i} \mathbf{p}^i u \right. \\ &\quad \left. + \sum_{i=0}^{\bar{d}} \sum_{j=0}^{i-1} \alpha_i CA^{i-1-j} \mathbf{p}^j w - \sum_{i=0}^{\bar{d}-1} \beta_i \mathbf{p}^i r \right] \end{aligned}$$

$$= H_d^{-1} K_x x + H_d^{-1} \Phi + u + \sum_{i=0}^{\bar{d}-d} H_d^{-1} K_i \mathbf{p}^i u, \quad (3.10)$$

where for  $i \in \{0, 1, \dots, \bar{d} - d\}$ ,

$$K_i \triangleq - \sum_{j=d+i}^{\bar{d}} \alpha_j H_{j-i} \in \mathbb{R}^{m \times m}, \quad (3.11)$$

and

$$K_x \triangleq - \sum_{i=0}^{\bar{d}} \alpha_i C A^i \in \mathbb{R}^{m \times n}, \quad (3.12)$$

$$\Phi(t) \triangleq \sum_{i=0}^{\bar{d}-1} \beta_i \mathbf{p}^i r(t) - \sum_{i=0}^{\bar{d}} \sum_{j=0}^{i-1} \alpha_i C A^{i-1-j} \mathbf{p}^j w(t). \quad (3.13)$$

Note that, if  $\bar{d} = d$ , then

$$K_0 = -H_d, \quad (3.14)$$

$$K_x = - \sum_{i=0}^d \alpha_i C A^i, \quad (3.15)$$

$$\Phi(t) = \sum_{i=0}^{d-1} \left( \beta_i \mathbf{p}^i r(t) - C A^{d-1-i} \mathbf{p}^i w(t) - \sum_{j=0}^{i-1} \alpha_i C A^{i-1-j} \mathbf{p}^j w(t) \right), \quad (3.16)$$

which implies that (3.10) simplifies to (2.9), which is the IDI control for known relative degree.

Let  $x_*$  and  $y_*$  denote the solution to (3.1) and (3.2) with  $u = u_*(x_*, u_*, \dots, \mathbf{p}^{\bar{d}-d} u_*, \Phi)$  and  $x_*(0) = x(0)$ . Thus, it follows from (3.1), (3.2), and (3.10)–(3.13) that

$$\dot{x}_*(t) = A x_*(t) + B u_* \left( x_*(t), u_*(t), \dots, \mathbf{p}^{\bar{d}-d} u_*(t), \Phi(t) \right) + w(t), \quad (3.17)$$

$$y_*(t) = C x_*(t), \quad (3.18)$$

where  $u_*(x_*, u_*, \dots, \mathbf{p}^{\bar{d}-d}u_*, \Phi)$  satisfies

$$0 = H_d^{-1}K_x x_* + H_d^{-1}\Phi + \sum_{i=0}^{\bar{d}-d} H_d^{-1}K_i \mathbf{p}^i u_* \left( x_*, u_*, \dots, \mathbf{p}^{\bar{d}-d}u_*, \Phi \right), \quad (3.19)$$

or equivalently,

$$\begin{aligned} \mathbf{p}^{\bar{d}-d}u_* \left( x_*, u_*, \dots, \mathbf{p}^{\bar{d}-d}u_*, \Phi \right) &= H_d^{-1}K_x x_* + H_d^{-1}\Phi \\ &+ \sum_{i=0}^{\bar{d}-d-1} H_d^{-1}K_i \mathbf{p}^i u_* \left( x_*, u_*, \dots, \mathbf{p}^{\bar{d}-d}u_*, \Phi \right). \end{aligned} \quad (3.20)$$

Next, (3.20) has the state-space realization

$$\dot{x}_{c_*}(t) = A_{c_*}x_{c_*}(t) + B_{c_*}x_*(t) + E_{c_*}\Phi(t), \quad (3.21)$$

$$u_* \left( x_*(t), u_*(t), \dots, \mathbf{p}^{\bar{d}-d}u_*(t), \Phi(t) \right) = C_{c_*}x_{c_*}(t), \quad (3.22)$$

where

$$x_{c_*}(t) \triangleq \begin{bmatrix} u_* \left( x_*(t), u_*(t), \dots, \mathbf{p}^{\bar{d}-d}u_*(t), \Phi(t) \right) \\ \mathbf{p}u_* \left( x_*(t), u_*(t), \dots, \mathbf{p}^{\bar{d}-d}u_*(t), \Phi(t) \right) \\ \vdots \\ \mathbf{p}^{\bar{d}-d-1}u_* \left( x_*(t), u_*(t), \dots, \mathbf{p}^{\bar{d}-d}u_*(t), \Phi(t) \right) \end{bmatrix} \in \mathbb{R}^{m(\bar{d}-d)}, \quad (3.23)$$

and

$$A_{c_*} \triangleq \begin{bmatrix} 0_{m \times m} & I_{m \times m} & 0_{m \times m} & \dots & 0_{m \times m} \\ 0_{m \times m} & 0_{m \times m} & I_{m \times m} & & 0_{m \times m} \\ \vdots & \vdots & & \ddots & \\ 0_{m \times m} & 0_{m \times m} & 0_{m \times m} & & I_{m \times m} \\ H_d^{-1}K_0 & H_d^{-1}K_1 & H_d^{-1}K_2 & \dots & H_d^{-1}K_{\bar{d}-d-1} \end{bmatrix} \in \mathbb{R}^{m(\bar{d}-d) \times m(\bar{d}-d)}, \quad (3.24)$$

$$B_{c_*} \triangleq \begin{bmatrix} 0_{m(\bar{d}-d-1) \times n} \\ H_d^{-1} K_x \end{bmatrix} \in \mathbb{R}^{m(\bar{d}-d) \times n}, \quad (3.25)$$

$$E_{c_*} \triangleq \begin{bmatrix} 0_{m(\bar{d}-d-1) \times m} \\ H_d^{-1} \end{bmatrix} \in \mathbb{R}^{m(\bar{d}-d) \times m}, \quad (3.26)$$

$$C_{c_*} \triangleq \begin{bmatrix} I_{m \times m} & 0_{m \times (m(\bar{d}-d-1))} \end{bmatrix} \in \mathbb{R}^{m \times m(\bar{d}-d)}. \quad (3.27)$$

Thus, the ideal closed-loop system (3.17), (3.18), and (3.21)–(3.27) is given by

$$\dot{\tilde{x}}_*(t) = \tilde{A}_* \tilde{x}_*(t) + \tilde{B}_* \Phi(t) + \tilde{E}_* w(t), \quad (3.28)$$

$$y_*(t) = \tilde{C}_* \tilde{x}_*(t), \quad (3.29)$$

where

$$\tilde{x}_*(t) \triangleq \begin{bmatrix} x_*(t) \\ x_{c_*}(t) \end{bmatrix} \in \mathbb{R}^{n+m(\bar{d}-d)}, \quad (3.30)$$

and

$$\tilde{A}_* \triangleq \begin{bmatrix} A & BC_{c_*} \\ B_{c_*} & A_{c_*} \end{bmatrix} \in \mathbb{R}^{(n+m(\bar{d}-d)) \times (n+m(\bar{d}-d))}, \quad (3.31)$$

$$\tilde{B}_* \triangleq \begin{bmatrix} 0_{n+m(\bar{d}-d-1) \times m} \\ H_d^{-1} \end{bmatrix} \in \mathbb{R}^{(n+m(\bar{d}-d)) \times m}, \quad (3.32)$$

$$\tilde{E}_* \triangleq \begin{bmatrix} I_n \\ 0_{m(\bar{d}-d) \times n} \end{bmatrix} \in \mathbb{R}^{(n+m(\bar{d}-d)) \times n}, \quad (3.33)$$

$$\tilde{C}_* \triangleq \begin{bmatrix} C & 0_{m \times m(\bar{d}-d)} \end{bmatrix} \in \mathbb{R}^{m \times (n+m(\bar{d}-d))}. \quad (3.34)$$

Define the ideal performance  $z_* \triangleq y_* - y_m$ . The following result characterizes the stability and the performance of the ideal closed-loop system (3.28)–(3.34). This

result is an extension of Lemma 2.1 to address  $\bar{d} \geq d$ .

**Lemma 3.1.** Consider the ideal closed-loop system (3.28)–(3.34), which consists of (3.17), (3.19), and (3.21)–(3.27), and satisfies (A3.1), (A3.2), and (A3.4). Then, the following statements hold:

(i) Let  $\lambda \in \mathbb{C}$ . Then,  $\det(\lambda I_{n+m(\bar{d}-d)} - \tilde{A}_*) = 0$  if and only if  $\det \alpha_m(\lambda) = 0$  or

$$\det \begin{bmatrix} \lambda I_n - A & B \\ C & 0_{m \times m} \end{bmatrix} = 0.$$

(ii)  $\tilde{A}_*$  is Hurwitz.

(iii) For all initial condition  $\tilde{x}_*(0) \in \mathbb{R}^{n+m(\bar{d}-d)}$ ,  $\alpha_m(\mathbf{p})y_*(t) = \beta_m(\mathbf{p})r(t)$ .

(iv) For all initial condition  $\tilde{x}_*(0) \in \mathbb{R}^{n+m(\bar{d}-d)}$ ,  $\lim_{t \rightarrow \infty} z_*(t) = 0$  and  $\int_0^\infty z_*^\top(t)z_*(t)dt$  exists.

**Proof.** We consider two cases:  $\bar{d} = d$ , and  $\bar{d} > d$ . First, assume  $\bar{d} = d$ . Then,  $K_0$ ,  $K_x$ , and  $\Phi$  are given by (3.14)–(3.16). Thus, (3.10) is equivalent to (2.9), and (i)–(iv) follows from Lemma 2.1.

Next, assume  $\bar{d} > d$ . To show (i), let  $\lambda \in \mathbb{C}$ , and define  $\hat{d} \triangleq \bar{d} - d$ . Next, define

$$\chi(\lambda) \triangleq (\det H_d) \det(\lambda I_{n+m\hat{d}} - \tilde{A}_*), \quad (3.35)$$

and

$$L \triangleq \begin{bmatrix} I_n & 0_{n \times m} & 0_{n \times m} & \cdots & 0_{n \times m} & 0_{n \times m} \\ 0_{m \times n} & I_m & 0_{m \times m} & \cdots & 0_{m \times m} & 0_{m \times m} \\ 0_{m \times n} & \lambda I_m & I_m & & 0_{m \times m} & 0_{m \times m} \\ \vdots & \vdots & & \ddots & & \vdots \\ 0_{m \times n} & \lambda^{\hat{d}-2} I_m & \lambda^{\hat{d}-3} I_m & & I_m & 0_{m \times m} \\ 0_{m \times n} & \lambda^{\hat{d}-1} I_m & \lambda^{\hat{d}-2} I_m & \cdots & \lambda I_m & I_m \end{bmatrix} \in \mathbb{R}^{(n+m\hat{d}) \times (n+m\hat{d})}, \quad (3.36)$$

$$S \triangleq \begin{bmatrix} I_n & 0_{n \times m(\hat{d}-1)} & 0_{n \times m} \\ 0_{m \times n} & 0_{m \times m(\hat{d}-1)} & I_m \\ 0_{m(\hat{d}-1) \times n} & I_{m(\hat{d}-1)} & 0_{m(\hat{d}-1) \times m} \end{bmatrix} \in \mathbb{R}^{(n+m\hat{d}) \times (n+m\hat{d})}, \quad (3.37)$$

and note that  $\det L = 1$  and  $\det S = (-1)^{m(\hat{d}-1)}$ . Thus,

$$\begin{aligned} \chi(\lambda) &= (-1)^{m(\hat{d}-1)} (\det S) (\det H_d) (\det(\lambda I_{n+m\hat{d}} - \tilde{A}_*)) \det L \\ &= (-1)^{m(\hat{d}-1)} (\det S) \left( \det \begin{bmatrix} I_{n+m(\hat{d}-1)} & 0 \\ 0_{m \times (n+m(\hat{d}-1))} & H_d \end{bmatrix} \right) \left( \det \begin{bmatrix} \lambda I_n - A & -BC_{c_*} \\ -B_{c_*} & \lambda I_{m\hat{d}} - A_{c_*} \end{bmatrix} \right) \\ &\quad \times \det L \\ &= (-1)^{m(\hat{d}-1)} \det S \begin{bmatrix} I_{n+m(\hat{d}-1)} & 0 \\ 0_{m \times (n+m(\hat{d}-1))} & H_d \end{bmatrix} \begin{bmatrix} \lambda I_n - A & -BC_{c_*} \\ -B_{c_*} & \lambda I_{m\hat{d}} - A_{c_*} \end{bmatrix} L \\ &= (-1)^{m(\hat{d}-1)} \det S \begin{bmatrix} I_{n+m(\hat{d}-1)} & 0 \\ 0_{m \times (n+m(\hat{d}-1))} & H_d \end{bmatrix} \\ &\quad \times \begin{bmatrix} \lambda I_n - A & -B & 0_{n \times m} & \dots & 0_{n \times m} & 0_{n \times m} \\ 0_{m \times n} & \lambda I_m & -I_m & & 0_{m \times m} & 0_{m \times m} \\ 0_{m \times n} & 0_{m \times m} & \lambda I_m & & & 0_{m \times m} \\ \vdots & \vdots & & \ddots & & \\ 0_{m \times n} & 0_{m \times m} & 0_{m \times m} & & \lambda I_m & -I_m \\ -H_d^{-1}K_x & -H_d^{-1}K_0 & -H_d^{-1}K_1 & \dots & -H_d^{-1}K_{\hat{d}-2} & \lambda I_m - H_d^{-1}K_{\hat{d}-1} \end{bmatrix} L \\ &= (-1)^{m(\hat{d}-1)} \det S \begin{bmatrix} \lambda I_n - A & -B & 0_{n \times m} & \dots & 0_{n \times m} & 0_{n \times m} \\ 0_{m \times n} & \lambda I_m & -I_m & & 0_{m \times m} & 0_{m \times m} \\ 0_{m \times n} & 0_{m \times m} & \lambda I_m & & & 0_{m \times m} \\ \vdots & \vdots & & \ddots & & \\ 0_{m \times n} & 0_{m \times m} & 0_{m \times m} & & \lambda I_m & -I_m \\ -K_x & -K_0 & -K_1 & \dots & -K_{\hat{d}-2} & -\hat{K}_1(\lambda) \end{bmatrix} L \end{aligned}$$

$$\begin{aligned}
&= (-1)^{m(\hat{d}-1)} \det S \begin{bmatrix} \lambda I_n - A & -B & 0_{n \times m} & \dots & 0_{n \times m} & 0_{n \times m} \\ 0_{m \times n} & 0_{m \times m} & -I_m & & 0_{m \times m} & 0_{m \times m} \\ 0_{m \times n} & 0_{m \times m} & 0_{m \times m} & & & 0_{m \times m} \\ \vdots & \vdots & \vdots & \ddots & & \\ 0_{m \times n} & 0_{m \times m} & 0_{m \times m} & \dots & 0_{m \times m} & -I_m \\ -K_x & -\hat{K}_{\hat{d}}(\lambda) & -\hat{K}_{\hat{d}-1}(\lambda) & \dots & -\hat{K}_2(\lambda) & -\hat{K}_1(\lambda) \end{bmatrix} \\
&= (-1)^{m(\hat{d}-1)} \det \begin{bmatrix} \lambda I_n - A & -B & 0_{n \times m} & \dots & 0_{n \times m} & 0_{n \times m} \\ -K_x & -\hat{K}_{\hat{d}}(\lambda) & -\hat{K}_{\hat{d}-1}(\lambda) & \dots & -\hat{K}_2(\lambda) & -\hat{K}_1(\lambda) \\ 0_{m \times n} & 0_{m \times m} & -I_m & & 0_{m \times m} & 0_{m \times m} \\ \vdots & \vdots & & \ddots & & \vdots \\ 0_{m \times n} & 0_{m \times m} & 0_{m \times m} & & -I_m & 0_{m \times m} \\ 0_{m \times n} & 0_{m \times m} & 0_{m \times m} & \dots & 0_{m \times m} & -I_m \end{bmatrix}, \tag{3.38}
\end{aligned}$$

where for all  $i \in \{1, \dots, \hat{d}\}$ ,  $\hat{K}_i(\lambda) \triangleq \sum_{j=0}^i \lambda^{i-j} K_{\hat{d}-j}$ . Thus, it follows from (3.38) that

$$\begin{aligned}
\chi(\lambda) &= (-1)^{m(\hat{d}-1)} \left( \det \begin{bmatrix} \lambda I_n - A & -B \\ -K_x & -\hat{K}_{\hat{d}}(\lambda) \end{bmatrix} \right) (\det -I_{m(\hat{d}-1)}) \\
&= \det \begin{bmatrix} \lambda I_n - A & -B \\ -K_x & -\hat{K}_{\hat{d}}(\lambda) \end{bmatrix} \\
&= \det \begin{bmatrix} I_n & 0_{n \times m} \\ 0_{m \times n} & -I_m \end{bmatrix} \begin{bmatrix} \lambda I_n - A & B \\ K_x & -\hat{K}_{\hat{d}}(\lambda) \end{bmatrix} \begin{bmatrix} I_n & 0_{n \times m} \\ 0_{m \times n} & -I_m \end{bmatrix} \\
&= \det \begin{bmatrix} \lambda I_n - A & B \\ K_x & -\hat{K}_{\hat{d}}(\lambda) \end{bmatrix} \\
&= \det \begin{bmatrix} I_n & 0_{n \times m} \\ \Gamma(\lambda) & -\alpha_m(\lambda) \end{bmatrix} \begin{bmatrix} \lambda I_n - A & B \\ C & 0_{m \times m} \end{bmatrix}
\end{aligned}$$

$$= (-\det \alpha_m(\lambda)) \det \begin{bmatrix} \lambda I_n - A & B \\ C & 0_{m \times m} \end{bmatrix}, \quad (3.39)$$

where  $\Gamma(\lambda) \triangleq \sum_{i=1}^{\bar{d}} \sum_{j=0}^{i-1} \lambda^j \alpha_i C A^{i-j-1}$ . Therefore, (i) follows from (3.39).

Next, since the roots of  $\det \alpha_m$  and the invariant zeros of  $(A, B, C)$  are contained in the open-left-half complex plane, it follows from (i) that the eigenvalues of  $\tilde{A}_*$  are contained in the open-left-half complex plane, which confirms (ii).

To show (iii), it follows from (3.7) and (3.8) that  $0 = \sum_{i=0}^{\bar{d}} -\alpha_i \mathbf{P}^i y_* + \sum_{i=0}^{\bar{d}-1} \beta_i \mathbf{P}^i r$ , which implies that  $\alpha_m(\mathbf{p})y_* = \beta_m(\mathbf{p})r$ , and thus confirms (iii).

To show (iv), subtracting (3.5) from  $\alpha_m(\mathbf{p})y_* = \beta_m(\mathbf{p})r$  yields  $\alpha_m(\mathbf{p})[y_* - y_m] = 0$ , which implies that  $\alpha_m(\mathbf{p})z_* = 0$ . Since the roots of  $\det \alpha_m$  are contained in the open-left-half complex plane, it follows that  $\lim_{t \rightarrow \infty} z_*(t) = 0$  and  $\int_0^\infty z_*^\top(t) z_*(t) dt$  exists, which confirms (iv).  $\square$

### 3.3 Filtered Dynamic Inversion

In this section, we present the FDI controller that requires only an upper bound on the relative degree. The IDI control (3.10)–(3.13) relies on the knowledge of the plant parameters  $A$ ,  $B$ , and  $C$  as well as measurements of  $x$  and  $w$ . Since this information is not assumed to be known, the IDI control cannot be implemented. Thus, we use a linear filter to construct the FDI control, which is implementable and approximates the IDI control.

For all  $j \in \mathbb{N}$ , let  $F_j \geq 0$  be the  $j$ th Fibonacci number, where  $F_0 = 0, F_1 = 1, F_2 = 1, F_3 = 2, F_4 = 3, F_5 = 5, F_6 = 8, \dots$ , and define  $f_h \triangleq F_{\rho+1} - F_{h+1}$ . Next, define

$$\eta_k(s) \triangleq \eta_\rho s^\rho + k^{f_{\rho-1}} \eta_{\rho-1} s^{\rho-1} + \dots + k^{f_1} \eta_1 s + k^{F_{\rho+1}} \eta_0, \quad (3.40)$$



where  $\eta_1, \dots, \eta_{\rho-1} \in \mathbb{R}$ ,  $\eta_\rho = 1$ , and  $\eta_0 \geq 1$ . Define the transfer function

$$\Delta_k(s) \triangleq \frac{\bar{\eta}_k(s)}{\eta_k(s)}, \quad (3.41)$$

where

$$\bar{\eta}_k(s) \triangleq \eta_\rho s^{\rho-1} + k^{f_{\rho-1}} \eta_{\rho-1} s^{\rho-2} + \dots + k^{f_2} \eta_2 s + k^{f_1} \eta_1. \quad (3.42)$$

Note that for all  $k \geq 0$ ,  $\Delta_k$  is well defined, that is,  $\eta_k(s) \neq 0$ . Next, consider the following condition:

(C3.1) If  $\rho = 1$ , then  $\eta_1 s + \eta_0$  is Hurwitz. If  $\rho = 2$ , then  $\eta_2 s^2 + \eta_1 s + \eta_0$  is Hurwitz.

If  $\rho \in \{3, 4, 5, \dots\}$ , then for all  $i \in \{0, 1, \dots, \rho - 3\}$  the polynomials

$$N_i(s) \triangleq \eta_{i+3} s^3 + \eta_{i+2} s^2 + \eta_{i+1} s + \eta_0 \quad (3.43)$$

are Hurwitz.

If  $\eta_k$  satisfies (C3.1), then it follows from [23, Lemma 6.1] that there exists  $k_0 > 0$  such that for all  $k > k_0$ ,  $\eta_k$  is Hurwitz. Next, consider the following condition:

(C3.2) For all  $\varepsilon > 0$  there exists  $k_\varepsilon > k_0$  such that for all  $k > k_\varepsilon$ ,

$$\gamma_k \triangleq \sup_{\omega \in \mathbb{R}} |\Delta_k(j\omega)| < \varepsilon. \quad (3.44)$$

Condition (C3.2) states that for sufficiently large  $k$ , the  $\mathcal{H}_\infty$  norm of  $\Delta_k$  is arbitrarily small. Next, we present examples for  $\rho = 1$ ,  $\rho = 2$ ,  $\rho = 3$ , and  $\rho = 4$  that satisfy (C3.1) and (C3.2).

**Example 3.1.** Let  $\rho = 1$ , and consider  $\eta_k(s) = s + k$ , which satisfies (C3.1). It follows from (3.41) and (3.42) that  $\Delta_k(s) = 1/(s + k)$ . Thus,  $\gamma_k = \sup_{\omega \in \mathbb{R}} |\Delta_k(j\omega)| = |\Delta_k(0)| = 1/k$ , which satisfies (C3.2).  $\triangle$

**Example 3.2.** Let  $\rho = 2$ , and consider  $\eta_k(s) = (s + k)^2$ , which satisfies (C3.1). It follows from (3.41) and (3.42) that  $\Delta_k(s) = (s + 2k)/(s + k)^2$ . Thus,  $\gamma_k = \sup_{\omega \in \mathbb{R}} |\Delta_k(j\omega)| = |\Delta_k(0)| = 2/k$ , which satisfies (C3.2).  $\triangle$

**Example 3.3.** Let  $\rho = 3$ , and consider  $\eta_k(s) = s^3 + 6ks^2 + 3k^2s + k^3$ , which satisfies (C3.1). It follows from (3.41) and (3.42) that  $\Delta_k(s) = (s^2 + 6ks + 3k^2)/(s^3 + 6ks^2 + 3k^2s + k^3)$ . Thus,  $|\Delta_k(j\omega)|^2 = (\omega^4 + 30k^2\omega^2 + 9k^4)/(\omega^6 + 30k^2\omega^4 - 3k^4\omega^2 + k^6)$ . Taking the derivative of  $|\Delta_k(j\omega)|^2$  with respect to  $\omega$  yields

$$\frac{d}{d\omega} (|\Delta_k(j\omega)|^2) = \frac{2\omega(-\omega^8 - 60k^2\omega^6 - 930k^4\omega^4 - 538k^6\omega^2 + 57k^8)}{(\omega^6 + 30k^2\omega^4 - 3k^4\omega^2 + k^6)^2}. \quad (3.45)$$

Thus,  $\frac{d}{d\omega} (|\Delta_k(j\omega)|^2) = 0$  if  $\omega \in \{0, 0.3024k\}$ . Next, taking the second derivative of  $|\Delta_k(j\omega)|^2$  with respect to  $\omega$  implies that  $|\Delta_k(j\omega)|^2$  is maximized at  $\omega = 0.3024k$ . Thus,  $\gamma_k = \sup_{\omega \in \mathbb{R}} |\Delta_k(j\omega)| = |\Delta_k(j0.3024k)| = 3.4676/k$ , which satisfies (C3.2).  $\triangle$

**Example 3.4.** Let  $\rho = 4$ , and consider  $\eta_k(s) = s^4 + 2k^2s^3 + 4k^3s^2 + 2k^4s + k^5$ , which satisfies (C3.1). It follows from (3.41) and (3.42) that  $\Delta_k(s) = (s^3 + 2k^2s^2 + 4k^3s + 2k^4)/(s^4 + 2k^2s^3 + 4k^3s^2 + 2k^4s + k^5)$ . Thus,  $|\Delta_k(j\omega)|^2 = (\omega^6 + (4k^4 - 8k^3)\omega^4 + 8k^6\omega^2 + 4k^8)/(\omega^8 + (4k^4 - 8k^3)\omega^6 + (8k^6 + 2k^5)\omega^4 - 4k^8\omega^2 + k^{10})$ . Taking the derivative of  $|\Delta_k(j\omega)|^2$  with respect to  $\omega$  yields

$$\frac{d}{d\omega} (|\Delta_k(j\omega)|^2) = \frac{a(\omega)}{(\omega^8 + (4k^4 - 8k^3)\omega^6 + (8k^6 + 2k^5)\omega^4 - 4k^8\omega^2 + k^{10})^2}, \quad (3.46)$$

where

$$\begin{aligned} a(\omega) \triangleq & 2\omega(-\omega^{12} - 8(k-2)k^3\omega^{10} + 2(1-8k((k-4)k+5))k^5\omega^8 \\ & - 8(8(k-2)k+3)k^8\omega^6 + (16(7-8k)k+3)k^{10}\omega^4 - 8(7k+4)k^{13}\omega^2 + 24k^{16}). \end{aligned} \quad (3.47)$$

Thus,  $\frac{d}{d\omega} (|\Delta_k(j\omega)|^2) = 0$  if  $\omega \in \{0, 0.5189k\}$ . Next, taking the second derivative

of  $|\Delta_k(j\omega)|^2$  with respect to  $\omega$  implies that  $|\Delta_k(j\omega)|^2$  is maximized at  $\omega = 0.5189k$ . Thus,  $\gamma_k = \sup_{\omega \in \mathbb{R}} |\Delta_k(j\omega)| = |\Delta_k(j0.5189k)| = 3.198/k$ , which satisfies (C3.2).  $\triangle$

Examples 3.1–3.4 provide constructions of  $\eta_k$  that satisfy (C3.1) and (C3.2) for  $\rho \in \{1, 2, 3, 4\}$ . We conjecture that for all  $\rho \geq 1$ , if (C3.1) is satisfied, then (C3.2) is satisfied. However, a proof of this conjecture is open.

To derive the FDI control, consider the control  $u$  that satisfies

$$\eta_k(\mathbf{p})u = \eta_k(0)u_*(x, u, \dots, \mathbf{p}^{\bar{d}-d}u, \Phi), \quad (3.48)$$

where  $u_*(x, u, \dots, \mathbf{p}^{\bar{d}-d}u, \Phi)$  is given by (3.10)–(3.13). The transfer function from  $u_*$  to  $u$  is given by

$$\zeta_k(s) \triangleq \frac{\eta_k(0)}{\eta_k(s)} I_m = (I - s\Delta_k(s))I_m, \quad (3.49)$$

which is a low-pass filter. It follows from (C3.2) that as  $k$  tends to infinity, the cutoff frequency of  $\zeta_k$  tends to infinity, suggesting that  $u$  approximates  $u_*(x, u, \dots, \mathbf{p}^{\bar{d}-d}u, \Phi)$  for sufficiently large  $k$ .

To express (3.48) as an implementable control, it follows from (3.9) that

$$u_* = u - H_d^{-1}[\alpha_m(\mathbf{p})y - \beta_m(\mathbf{p})r]. \quad (3.50)$$

Substituting (3.50) into (3.48) yields the FDI controller

$$\mathbf{p}\bar{\eta}_k(\mathbf{p})u(t) = k^{F_{\rho+1}}\eta_0 H_d^{-1}[\beta_m(\mathbf{p})r(t) - \alpha_m(\mathbf{p})y(t)]. \quad (3.51)$$

The controller (3.51) is a dynamic output-feedback controller, which uses  $y$  for feedback,  $r$  for feedforward, and can be implemented for  $k > k_0$  using knowledge of only  $H_d$  as well as the design parameters  $\alpha_m, \beta_m$ , and  $\eta_k$ .

The transfer function from  $\begin{bmatrix} y^T & r^T \end{bmatrix}^T$  to  $u$  is given by

$$G_c(s) \triangleq \frac{k^{F_{\rho+1}}\eta_0}{s\bar{\eta}_k(s)} H_d^{-1} \begin{bmatrix} -\alpha_m(s) & \beta_m(s) \end{bmatrix}. \quad (3.52)$$

which characterizes the forced response of (3.51). Next, for all  $k > k_0$ , let  $G_c$  have the  $\rho m$ -order state-space realization

$$\dot{x}_c(t) = A_c x_c(t) + B_c y(t) + E_c r(t), \quad (3.53)$$

$$u(t) = C_c x_c(t) + D_c y(t), \quad (3.54)$$

where  $x_c \in \mathbb{R}^{\rho m}$ , and for all  $k > k_0$ ,  $A_c \in \mathbb{R}^{\rho m \times \rho m}$ ,  $B_c \in \mathbb{R}^{\rho m \times m}$ ,  $C_c \in \mathbb{R}^{m \times \rho m}$ ,  $D_c \in \mathbb{R}^{m \times m}$ , and  $E_c \in \mathbb{R}^{\rho m \times m}$ . To demonstrate that such a realization exists, consider the block-observable realization

$$A_c = \begin{bmatrix} -k^{f_{\rho-1}}\eta_{\rho-1} & 1 & 0 & \dots & 0 \\ -k^{f_{\rho-2}}\eta_{\rho-2} & 0 & 1 & & 0 \\ \vdots & \vdots & \ddots & & \\ -k^{f_1}\eta_1 & 0 & 0 & & 1 \\ 0 & 0 & 0 & \dots & 0 \end{bmatrix} \otimes I_m \in \mathbb{R}^{\rho m \times \rho m}, \quad (3.55)$$

$$B_c = \begin{bmatrix} -k^{F_{\rho+1}}\eta_0 H_d^{-1} \alpha_{\rho-1} - k^{f_{\rho-1}}\eta_{\rho-1} D_c \\ \vdots \\ -k^{F_{\rho+1}}\eta_0 H_d^{-1} \alpha_1 - k^{f_{\rho-1}}\eta_1 D_c \\ -k^{F_{\rho+1}}\eta_0 H_d^{-1} \alpha_0 \end{bmatrix} \in \mathbb{R}^{\rho m \times m}, \quad (3.56)$$

$$E_c = \begin{bmatrix} 0_{(\rho-\bar{d})m \times m} \\ -k^{F_{\rho+1}}\eta_0 H_d^{-1} \beta_{\bar{d}-1} \\ \vdots \\ -k^{F_{\rho+1}}\eta_0 H_d^{-1} \beta_0 \end{bmatrix} \in \mathbb{R}^{\rho m \times m}, \quad (3.57)$$

$$C_c = \begin{bmatrix} 1 & 0_{1 \times \rho-1} \end{bmatrix} \otimes I_m \in \mathbb{R}^{m \times \rho m}, \quad (3.58)$$

$$D_c = -k^{F_{\rho+1}} \eta_0 H_d^{-1} \alpha_\rho \in \mathbb{R}^{m \times m}, \quad (3.59)$$

where  $\otimes$  is the Kronecker product and  $\alpha_{\bar{d}+1} = \alpha_{\bar{d}+2} = \dots = 0_{m \times m}$ .

The closed-loop system (3.1), (3.2) and (3.53)–(3.59) is given by

$$\dot{\tilde{x}}(t) = \tilde{A}\tilde{x}(t) + \tilde{B}w(t) + \tilde{E}r(t), \quad (3.60)$$

$$y(t) = \tilde{C}\tilde{x}(t), \quad (3.61)$$

where

$$\tilde{x}(t) \triangleq \begin{bmatrix} x(t) \\ x_c(t) \end{bmatrix} \in \mathbb{R}^{n+\rho m}, \quad (3.62)$$

and

$$\tilde{A} \triangleq \begin{bmatrix} A + BD_c C & BC_c \\ B_c C & A_c \end{bmatrix} \in \mathbb{R}^{(n+\rho m) \times (n+\rho m)}, \quad \tilde{B} \triangleq \begin{bmatrix} I_n \\ 0_{\rho m \times n} \end{bmatrix} \in \mathbb{R}^{(n+\rho m) \times n}, \quad (3.63)$$

$$\tilde{E} \triangleq \begin{bmatrix} 0_{n \times m} \\ E_c \end{bmatrix} \in \mathbb{R}^{(n+\rho m) \times m}, \quad \tilde{C} \triangleq \begin{bmatrix} C & 0_{m \times \rho m} \end{bmatrix} \in \mathbb{R}^{m \times (n+\rho m)}. \quad (3.64)$$

The following result characterizes the stability of the closed-loop system (3.60)–(3.64) for the case where the open-loop system (3.1) and (3.2) is SISO (i.e.,  $m = 1$ ).

**Theorem 3.1.** Consider the closed-loop system (3.60)–(3.64), which consists of (3.1), (3.2), and (3.53)–(3.59), where (A3.1)–(A3.5) are satisfied,  $\eta_k$  satisfies (C3.1) and (C3.2), and  $m = 1$ . Then, there exists  $k_s > k_0$  such that for all  $k > k_s$ ,  $\tilde{A}$  is Hurwitz.

**Proof.** Let  $P$  and  $Q$  be coprime polynomials such that  $P(s)/Q(s) = C(sI_n -$

$A)^{-1}B$ . The transfer function from  $r$  to  $y$  is

$$\tilde{G}_{yr}(s) \triangleq \frac{k^{F_{\rho+1}}\eta_0 H_d^{-1}P(s)\beta_m(s)}{\tilde{Q}(s)}, \quad (3.65)$$

and the transfer function from  $w$  to  $y$  is

$$\tilde{G}_{yw}(s) \triangleq \frac{Q(s)s\bar{\eta}_k(s)C(sI_n - A)^{-1}}{\tilde{Q}(s)}, \quad (3.66)$$

where

$$\tilde{Q}(s) \triangleq Q(s)s\bar{\eta}_k(s) + k^{F_{\rho+1}}\eta_0 H_d^{-1}P(s)\alpha_m(s). \quad (3.67)$$

Next, it follows from (3.42) that

$$\tilde{Q}(s) = Q(s)s^\rho + k^{f_{\rho-1}}\eta_{\rho-1}Q(s)s^{\rho-1} + \cdots + k^{f_1}\eta_1Q(s)s + k^{F_{\rho+1}}\eta_0 H_d^{-1}P(s)\alpha_m(s). \quad (3.68)$$

Note that (A3.2) implies that the roots of  $P$  are contained in the open-left-half complex plane. Since  $\alpha_m(\mathbf{p})$  is Hurwitz, it follows from [23, Lemma 6.1] that there exists  $k_s > k_0$  such that for all  $k > k_s$ , the roots of  $\tilde{Q}$  are contained in the open-left-half complex plane. Finally, since the eigenvalues of  $\tilde{A}$  coincide with the roots of  $\tilde{Q}$ , it follows that for all  $k > k_s$ ,  $\tilde{A}$  is Hurwitz.  $\square$

# Chapter 4

---

## Numerical Simulations

In this chapter, we present numerical simulations demonstrating the filtered-dynamic-inversion (FDI) control for unknown relative degree. We demonstrate that the performance  $z$  is made small by sufficiently large choice of  $k$ .

### 4.1 Numerical Simulations of Mathematical Examples

In this section, we simulate single-input single-output (SISO) systems and a multi-input multi-output (MIMO) system with FDI controller (3.53)–(3.59) implemented in feedback. We demonstrate stabilization, command following, and disturbance rejection. We compare the performance  $z$  for different parameters of  $k$  for each example.

#### 4.1.1 Single Integrator, Double Integrator and Triple Integrator

Consider the single integrator

$$\dot{y}(t) = u(t) + \mu(t), \tag{4.1}$$

where  $t \geq 0$ ,  $y(t) \in \mathbb{R}$  is the measured output,  $u(t) \in \mathbb{R}$  is the control,  $\mu(t) \in \mathbb{R}$  is the unknown and unmeasured disturbance. It follows that (4.1) can be expressed as (3.1) and (3.2), where

$$x(t) \triangleq y(t), \quad w(t) \triangleq \mu(t), \quad (4.2)$$

and

$$A \triangleq 0, \quad B \triangleq 1, \quad C \triangleq 1. \quad (4.3)$$

Note that the relative degree  $d = 1$ , and the first nonzero Markov parameter is given by  $H_d = CB = 1$ . Also, (A3.1), (A3.2), and (A3.4) are satisfied.

Next, consider the double integrator

$$\ddot{y}(t) = u(t) + \mu(t), \quad (4.4)$$

where  $t \geq 0$ ,  $y(t) \in \mathbb{R}$  is the measured output,  $u(t) \in \mathbb{R}$  is the control,  $\mu(t) \in \mathbb{R}$  is the unknown and unmeasured disturbance. It follows that (4.4) can be expressed as (3.1) and (3.2), where

$$x(t) \triangleq \begin{bmatrix} y(t) \\ \dot{y}(t) \end{bmatrix}, \quad w(t) \triangleq \begin{bmatrix} 0 \\ 1 \end{bmatrix} \mu(t), \quad (4.5)$$

and

$$A \triangleq \begin{bmatrix} 0 & 1 \\ 0 & 0 \end{bmatrix}, \quad B \triangleq \begin{bmatrix} 0 \\ 1 \end{bmatrix}, \quad C \triangleq \begin{bmatrix} 1 & 0 \end{bmatrix}. \quad (4.6)$$

Note that the relative degree  $d = 2$ , and the first nonzero Markov parameter is given by  $H_d = CB = 1$ . Also, (A3.1), (A3.2), and (A3.4) are satisfied.



Finally, consider the triple integrator

$$\ddot{y}(t) = u(t) + \mu(t), \quad (4.7)$$

where  $t \geq 0$ ,  $y(t) \in \mathbb{R}$  is the measured output,  $u(t) \in \mathbb{R}$  is the control,  $\mu(t) \in \mathbb{R}$  is the unknown and unmeasured disturbance. It follows that (4.7) can be expressed as (3.1) and (3.2), where

$$x(t) = \begin{bmatrix} y(t) \\ \dot{y}(t) \\ \ddot{y}(t) \end{bmatrix}, \quad w(t) \triangleq \begin{bmatrix} 0 \\ 0 \\ 1 \end{bmatrix} \mu(t), \quad (4.8)$$

and

$$A \triangleq \begin{bmatrix} 0 & 1 & 0 \\ 0 & 0 & 1 \\ 0 & 0 & 0 \end{bmatrix}, \quad B \triangleq \begin{bmatrix} 0 \\ 0 \\ 1 \end{bmatrix}, \quad C \triangleq [1 \ 0 \ 0]. \quad (4.9)$$

Note that the relative degree  $d = 3$ , and the first nonzero Markov parameter is given by  $H_d = CB = 1$ . Also, (A3.1), (A3.2), and (A3.4) are satisfied.

The objective is to design an FDI controller to control the single integrator (4.1), the double integrator (4.4), and the triple integrator (4.7). The upper bound on the relative degree is  $\bar{d} = 3$ . We select the reference-model polynomials

$$\alpha_m(\mathbf{p}) = (\mathbf{p} + 5)^3, \quad \beta_m(\mathbf{p}) = 125. \quad (4.10)$$

Next, let  $\rho = 4 > \bar{d}$ , and let

$$\eta_k(s) \triangleq s^4 + 2k^2s^3 + 4k^3s^2 + 2k^4s + k^5, \quad (4.11)$$

which satisfies (C3.1) and (C3.2). We select the initial condition of the FDI controller (3.53)–(3.59) as  $x_c(0) = 0$ .

**Example 4.1.** *SISO, stabilization, disturbance free, and no command following.* Consider the single integrator (4.1), the double integrator (4.4), and the triple integrator (4.7). The disturbance is identically 0 (i.e.,  $w = 0$ ). The control objective is to stabilize the the single integrator (4.1), the double integrator (4.4), and the triple integrator (4.4).

First, we stabilize the single integrator. The initial condition is  $x(0) = -5$ . The FDI controller (3.53)–(3.59) is implemented in feedback, where  $\eta_k$  is given by (4.11) and  $k = 2.9$ , which is close to but greater than the minimum stabilizing value  $k = 2.69$ . We also consider  $k = 3.1$  and  $k = 5$ . The closed-loop system consists of the single integrator (3.1)–(3.2) and (4.2)–(4.3); and the FDI controller (3.53)–(3.59), which consists of (4.11), where  $k \in \{2.9, 3.1, 5\}$ . Figure 4.1 shows the time history of  $y$  and  $u$ . We observe that by increasing  $k$  the time it takes  $y$  to converge to the origin decreases.

Next, we stabilize the double integrator. The initial condition is

$$x(0) = \begin{bmatrix} -5 \\ 0 \end{bmatrix}. \quad (4.12)$$

The FDI controller (3.53)–(3.59) is implemented in feedback, where  $\eta_k$  is given by (4.11) and  $k = 9$ , which is close to but greater than the minimum stabilizing value  $k = 8.45$ . We also consider  $k = 10$  and  $k = 14$ . The closed-loop system consists of the double integrator (3.1)–(3.2) and (4.5)–(4.6); and the FDI controller (3.53)–(3.59), which consists of (4.11), where  $k \in \{9, 10, 14\}$ . Figure 4.2 shows the time history of  $y$  and  $u$ . Similar to the single integrator, increasing  $k$  tends to improve performance.

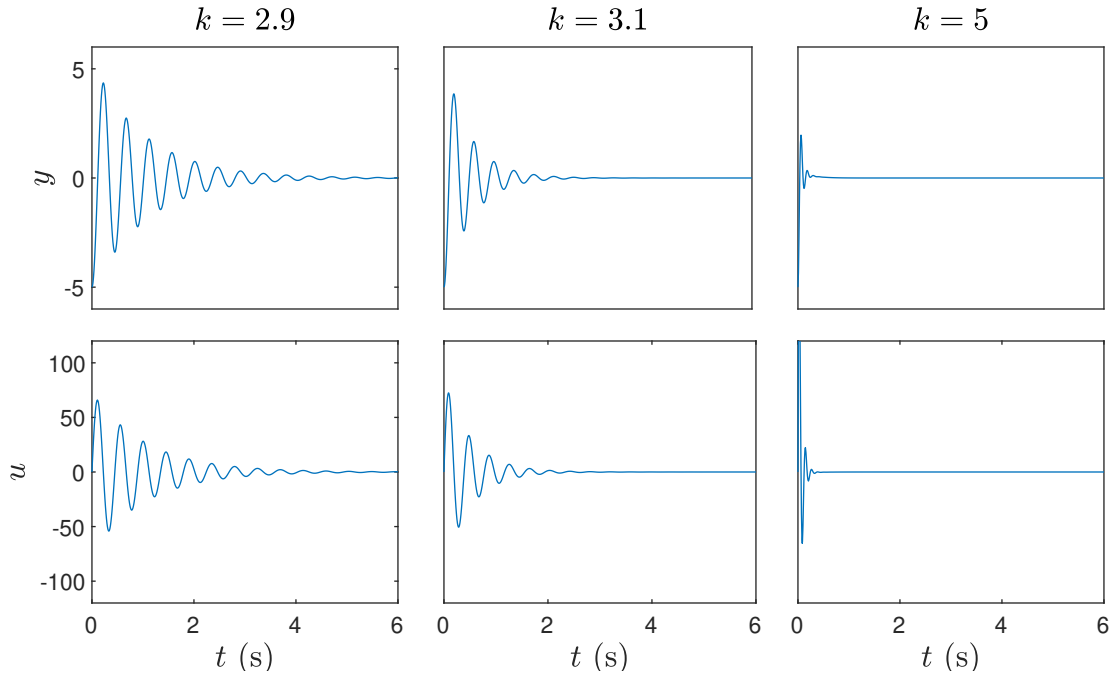


Figure 4.1: The FDI controller (3.53)–(3.59), where  $k \in \{2.9, 3.1, 5\}$ , is implemented in feedback with the single integrator (4.1)–(4.3). By increasing  $k$ , the time it takes  $y$  to converge to the origin decreases.

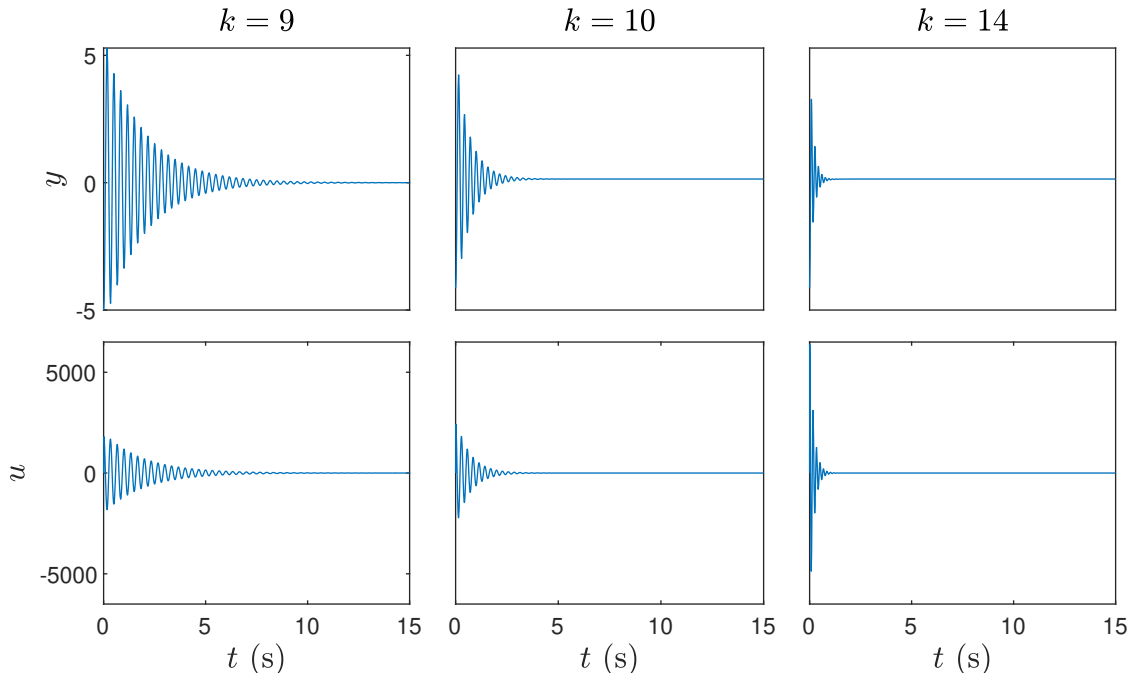


Figure 4.2: The FDI controller (3.53)–(3.59), where  $k \in \{9, 10, 14\}$ , is implemented in feedback with the double integrator (4.4)–(4.6). By increasing  $k$ , the time it takes  $y$  to converge to the origin decreases.

Finally, we stabilize the triple integrator. The initial condition is

$$x(0) = \begin{bmatrix} -5 \\ 0 \\ 0 \end{bmatrix}. \quad (4.13)$$

The FDI controller (3.53)–(3.59) is implemented in feedback, where  $\eta_k$  is given by (4.11) and  $k = 47$ , which is close to but greater than the minimum stabilizing value  $k = 46.2$ . We also consider  $k = 50$  and  $k = 55$ . The closed-loop system consists of the triple integrator (3.1)–(3.2) and (4.8)–(4.9); and the FDI controller (3.53)–(3.59), which consists of (4.11), where  $k \in \{47, 50, 55\}$ . Figure 4.3 shows the time history of  $y$  and  $u$ . Similar to the single integrator and double integrator, increasing  $k$  tends to improve performance. Thus, we have designed a controller capable of stabilizing the single, double, and triple integrator.  $\triangle$

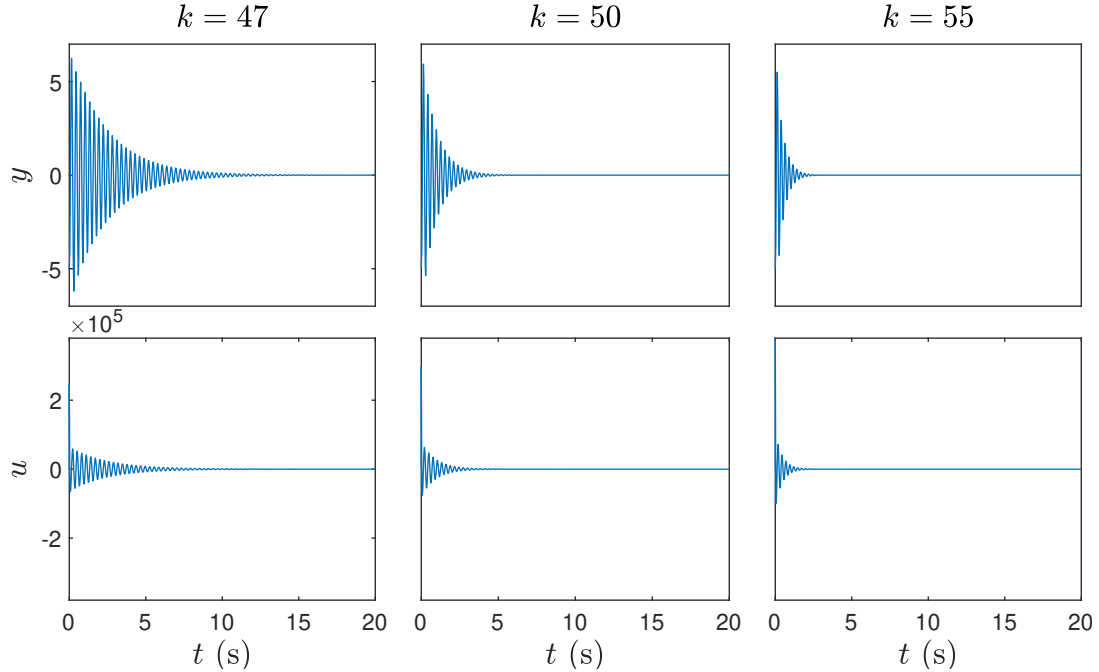


Figure 4.3: The FDI controller (3.53)–(3.59), where  $k \in \{47, 50, 55\}$ , is implemented in feedback with the triple integrator (4.7)–(4.9). By increasing  $k$ , the time it takes  $y$  to converge to the origin decreases.

**Example 4.2.** *SISO, command following, and disturbance free.* Consider the single integrator (4.1), the double integrator (4.4), and the triple integrator (4.7). The disturbance is identically 0 (i.e.,  $w = 0$ ). The control objective is to force the output  $y$  to follow the reference output  $y_m$  of the reference model (3.5). The reference command is a series of step inputs which are passed through the filter  $G_r(s) = 10^3/(s + 10)^3$ , which makes the reference  $\bar{d}$  times differentiable and  $r, \mathbf{p}r, \dots, \mathbf{p}^{\bar{d}}r$  are bounded.

First, we control the single integrator. The initial condition is  $x(0) = 0$ . The closed-loop system consists of the single integrator (3.1)–(3.2) and (4.2)–(4.3); and the FDI controller (3.53)–(3.59), which consists of (4.11), where  $k \in \{3, 4, 9\}$ . Figure 4.4 shows the time history of  $y, y_m, z$ , and  $u$ .

Next, we control the double integrator. The initial condition is  $x(0) = 0$ . The closed-loop system consists of the double integrator (3.1)–(3.2) and (4.5)–(4.6); and the FDI controller (3.53)–(3.59), which consists of (4.11), where  $k \in \{10, 15, 30\}$ . Figure 4.5 shows the time history of  $y, y_m, z$ , and  $u$ .

Finally, we control the triple integrator. The initial condition of the open-loop system of the triple integrator is  $x(0) = 0$ . The closed-loop system consists of the triple integrator (3.1)–(3.2) and (4.8)–(4.9); and the FDI controller (3.53)–(3.59), which consists of (4.11), where  $k \in \{50, 70, 100\}$ . Figure 4.6 shows the time history of  $y, y_m, z$ , and  $u$ .

We observe in Figure 4.4, Figure 4.5, and Figure 4.6, that  $y$  follows  $y_m$  with a small nonzero asymptotic error. We also observe that increasing  $k$  tends to improve the performance  $z$ . △

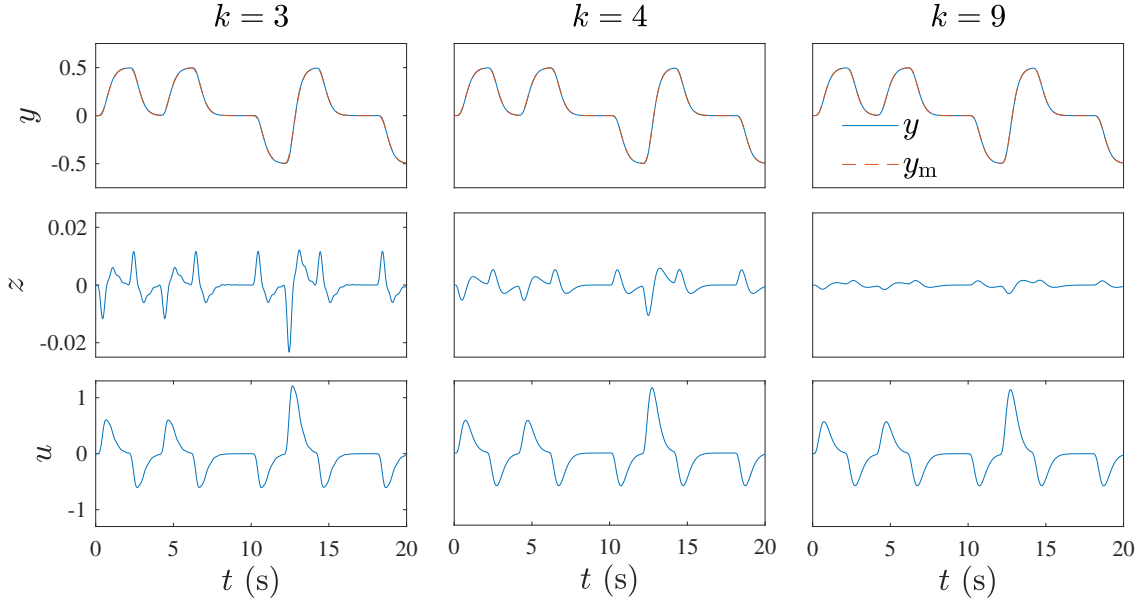


Figure 4.4: The FDI controller (3.53)–(3.59), where  $k \in \{3, 4, 9\}$ , is implemented in feedback with the single integrator (4.1)–(4.3). The command  $r$  is a series of steps passed through a filter  $G_r(s) = 10^3/(s + 10)^3$ . The average power of performance  $z$  decreases with increase of  $k$ .

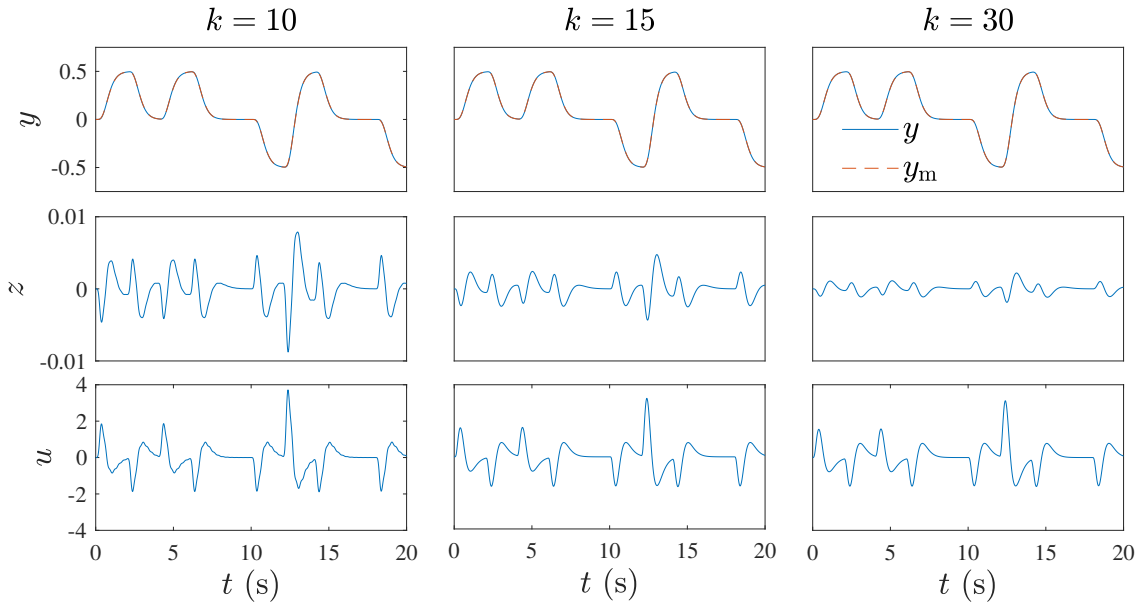


Figure 4.5: The FDI controller (3.53)–(3.59), where  $k \in \{10, 15, 30\}$ , is implemented in feedback with the double integrator (4.4)–(4.6). The command  $r$  is a series of steps passed through a filter  $G_r(s) = 10^3/(s + 10)^3$ . The average power of performance  $z$  decreases with increase of  $k$ .

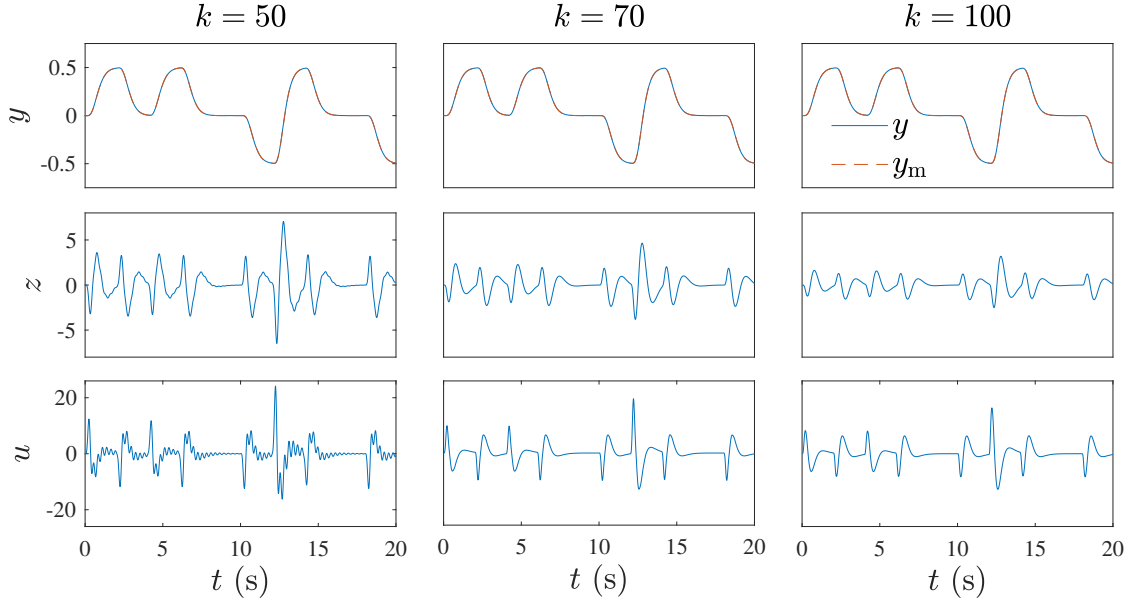


Figure 4.6: The FDI controller (3.53)–(3.59), where  $k \in \{50, 70, 100\}$ , is implemented in feedback with the triple integrator (4.7)–(4.9). The command  $r$  is a series of steps passed through a filter  $G_r(s) = 10^3/(s + 10)^3$ . The average power of performance  $z$  decreases with increase of  $k$ .

**Example 4.3.** *SISO, command following, and white-noise disturbance.* Consider the single integrator (4.1), double integrator (4.4), and triple integrator (4.7). The control objective is to force the output  $y$  to follow the reference output  $y_m$  in the presence of zero-mean 20-variance Gaussian white-noise distribution. The reference command is a series of step inputs, which are passed through the filter  $G_r(s) = 10^3/(s + 10)^3$ . The initial conditions of the open-loop systems are the same as Example 4.2.

First, we control the single integrator. The FDI controller (3.53)–(3.59), where  $\eta_k$  is given by (4.11) and  $k \in \{3, 4, 9, 30\}$ , is implemented in feedback with the single integrator. Figure 4.7 shows the time history of  $y$ ,  $y_m$ ,  $z$ , and  $u$ . By comparing Figure 4.7 with Figure 4.4, we observe that the performance  $z$  degrades slightly in comparison to the disturbance free case. By increasing  $k$  to 30, the performance  $z$  improves.

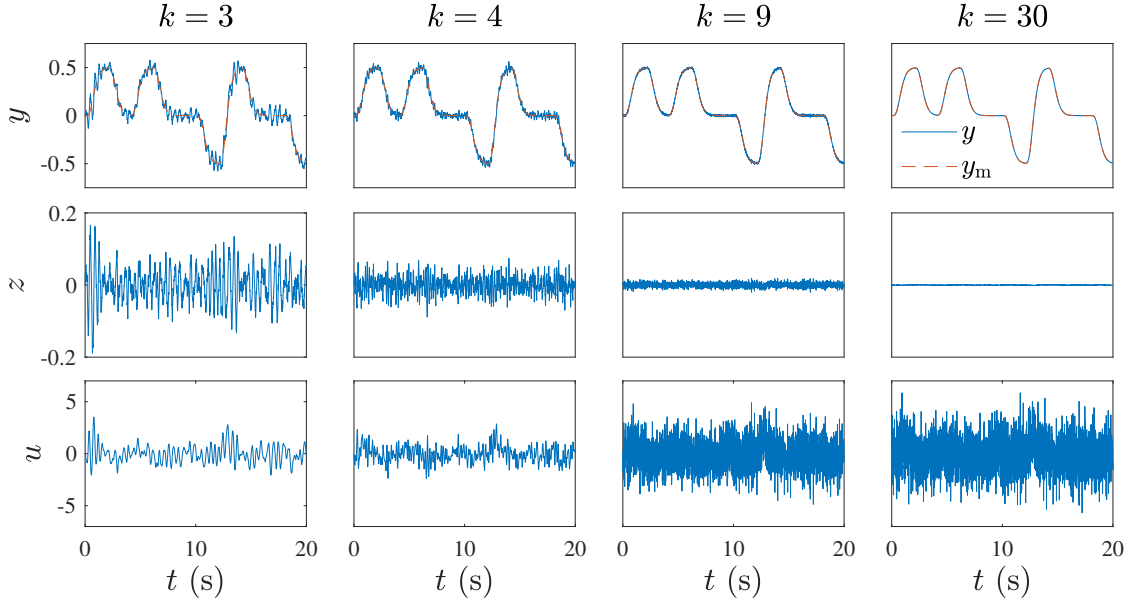


Figure 4.7: The FDI controller (3.53)–(3.59), where  $k \in \{3, 4, 9, 30\}$ , is implemented in feedback with the single integrator (4.1)–(4.3) with white-noise disturbance. The command  $r$  is a series of steps passed through the filter  $G_r(s) = 10^3/(s + 10)^3$ . The performance  $z$  degrades with the introduction of disturbance in comparison to the performance in Figure 4.4. By increasing  $k$  to 30, the performance improves.

Next, we control the double integrator. The FDI controller (3.53)–(3.59), where  $\eta_k$  is given by (4.11) and  $k \in \{10, 15, 30, 80\}$ , is implemented in feedback with the double integrator. Figure 4.8 shows the time history of  $y$ ,  $y_m$ ,  $z$ , and  $u$ . By comparing Figure 4.8 with Figure 4.5, the performance  $z$  degrades slightly in comparison to the disturbance free case. By increasing  $k$  to 80, the performance  $z$  improves.

Finally, we control the triple integrator. The FDI controller (3.53)–(3.59), where  $\eta_k$  is given by (4.11) and  $k \in \{50, 70, 100, 200\}$ , is implemented in feedback with the triple integrator. Figure 4.9 shows the time history of  $y$ ,  $y_m$ ,  $z$ , and  $u$ . By comparing Figure 4.9 with Figure 4.6, we observe that the performance  $z$  degrades slightly in comparison to the disturbance free case. By increasing  $k$  to 200, the performance  $z$  improves. △



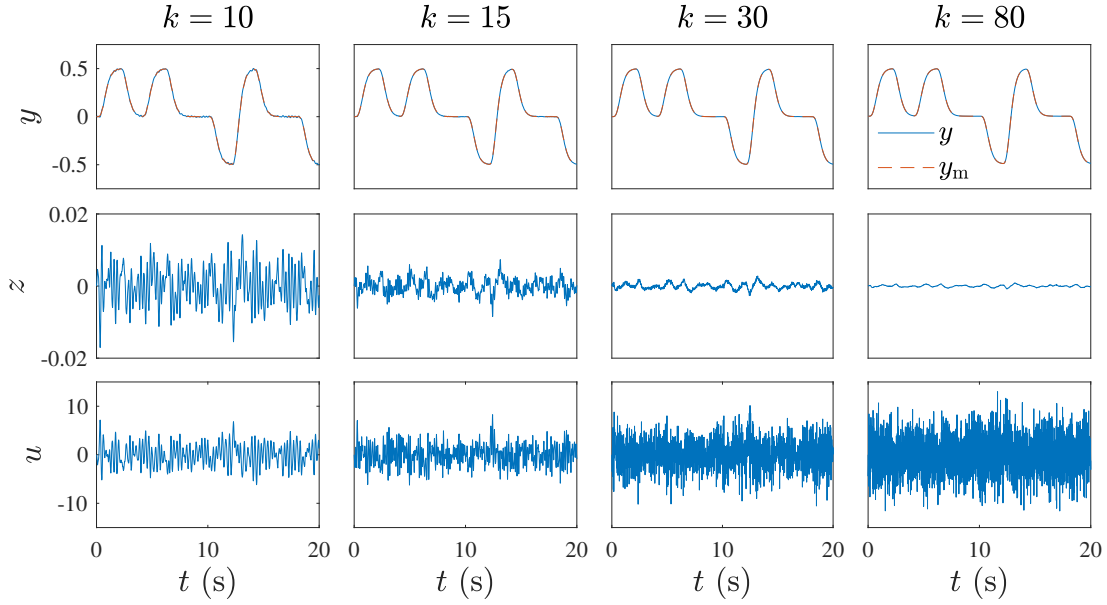


Figure 4.8: The FDI controller (3.53)–(3.59), where  $k \in \{10, 15, 30, 80\}$ , is implemented in feedback with the double integrator (4.4)–(4.6) with white-noise disturbance. The command  $r$  is a series of steps passed through the filter  $G_r(s) = 10^3/(s + 10)^3$ . The performance  $z$  degrades with the introduction of disturbance in comparison to the performance in Figure 4.5. By increasing  $k$  to 80, the performance improves.

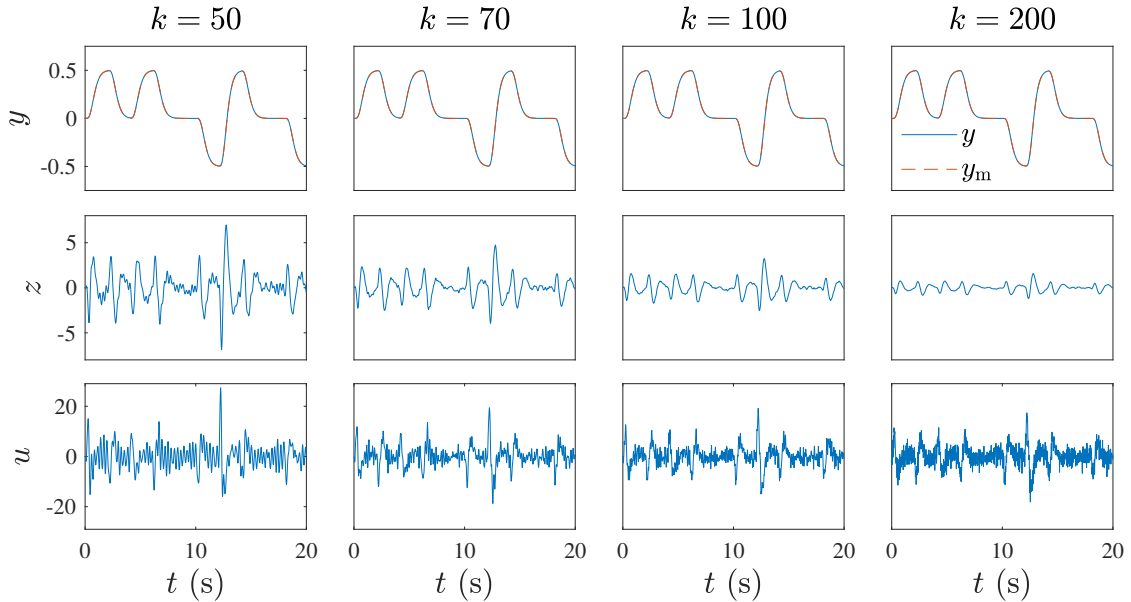


Figure 4.9: The FDI controller (3.53)–(3.59), where  $k \in \{50, 70, 100, 200\}$ , is implemented in feedback with the triple integrator (4.7)–(4.9) with white-noise disturbance. The command  $r$  is a series of steps passed through the filter  $G_r(s) = 10^3/(s + 10)^3$ . The performance  $z$  degrades with the introduction of disturbance in comparison to the performance in Figure 4.6. By increasing  $k$  to 200, the performance improves.

### 4.1.2 Multi-Input Multi-Output Example

In this section, we simulate a MIMO system with FDI control for unknown relative degree implemented in feedback. We demonstrate that the performance  $z$  improves as  $k$  is increased.

Consider (3.1) and (3.2), where

$$x(t) \triangleq \begin{bmatrix} x_1(t) \\ x_2(t) \\ \vdots \\ x_6(t) \end{bmatrix}, \quad u(t) \triangleq \begin{bmatrix} u_1(t) \\ u_2(t) \end{bmatrix}, \quad w(t) \triangleq \begin{bmatrix} \psi_1(t) \\ \psi_2(t) \\ \psi_3(t) \\ \psi_4(t) \end{bmatrix}, \quad (4.14)$$

and

$$A \triangleq \begin{bmatrix} -1 & 0 & 0 & 0 & 0 & 0 \\ 0 & -4 & -1.5 & 0 & 0 & 0 \\ 0 & 2 & 0 & 0 & 0 & 0 \\ 0 & 0 & 0 & -5 & -3 & 0 \\ 0 & 0 & 0 & 2 & 0 & 0 \\ 0 & 0 & 0 & 0 & 0 & -2 \end{bmatrix}. \quad (4.15)$$

We consider several different choices of  $B$  and  $C$  (e.g., different sensor and actuator

placements). First, consider

$$B \triangleq \begin{bmatrix} 1 & 0 \\ 0 & 0 \\ 0 & 0 \\ 0 & 0 \\ 0 & 0 \\ 0 & 1 \end{bmatrix}, \quad C \triangleq \begin{bmatrix} 1 & 0 & 0 & 0 & 0 & 0 \\ 0 & 0 & 0 & 0 & 0 & 1 \end{bmatrix}. \quad (4.16)$$

In this case,  $d = 1$ , and the first nonzero Markov parameter is  $H_d = CB = I_2$ . Also, (A3.1), (A3.2), and (A3.4) are satisfied. Next, consider

$$B \triangleq \begin{bmatrix} 0 & 0 \\ 1 & 0 \\ 0 & 0 \\ 0 & 1 \\ 0 & 0 \\ 0 & 0 \end{bmatrix}, \quad C \triangleq \begin{bmatrix} 0 & 0 & 0.5 & 0 & 0 & 0 \\ 0 & 0 & 0 & 0 & 0.5 & 0 \end{bmatrix}. \quad (4.17)$$

In this case,  $d = 2$ , and the first nonzero Markov parameter is  $H_d = CAB = I_2$ . Also, (A3.1), (A3.2), and (A3.4) are satisfied.

The objective is to design an FDI controller to control the MIMO system (3.1), (3.2), (4.14), and (4.15), where  $B$  and  $C$  could be either of the choices above, which have different relative degree. Note that the upper bound on the relative degree is  $\bar{d} = 2$ . We select the reference-model polynomials as

$$\alpha_m(\mathbf{p}) = (\mathbf{p} + 5)^2, \quad \beta_m(\mathbf{p}) = 25. \quad (4.18)$$

Next, let  $\rho = 3 > \bar{d}$ , and let

$$\eta_k(s) \triangleq s^3 + 4k^2s^2 + 2k^2s + k^3, \quad (4.19)$$

which satisfies (C3.1) and (C3.2). The initial conditions are  $x(0) = 0$  and  $x_c(0) = 0$ .

**Example 4.4.** *MIMO, command following and disturbance free.* Consider the MIMO system (3.1), (3.2), and (4.14)–(4.16), where the relative degree is  $d = 1$ . Also, consider the MIMO system (3.1), (3.2), (4.14), (4.15), and (4.17), where the relative degree is  $d = 2$ . The disturbances are identically 0 (i.e.,  $\psi_1 = \psi_2 = \psi_3 = \psi_4 = 0$ ). The control objective is to force the output  $y$  to follow the reference output  $y_m$  of the reference model (3.5). The reference-model command is  $r = \begin{bmatrix} r_1 & r_2 \end{bmatrix}^T$ , where  $r_1$  is a sequence of steps, which are passed through the filter  $G_r(s) = 10^2/(s + 10)^2$ , and  $r_2(t) = 0.3 \sin 2\pi t$ .

The FDI controller, where  $k \in \{5, 6, 8\}$ , is implemented in feedback with the MIMO system, where  $B$  and  $C$  are given by (4.16). Figure 4.10 shows the time history of  $y$ ,  $y_m$ ,  $z$ , and  $u$ . We notice that  $y$  follows  $y_m$  with a small but noticeable error. By increasing  $k$ , the average power of the performance decreases.

Next, the FDI controller, where  $k \in \{15, 20, 30\}$ , is implemented in feedback with the MIMO system, where  $B$  and  $C$  are given by (4.17). Figure 4.11 shows the time history of  $y$ ,  $y_m$ ,  $z$ , and  $u$ . We notice that  $y$  follows  $y_m$  with a small but noticeable error. By increasing  $k$ , the average power of the performance  $z$  decreases.  $\triangle$

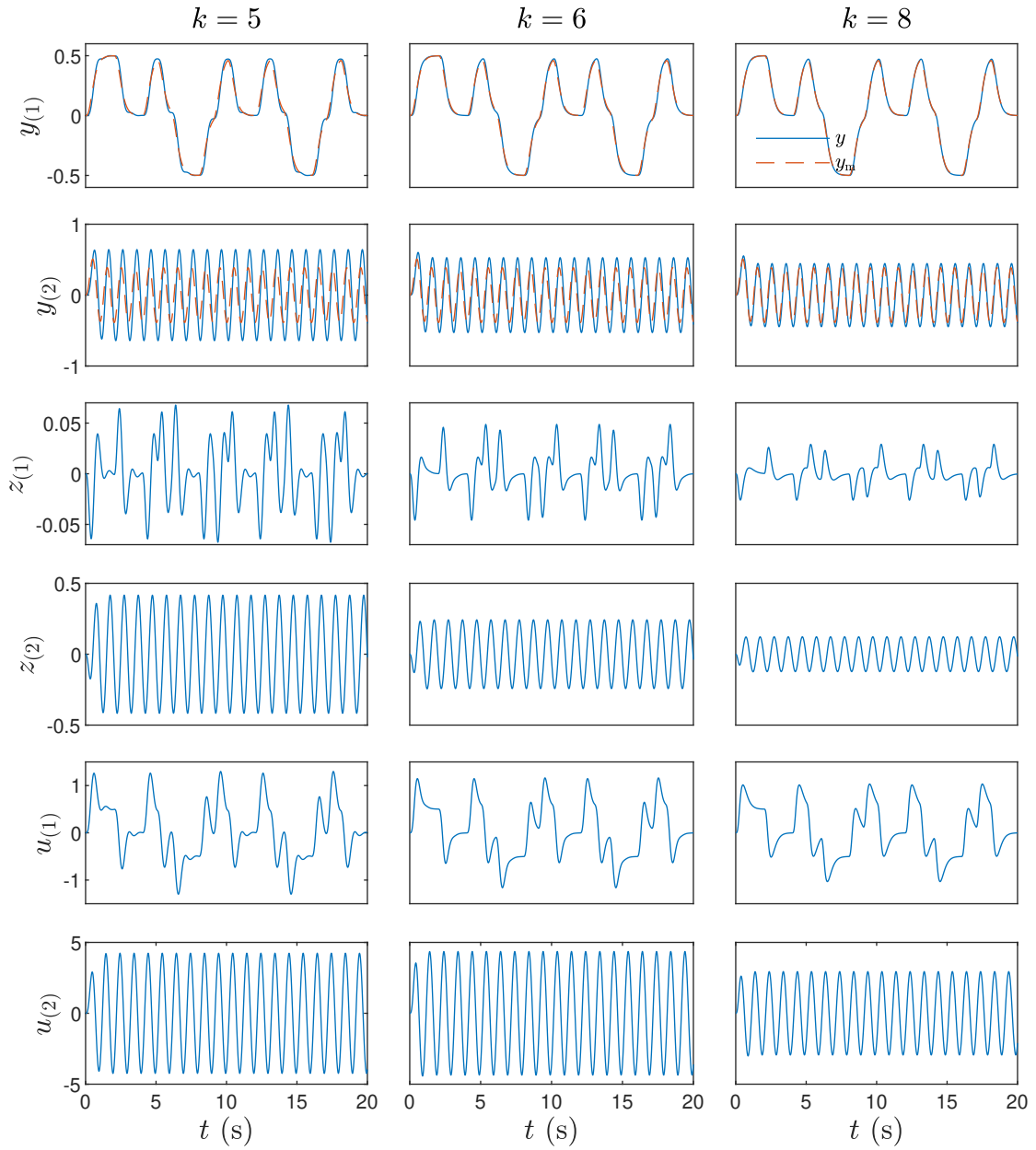


Figure 4.10: The FDI controller (3.53)–(3.59), where  $k \in \{5, 6, 8\}$ , is implemented in feedback with the MIMO system (4.14)–(4.16). In this case,  $d = 1$ . There is a noticeable error between  $y$  and  $y_m$ . By increasing  $k$ , the average power of the performance is reduced.

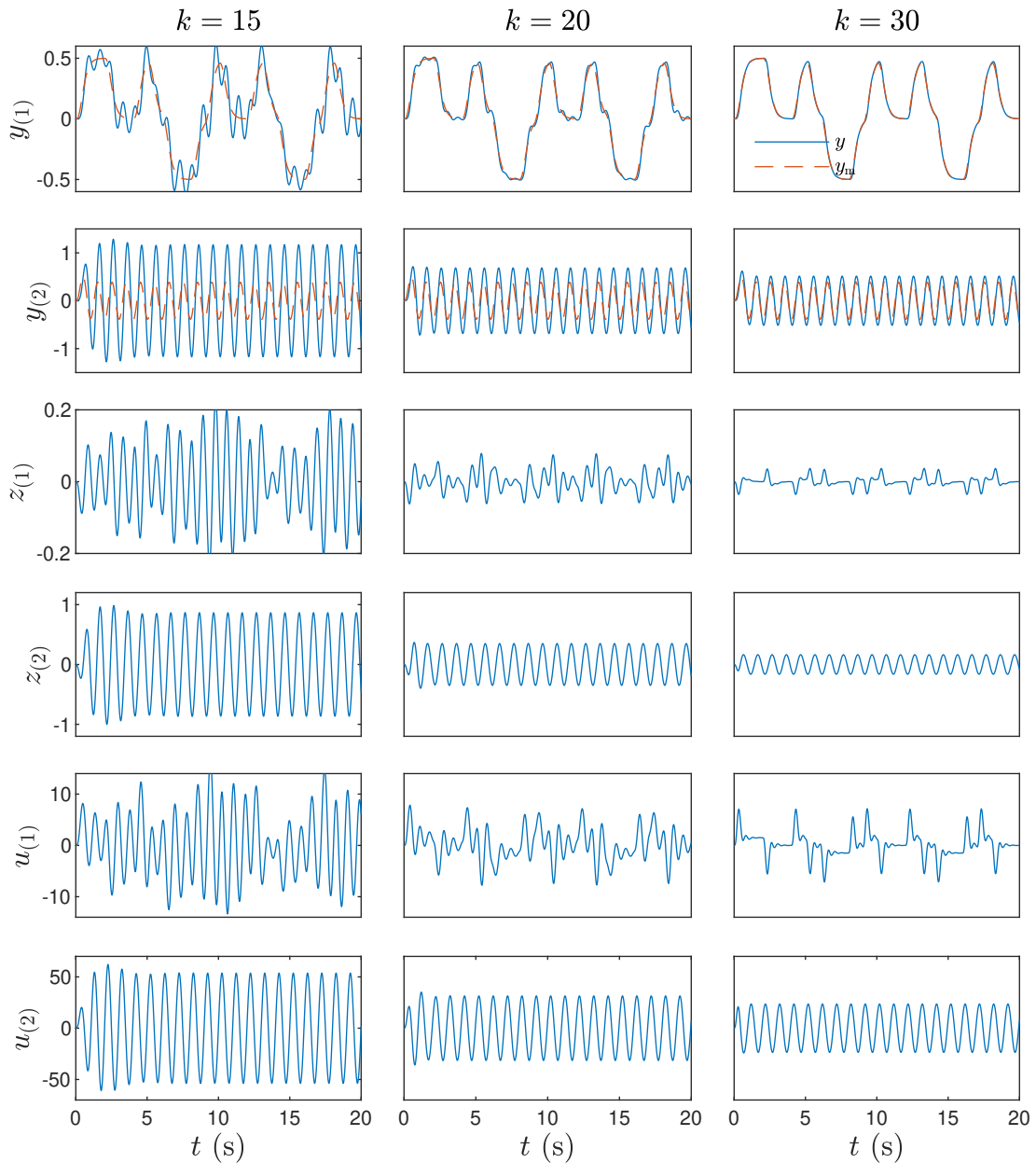


Figure 4.11: The FDI controller (3.53)–(3.59), where  $k \in \{15, 20, 30\}$ , is implemented in feedback with the MIMO system (4.14), (4.15), and (4.17). In this case,  $d = 2$ . There is a noticeable error between  $y$  and  $y_m$ . By increasing  $k$ , the average power of the performance is reduced.

**Example 4.5.** *MIMO, command following, and white-noise disturbance.* Consider the MIMO system (3.1), (3.2), and (4.14)–(4.16), where the relative degree is  $d = 1$ . Also, consider the MIMO system (3.1), (3.2), (4.14), (4.15), and (4.17), where the relative degree is  $d = 2$ . The disturbances  $\psi_1$ ,  $\psi_2$ ,  $\psi_3$ , and  $\psi_4$ , are generated from independent zero-mean 20-variance Gaussian white-noise distributions. The control objective is to force the output  $y$  to follow the reference output  $y_m$  of the reference model (3.5). The reference-model command is  $r = \begin{bmatrix} r_1 & r_2 \end{bmatrix}^T$ , where  $r_1$  is a sequence of steps, which are passed through the filter  $G_r(s) = 10^2/(s + 10)^2$ , and  $r_2(t) = 0.3 \sin 2\pi t$ .

The FDI controller, where  $k \in \{5, 6, 8, 20\}$ , is implemented in feedback with the MIMO system, where  $B$  and  $C$  are given by (4.16). Figure 4.12 shows the time history of  $y$ ,  $y_m$ ,  $z$ , and  $u$ . By comparing Figure 4.12 with Figure 4.10, we observe that the performance  $z$  degrades slightly in comparison to the disturbance free case. By increasing  $k$  to 20, the performance  $z$  improves.

Next, the FDI controller, and where  $k \in \{15, 20, 30, 100\}$ , is implemented in feedback with the MIMO system, where  $B$  and  $C$  are given by (4.17). Figure 4.13 shows the time history of  $y$ ,  $y_m$ ,  $z$ , and  $u$ . By comparing Figure 4.13 with Figure 4.11, we observe that the performance  $z$  degrades slightly in comparison to the disturbance free case. By increasing  $k$  to 100, the performance  $z$  improves. △

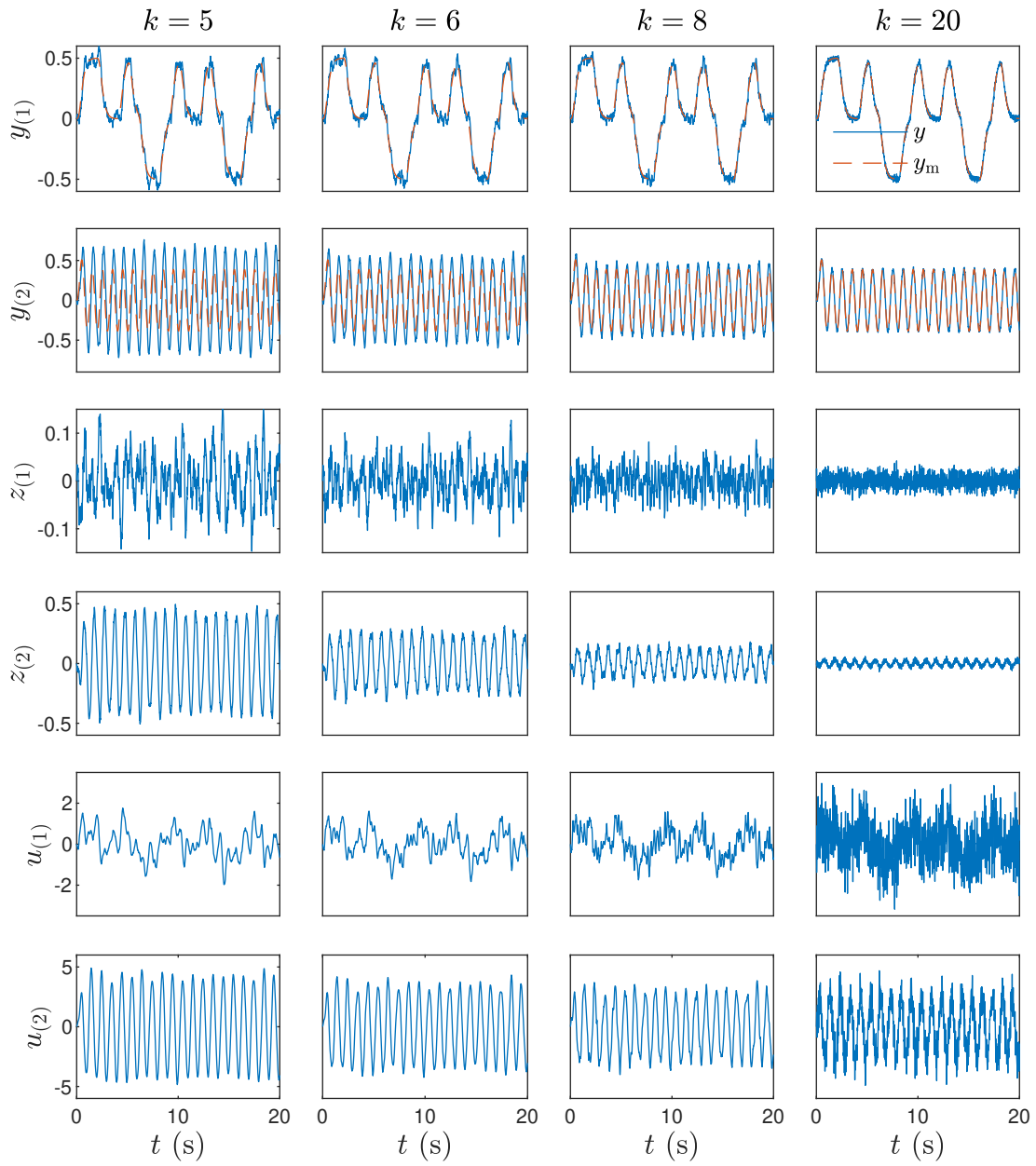


Figure 4.12: The FDI controller (3.53)–(3.59), where  $k \in \{5, 6, 8, 20\}$ , is implemented in feedback with the MIMO system (4.14)–(4.16). In this case,  $d = 1$ . The performance  $z$  degrades slightly in comparison to the disturbance free case, which is shown in Figure 4.10. By increasing  $k$  to 20, the performance  $z$  improves.



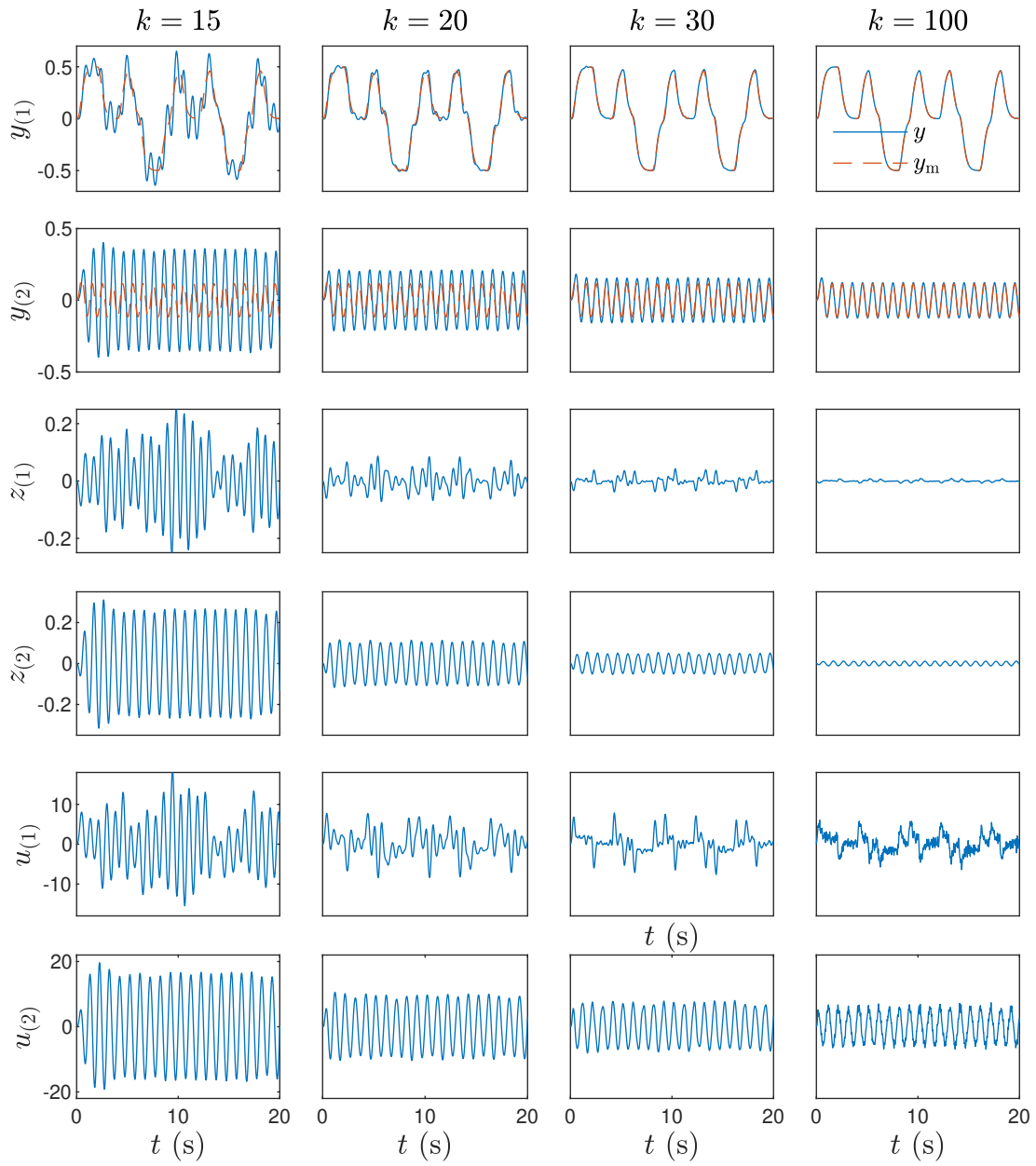


Figure 4.13: The FDI controller (3.53)–(3.59), where  $k \in \{15, 20, 30, 100\}$ , is implemented in feedback with the MIMO system (4.14), (4.15), and (4.17). In this case,  $d = 2$ . The performance  $z$  degrades slightly in comparison to the disturbance free case, which is shown in Figure 4.11. By increasing  $k$  to 100, the performance  $z$  improves.

## 4.2 Numerical Simulations of Physical Examples

### 4.2.1 Serially Connected Mass-Spring-Damper System (SISO)

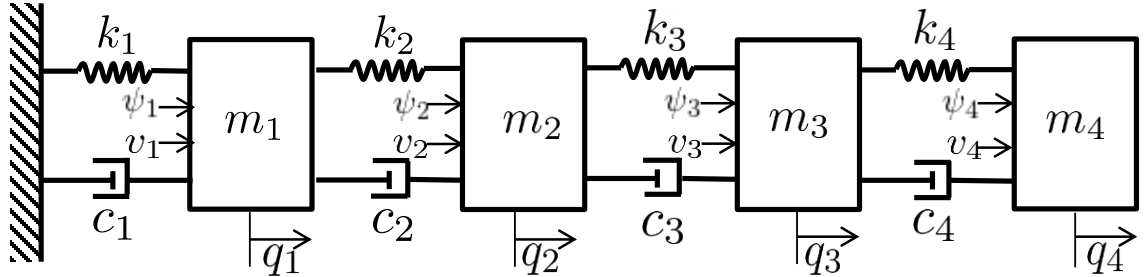


Figure 4.14: A serially connected four-mass structure.

Consider the serially connected four mass-spring-damper system shown in Figure 4.14, which has the equation of motion

$$M_0 \ddot{q}(t) + C_0 \dot{q}(t) + K_0 q(t) = \begin{bmatrix} v_1(t) & v_2(t) & v_3(t) & v_4(t) \end{bmatrix}^T + \begin{bmatrix} \psi_1(t) & \psi_2(t) & \psi_3(t) & \psi_4(t) \end{bmatrix}^T, \quad (4.20)$$

where

$$q(t) \triangleq \begin{bmatrix} q_1(t) \\ q_2(t) \\ q_3(t) \\ q_4(t) \end{bmatrix}, \quad (4.21)$$

and

$$M_0 \triangleq \begin{bmatrix} m_1 & 0 & 0 & 0 \\ 0 & m_2 & 0 & 0 \\ 0 & 0 & m_3 & 0 \\ 0 & 0 & 0 & m_4 \end{bmatrix}, \quad (4.22)$$

$$C_0 \triangleq \begin{bmatrix} c_1 + c_2 & -c_2 & 0 & 0 \\ -c_2 & c_2 + c_3 & -c_3 & 0 \\ 0 & -c_3 & c_3 + c_4 & -c_4 \\ 0 & 0 & -c_4 & c_4 \end{bmatrix}, \quad (4.23)$$

$$K_0 \triangleq \begin{bmatrix} k_1 + k_2 & -k_2 & 0 & 0 \\ -k_2 & k_2 + k_3 & -k_3 & 0 \\ 0 & -k_3 & k_3 + k_4 & -k_4 \\ 0 & 0 & -k_4 & -k_4 \end{bmatrix}. \quad (4.24)$$

The masses are  $m_1 = 1$  kg and  $m_2 = m_3 = m_4 = 2$  kg; the damping coefficients are  $c_1 = c_2 = c_3 = c_4 = 2$  kg/s; the spring coefficients are  $k_1 = 2$  kg/s<sup>2</sup>,  $k_2 = 4$  kg/s<sup>2</sup>,  $k_3 = 1$  kg/s<sup>2</sup>, and  $k_4 = 3$  kg/s<sup>2</sup>;  $v_1, v_2, v_3$ , and  $v_4$  are the control forces acting on the first, the second, the third, and the fourth mass respectively; and  $\psi_1, \psi_2, \psi_3$ , and  $\psi_4$  are the disturbance forces acting on the first, the second, the third, and the fourth mass. It follows that (4.24) with  $u(t) = v_1(t)$  can be expressed as (3.1), where

$$x(t) \triangleq \begin{bmatrix} q(t) \\ \dot{q}(t) \end{bmatrix}, \quad w(t) \triangleq \begin{bmatrix} 0_{4 \times 1} \\ \psi_1(t) \\ \psi_2(t) \\ \psi_3(t) \\ \psi_4(t) \end{bmatrix}, \quad (4.25)$$

and

$$A \triangleq \begin{bmatrix} 0_{4 \times 4} & I_4 \\ -M_0^{-1}K_0 & -M_0^{-1}C_0 \end{bmatrix}, \quad B \triangleq \begin{bmatrix} 0_{4 \times 1} \\ \begin{bmatrix} 1 \\ 0 \\ 0 \\ 0 \end{bmatrix} \\ -M_0^{-1} \end{bmatrix}. \quad (4.26)$$

We consider several different choices of  $C$  (sensor placements). First, consider

$$C \triangleq \begin{bmatrix} 1 & 0_{1 \times 7} \end{bmatrix}. \quad (4.27)$$

The output is the position  $q_1$  of the first mass. In this case,  $d = 2$ , and the first nonzero Markov parameter is  $H_d = CAB = 1$ . Also, (A3.1), (A3.2), and (A3.4) are satisfied. Next, consider

$$C \triangleq \begin{bmatrix} 0 & 1 & 0_{1 \times 6} \end{bmatrix}. \quad (4.28)$$

The output is the position  $q_2$  of the second mass. In this case,  $d = 3$ , and the first nonzero Markov parameter is given by  $H_d = CA^2B = 1$ . Also, (A3.1), (A3.2), and (A3.4) are satisfied. Next, consider

$$C \triangleq \begin{bmatrix} 0 & 0 & 1 & 0_{1 \times 5} \end{bmatrix}. \quad (4.29)$$

The output is the position  $q_3$  of the third mass. In this case,  $d = 4$ , and the first nonzero Markov parameter is given by  $H_d = CA^3B = 1$ . Also, (A3.1), (A3.2), and (A3.4) are satisfied. Finally, consider

$$C \triangleq \begin{bmatrix} 0 & 0 & 0 & 1 & 0_{1 \times 4} \end{bmatrix}. \quad (4.30)$$

The output is the position  $q_4$  of the fourth mass. In this case,  $d = 5$ , and the first nonzero Markov parameter is given by  $H_d = CA^4B = 1$ . Also, (A3.1), (A3.2), and (A3.4) are satisfied.

The objective is to design an FDI controller for the mass-spring-damper system (4.20)–(4.24), which can be expressed as (3.1), (3.2), (4.25), and (4.26), and where  $C$  could be any of the above choices, which have different relative degree. Note that the upper bound on the relative degree is  $\bar{d} = 5$ . We select the reference-model polynomials as

$$\alpha_m(\mathbf{p}) = (\mathbf{p} + 5)^5, \quad \beta_m(\mathbf{p}) = 5^5. \quad (4.31)$$

Note that the reference model transfer function (3.5) has unity gain at dc. Next, let  $\rho = 5 = \bar{d}$ , and let

$$\eta_k(s) \triangleq s^5 + 12k^3s^4 + 6k^5s^3 + 12k^6s^2 + 6k^7s + 3k^8, \quad (4.32)$$

which satisfies (C3.1) and (C3.2). The initial conditions are  $x(0) = 0$  and  $x_c(0) = 0$ .

**Example 4.6.** *SISO, disturbance free, and stable mass-spring-damper system with command following and disturbance free.* Consider the mass-spring-damper system shown in Figure 4.14. The disturbances are identically 0 (i.e.,  $\psi_1 = \psi_2 = \psi_3 = \psi_4 = 0$ ). The control objective is to force  $y$  to follow the output  $y_m$  of the reference model (3.5). The reference-model command  $r$  is a sequence of steps, which are passed through the filter  $G_r(s) = 10^5/(s + 10)^5$ .

The FDI controller, where  $k \in \{3, 4, 6\}$ , is implemented in feedback with the mass-spring-damper system, where  $C$  is given by (4.27). The parameter  $k = 3$  is selected near but above the minimum stabilizing value of approximately 1.9. Figure 4.15 shows the time history of  $y$ ,  $y_m$ ,  $z$ , and  $u$ .

Next, the FDI controller, where  $k \in \{8, 12, 20\}$ , is implemented in feedback with the mass-spring-damper system, where  $C$  is given by (4.28). The parameter  $k = 8$  is selected near but above the minimum stabilizing value of approximately 6.6. Figure 4.16 shows the time history of  $y$ ,  $y_m$ ,  $z$ , and  $u$ .

Next, the FDI controller, where  $k \in \{20, 30, 50\}$ , is implemented in feedback with the mass-spring-damper system, where  $C$  is given by (4.29). The parameter  $k = 20$  is selected near but above the minimum stabilizing value of approximately 19.6. Figure 4.17 shows the time history of  $y$ ,  $y_m$ ,  $z$ , and  $u$ .

Finally, the FDI controller, where  $k \in \{65, 80, 110\}$ , is implemented in feedback with the mass-spring-damper system, where  $C$  is given by (4.30). The parameter  $k = 65$  is selected near but above the minimum stabilizing value of approximately 60.3. Figure 4.18 shows the time history of  $y$ ,  $y_m$ ,  $z$ , and  $u$ .

By observing Figure 4.15, Figure 4.16, Figure 4.17, and Figure 4.18, we notice that  $y$  follows  $y_m$  with a small but noticeable error. By increasing  $k$ , the average power of performance decreases. △

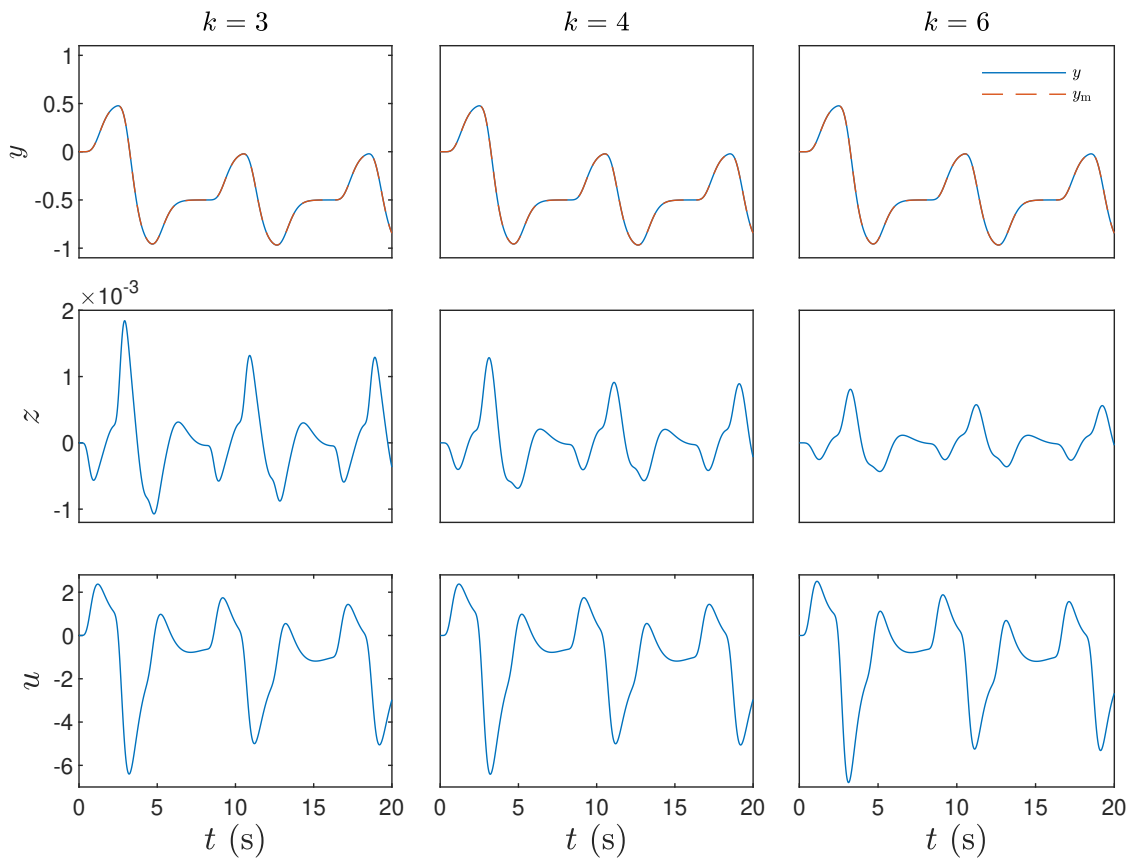


Figure 4.15: The FDI controller (3.53)–(3.59), where  $k \in \{3, 4, 6\}$ , is implemented in feedback with the mass-spring-damper system (4.25)–(4.27). In this case,  $d = 2$ . By increasing  $k$ , the average power of the performance  $z$  decreases.

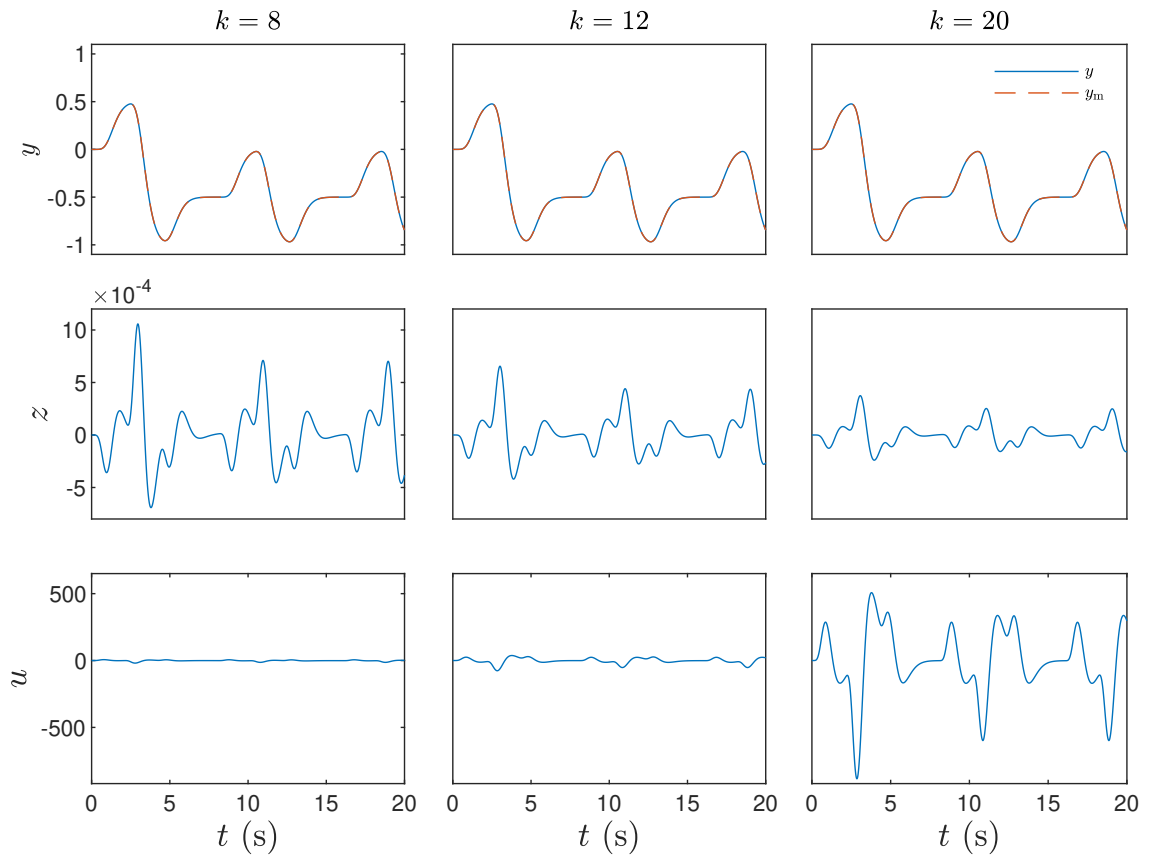


Figure 4.16: The FDI controller (3.53)–(3.59), where  $k \in \{8, 12, 20\}$ , is implemented in feedback with the mass-spring-damper system (4.25), (4.26), and (4.28). In this case,  $d = 3$ . By increasing  $k$ , the average power of the performance  $z$  decreases.



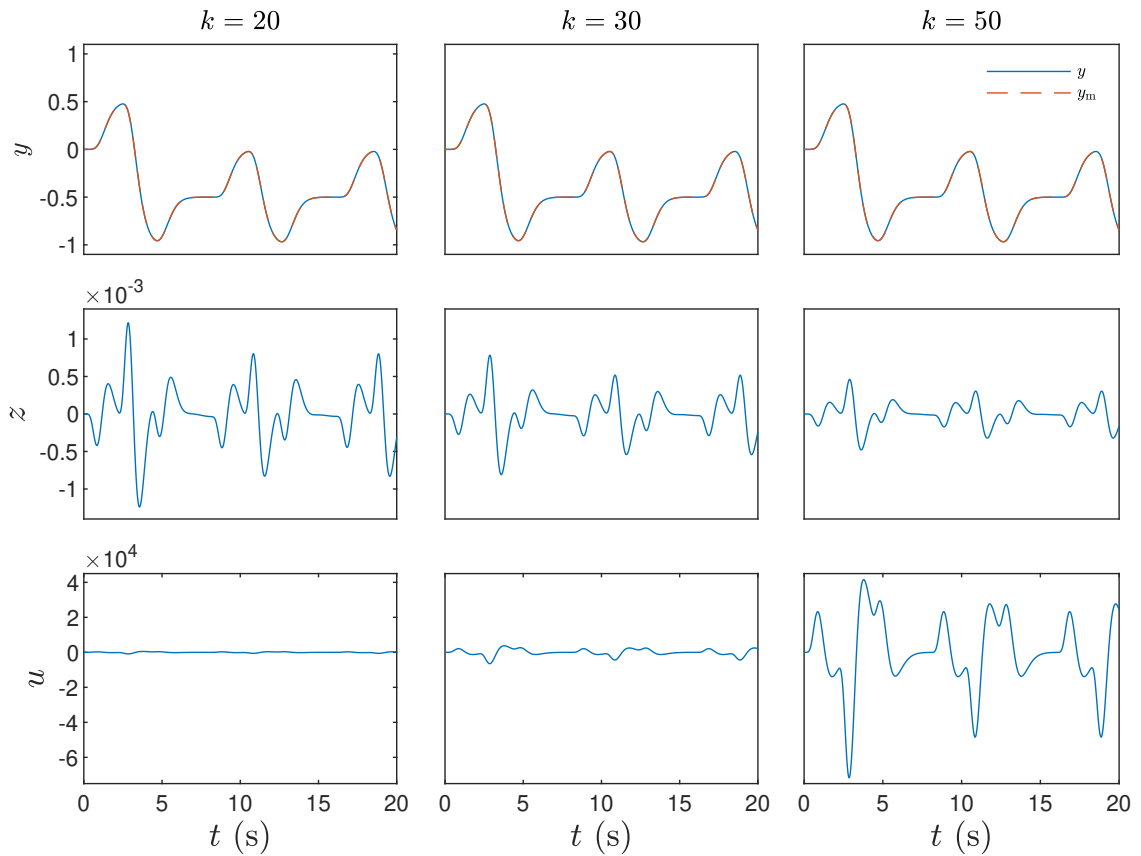


Figure 4.17: The FDI controller (3.53)–(3.59), where  $k \in \{20, 30, 50\}$ , is implemented in feedback with the mass-spring-damper system (4.25), (4.26), and (4.29). In this case,  $d = 4$ . By increasing  $k$ , the average power of the performance  $z$  decreases.

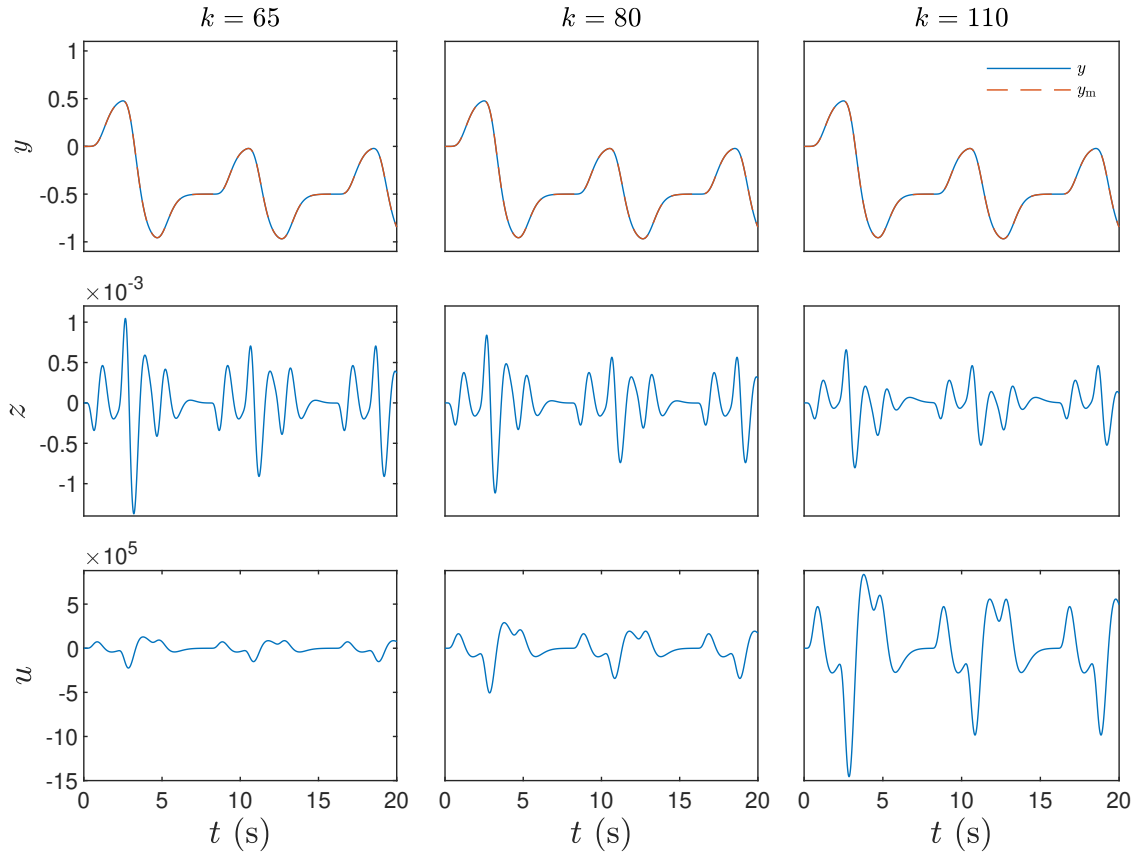


Figure 4.18: The FDI controller (3.53)–(3.59), where  $k \in \{65, 80, 110\}$ , is implemented in feedback with the mass-spring-damper system (4.25), (4.26), and (4.30). In this case,  $d = 5$ . By increasing  $k$ , the average power of the performance  $z$  decreases.

**Example 4.7.** *SISO and stable mass-spring-damper system, with command following and white-noise disturbance.* Consider the mass-spring-damper system (4.20) shown in Figure 4.14. The disturbances  $\psi_1$ ,  $\psi_2$ ,  $\psi_3$ , and  $\psi_4$ , are generated from independent zero-mean 20-variance Gaussian white-noise distributions. The control objective is to force  $y$  to follow the output  $y_m$  of the reference model (3.5). The reference-model command  $r$  is a sequence of steps, which are passed through the filter  $G_r(s) = 10^5/(s + 10)^5$ .

The FDI controller, where  $k \in \{3, 4, 6, 10\}$ , is implemented in feedback with the four mass-spring-damper system, where  $C$  is given by (4.27). Figure 4.19 shows the time history of  $y$ ,  $y_m$ ,  $z$ , and  $u$ . By comparing Figure 4.19 with Figure 4.15, we observe that the performance  $z$  degrades slightly in comparison to the disturbance free case. By increasing  $k$  to 10, the performance  $z$  improves.

Next, the FDI controller, where  $k \in \{8, 12, 20, 40\}$ , is implemented in feedback with the four mass-spring-damper system, where  $C$  is given by (4.28). Figure 4.20 shows the time history of  $y$ ,  $y_m$ ,  $z$ , and  $u$ . By comparing Figure 4.20 with Figure 4.16, we observe that the performance  $z$  degrades slightly in comparison to the disturbance free case. By increasing  $k$  to 40, the performance  $z$  improves.

Next, the FDI controller, where  $k \in \{20, 30, 50, 90\}$ , is implemented in feedback with the four mass-spring-damper system, where  $C$  is given by (4.29). Figure 4.21 shows the time history of  $y$ ,  $y_m$ ,  $z$ , and  $u$ . By comparing Figure 4.21 with Figure 4.17, we observe that the performance  $z$  degrades slightly in comparison to the disturbance free case. By increasing  $k$  to 90, the performance  $z$  improves.

Finally, the FDI controller, where  $k \in \{65, 80, 110, 160\}$ , is implemented in feedback with the four mass-spring-damper system, where  $C$  is given by (4.30). Figure 4.22 shows the time history of  $y$ ,  $y_m$ ,  $z$ , and  $u$ . By comparing Figure 4.22 with Figure 4.18, we observe that the performance  $z$  degrades slightly in comparison to the disturbance free case. By increasing  $k$  to 160, the performance  $z$  improves.  $\triangle$

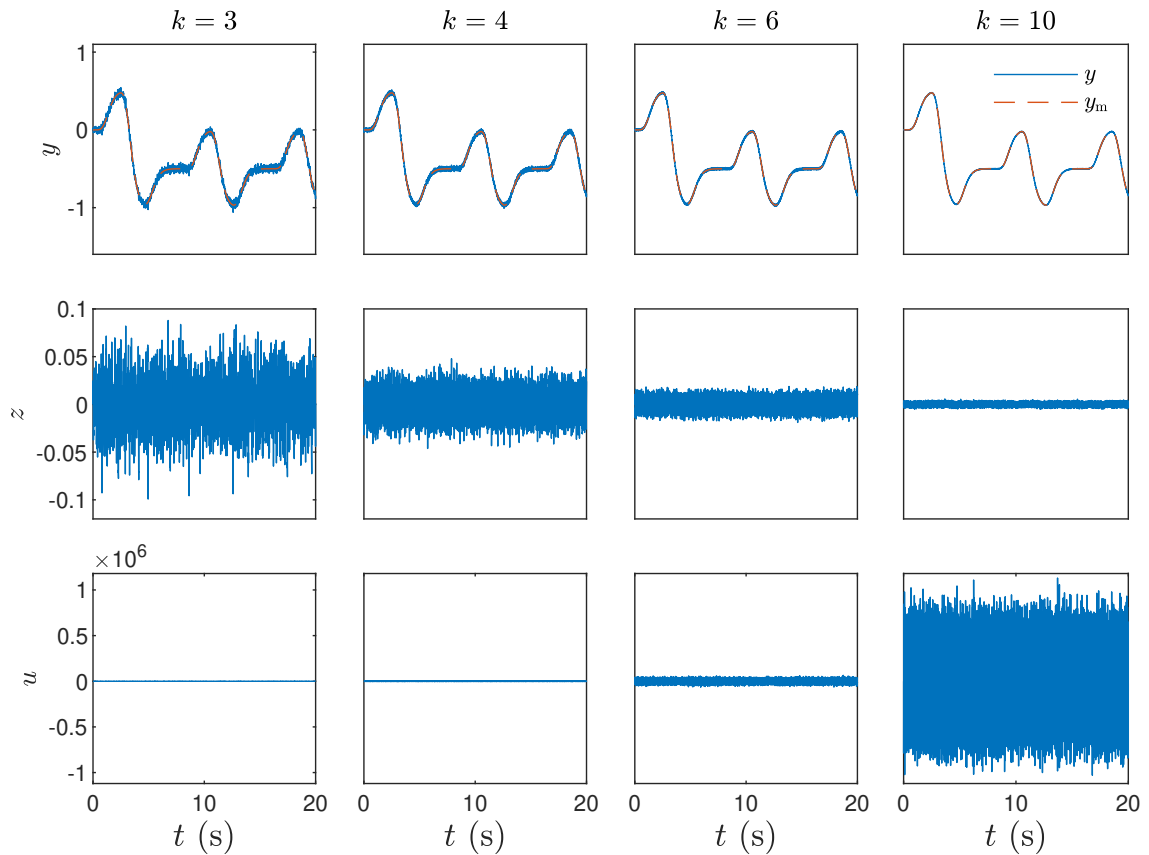


Figure 4.19: The FDI controller (3.53)–(3.59), where  $k \in \{3, 4, 6, 10\}$ , is implemented in feedback with the mass-spring-damper system (4.25)–(4.27). In this case,  $d = 2$ . In comparison to Figure 4.15, the performance  $z$  degrades slightly. By increasing  $k$  to 10, the performance  $z$  improves.

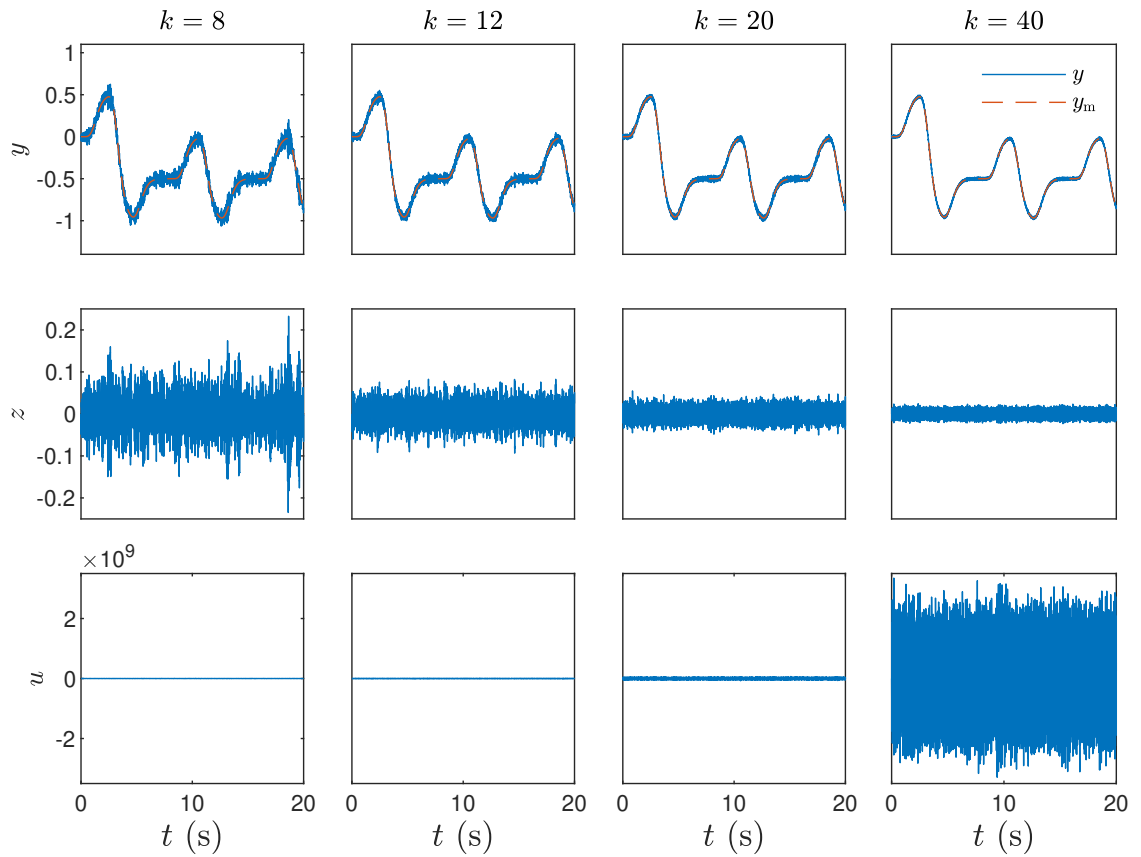


Figure 4.20: The FDI controller (3.53)–(3.59), where  $k \in \{8, 12, 20, 40\}$ , is implemented in feedback with the mass-spring-damper system (4.25), (4.26), and (4.28). In this case,  $d = 3$ . In comparison to Figure 4.16, the performance  $z$  degrades slightly. By increasing  $k$  to 40, the performance  $z$  improves.

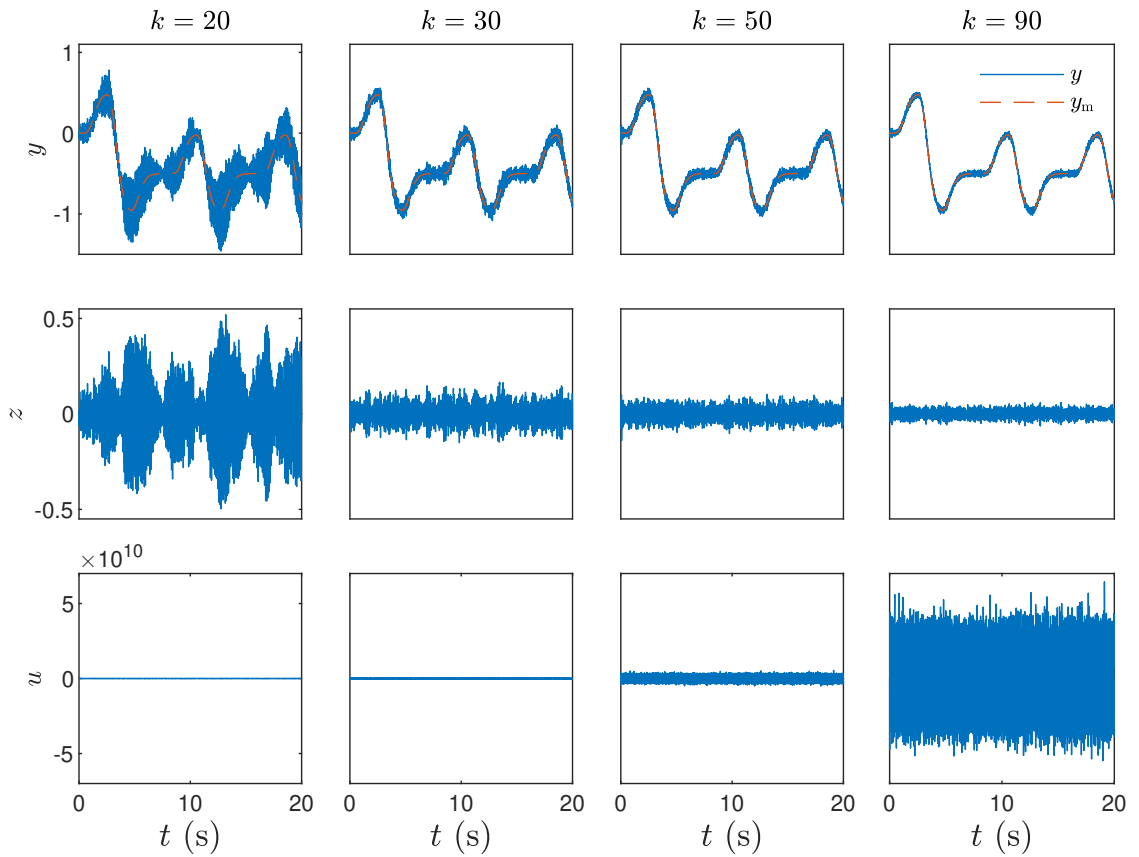


Figure 4.21: The FDI controller (3.53)–(3.59), where  $k \in \{20, 30, 50, 90\}$ , is implemented in feedback with the mass-spring-damper system (4.25), (4.26), and (4.29). In this case,  $d = 4$ . In comparison to Figure 4.17, the performance  $z$  degrades slightly. By increasing  $k$  to 90, the performance  $z$  improves.

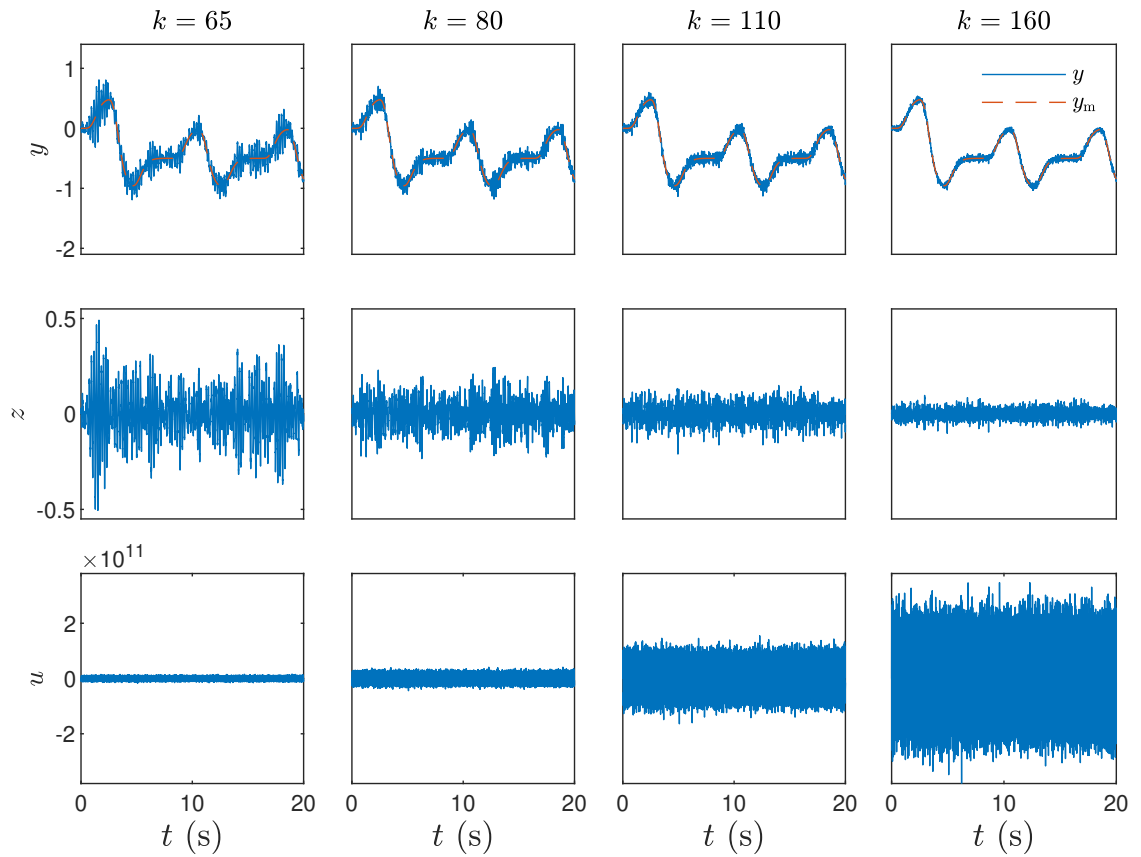


Figure 4.22: The FDI controller (3.53)–(3.59), where  $k \in \{65, 80, 110, 160\}$ , is implemented in feedback with the mass-spring-damper system (4.25), (4.26), and (4.30). In this case,  $d = 5$ . In comparison to Figure 4.18, we observe that the performance  $z$  degrades slightly. By increasing  $k$  to 160, the performance  $z$  improves.

**Example 4.8.** *SISO, disturbance free, and unstable mass-spring-damper system, with command following.* Consider the mass-spring-damper system (4.20) shown in Figure 4.14. By changing  $c_1$  to  $-10$ , the resulting open-loop system becomes unstable. The disturbance is identically 0 (i.e.,  $\psi_1 = \psi_2 = \psi_3 = \psi_4 = 0$ ). The control objective is to force  $y$  to follow the output  $y_m$  of the reference model (3.5). The reference-model command  $r$  is a sequence of steps, which are passed through the filter  $G_r(s) = 10^5/(s + 10)^5$ .

The FDI controller, where  $k \in \{3, 4, 6\}$ , is implemented in feedback with the mass-spring-damper system, where  $C$  is given by (4.27). The parameter  $k = 3$  is selected near but above the minimum stabilizing value of approximately 2.4. Figure 4.23 shows the time history of  $y$ ,  $y_m$ ,  $z$ , and  $u$ .

Next, the FDI controller, where  $k \in \{10, 15, 25\}$ , is implemented in feedback with the mass-spring-damper system, where  $C$  is given by (4.28). The parameter  $k = 10$  is selected near but above the minimum stabilizing value of approximately 8.3. Figure 4.24 shows the time history of  $y$ ,  $y_m$ ,  $z$ , and  $u$ .

Next, the FDI controller, where  $k \in \{35, 55, 85\}$ , is implemented in feedback with the mass-spring-damper system, where  $C$  is given by (4.29). The parameter  $k = 35$  is selected near but above the minimum stabilizing value of approximately 31.3. Figure 4.25 shows the time history of  $y$ ,  $y_m$ ,  $z$ , and  $u$ .

Finally, the FDI controller, where  $k \in \{100, 115, 140\}$ , is implemented in feedback with the mass-spring-damper system, where  $C$  is given by (4.30). The parameter  $k = 100$  is selected near but above the minimum stabilizing value of approximately 97.4. Figure 4.26 shows the time history of  $y$ ,  $y_m$ ,  $z$ , and  $u$ .

Note that the minimum stabilizing values for each case is greater than the minimum stabilizing value of the stable mass-spring damper system in Example 4.6 (i.e., SISO and stable mass-spring-damper system). By observing Figure 4.23, Figure 4.24, Figure 4.25, and Figure 4.26, we notice that  $y$  follows  $y_m$  with a small but noticeable



error. By increasing  $k$ , the average power of performance decreases. △

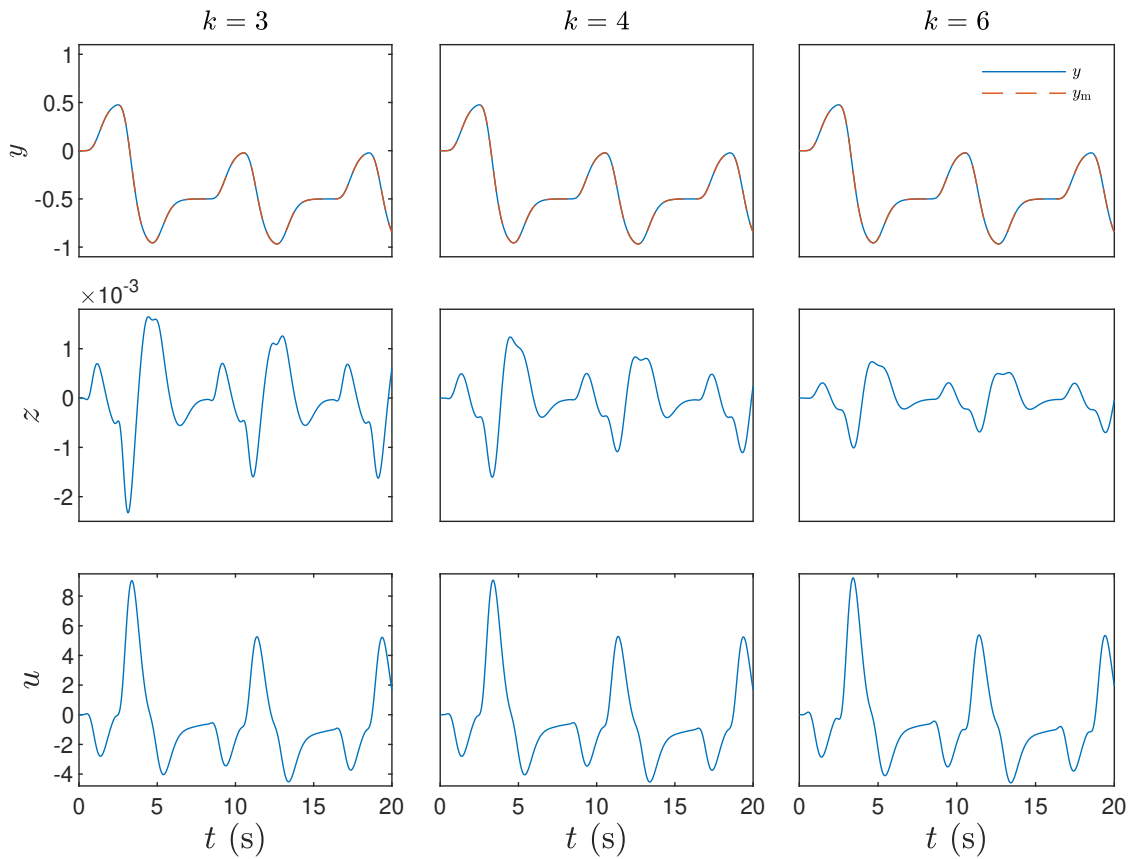


Figure 4.23: FDI control with  $k \in \{3, 4, 6\}$  for the disturbance free and unstable mass-spring-damper system shown in Figure 4.14. The FDI controller (3.53)–(3.59), where  $k \in \{3, 4, 6\}$ , is implemented in feedback with the mass-spring-damper system (4.25)–(4.27). In this case,  $d = 2$ . By increasing  $k$ , the average power of the performance  $z$  decreases.

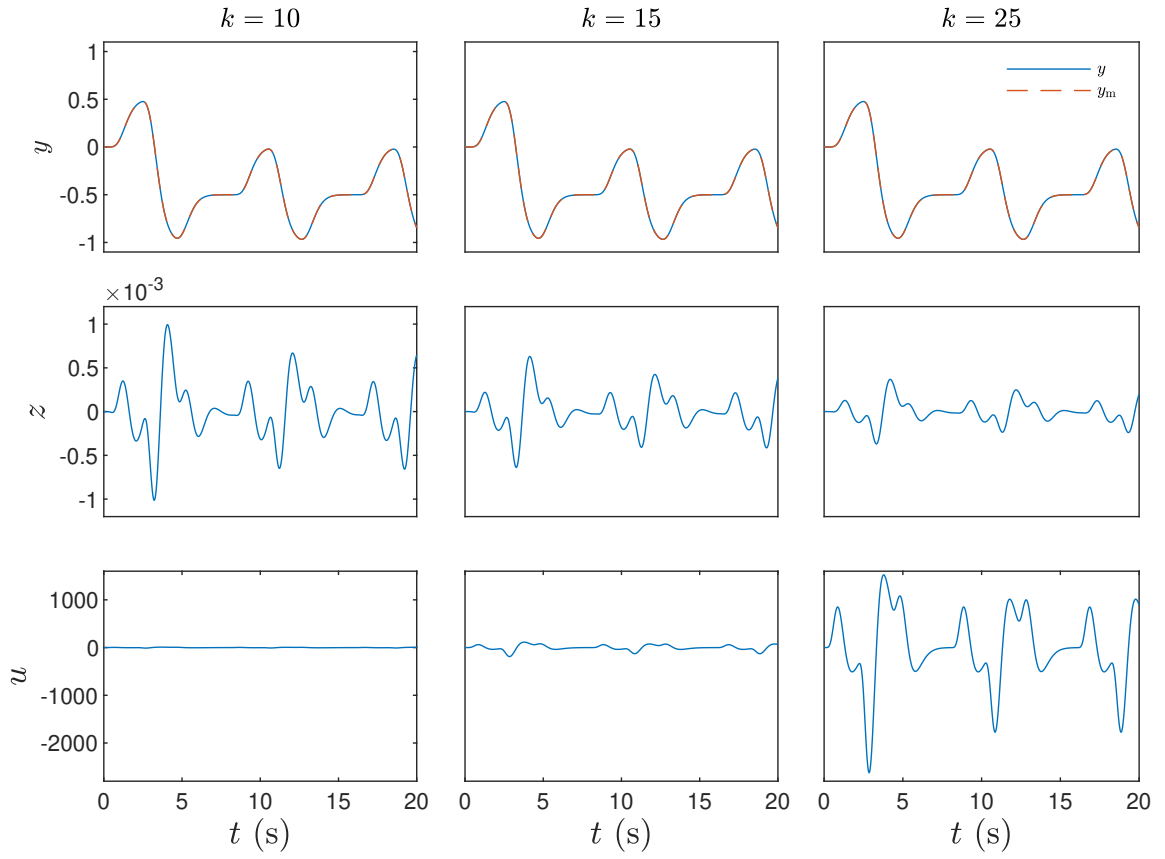


Figure 4.24: FDI control with  $k \in \{10, 15, 25\}$  for the disturbance free and unstable mass-spring-damper system shown in Figure 4.14. The FDI controller (3.53)–(3.59), where  $k \in \{10, 15, 25\}$ , is implemented in feedback with the mass-spring-damper system (4.25), (4.26), and (4.28). In this case,  $d = 3$ . By increasing  $k$ , the average power of the performance  $z$  decreases.

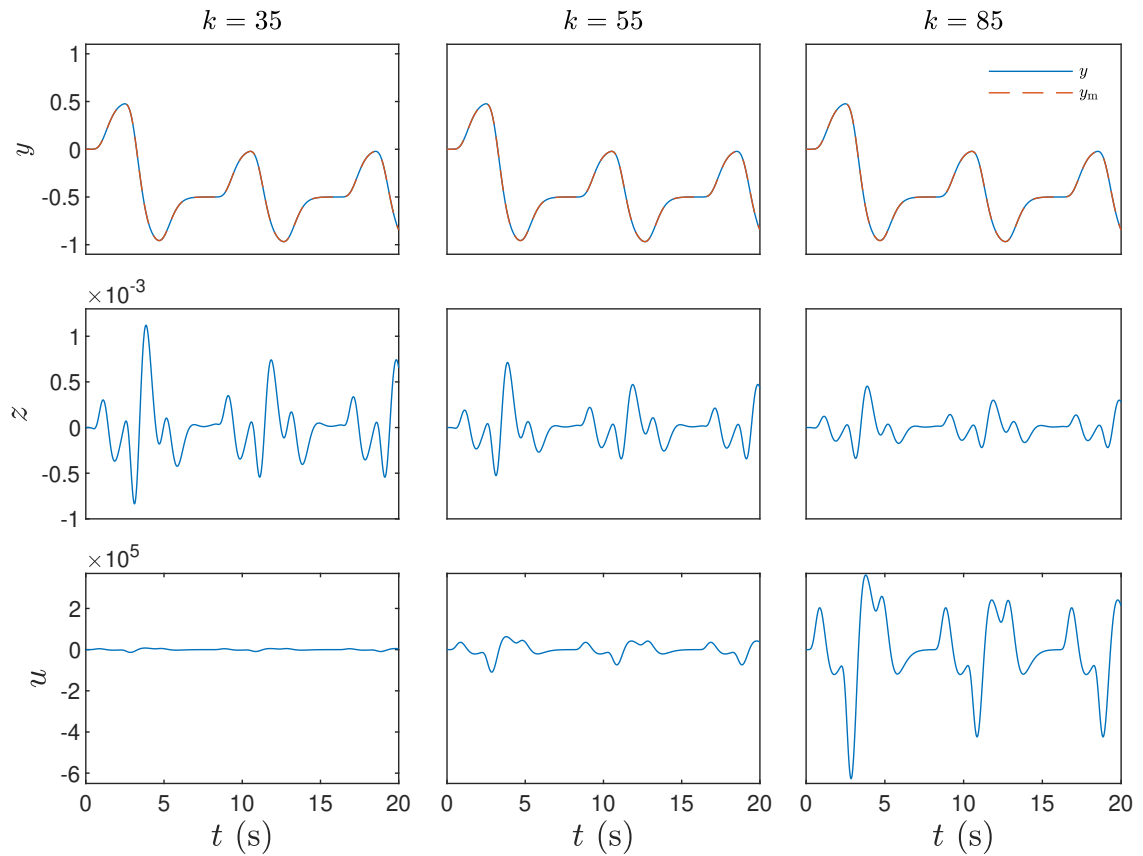


Figure 4.25: FDI control with  $k \in \{35, 55, 85\}$  for the disturbance free and unstable mass-spring-damper system shown in Figure 4.14. The FDI controller (3.53)–(3.59), where  $k \in \{35, 55, 85\}$ , is implemented in feedback with the mass-spring-damper system (4.25), (4.26), and (4.29). In this case,  $d = 4$ . By increasing  $k$ , the average power of the performance  $z$  decreases.

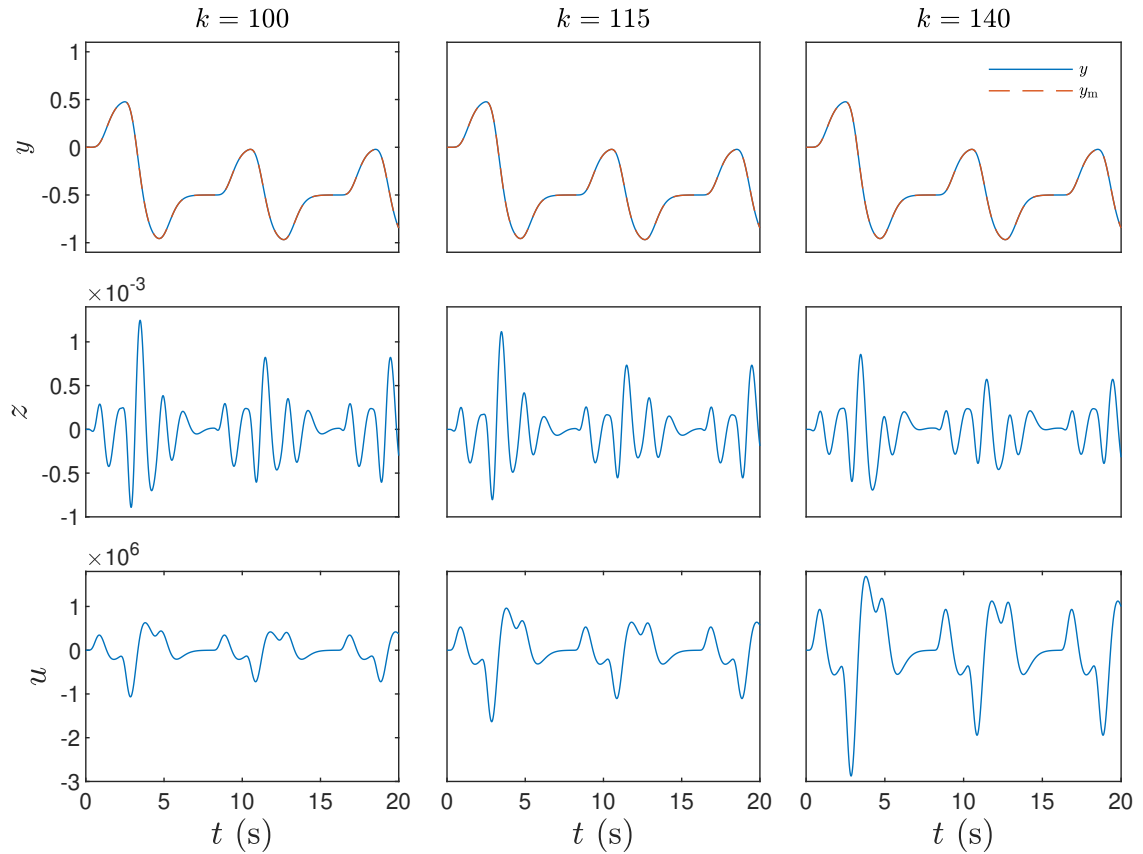


Figure 4.26: FDI control with  $k \in \{100, 115, 140\}$  for the disturbance free and unstable mass-spring-damper system shown in Figure 4.14. The FDI controller (3.53)–(3.59), where  $k \in \{100, 115, 140\}$ , is implemented in feedback with the mass-spring-damper system (4.25), (4.26), and (4.30). In this case,  $d = 5$ . By increasing  $k$ , the average power of the performance  $z$  decreases.

**Example 4.9.** *SISO and unstable mass-spring-damper system with command following, and white-noise disturbance.* Consider the four mass-spring-damper system (4.20) shown in Figure 4.14. By changing  $c_1$  to  $-10$ , the resulting open-loop system becomes unstable. The disturbances  $\psi_1$ ,  $\psi_2$ ,  $\psi_3$ , and  $\psi_4$ , are generated from independent zero-mean 20-variance Gaussian white-noise distributions. The control objective is to force  $y$  to follow the output  $y_m$  of the reference model (3.5). The reference-model command  $r$  is a sequence of steps, which are passed through the filter  $G_r(s) = 10^5/(s + 10)^5$ .

The FDI controller, where  $k \in \{3, 4, 6, 10\}$ , is implemented in feedback with the unstable mass-spring-damper system, where  $C$  is given by (4.27). Figure 4.27 shows the time history of  $y$ ,  $y_m$ ,  $z$ , and  $u$ . By comparing Figure 4.27 with Figure 4.23, we observe that the performance  $z$  degrades slightly in comparison to the disturbance free case. By increasing  $k$  to 10, the performance  $z$  improves.

Next, the FDI controller, where  $k \in \{10, 15, 25, 40\}$ , is implemented in feedback with the unstable mass-spring-damper system, where  $C$  is given by (4.28). Figure 4.28 shows the time history of  $y$ ,  $y_m$ ,  $z$ , and  $u$ . By comparing Figure 4.28 with Figure 4.24, we observe that the performance  $z$  degrades slightly in comparison to the disturbance free case. By increasing  $k$  to 40, the performance  $z$  improves.

Next, the FDI controller, where  $k \in \{35, 55, 85, 200\}$ , is implemented in feedback with the unstable mass-spring-damper system, where  $C$  is given by (4.29). Figure 4.29 shows the time history of  $y$ ,  $y_m$ ,  $z$ , and  $u$ . By comparing Figure 4.29 with Figure 4.25, we observe that the performance  $z$  degrades slightly in comparison to the disturbance free case. By increasing  $k$  to 200, the performance  $z$  improves.

Finally, the FDI controller, where  $k \in \{100, 115, 140, 245\}$ , is implemented in feedback with the unstable mass-spring-damper system, where  $C$  is given by (4.30). Figure 4.30 shows the time history of  $y$ ,  $y_m$ ,  $z$ , and  $u$ . By comparing Figure 4.30 with Figure 4.26, we observe that the performance  $z$  degrades slightly in comparison to

the disturbance free case. By increasing  $k$  to 245, the performance  $z$  improves.  $\triangle$

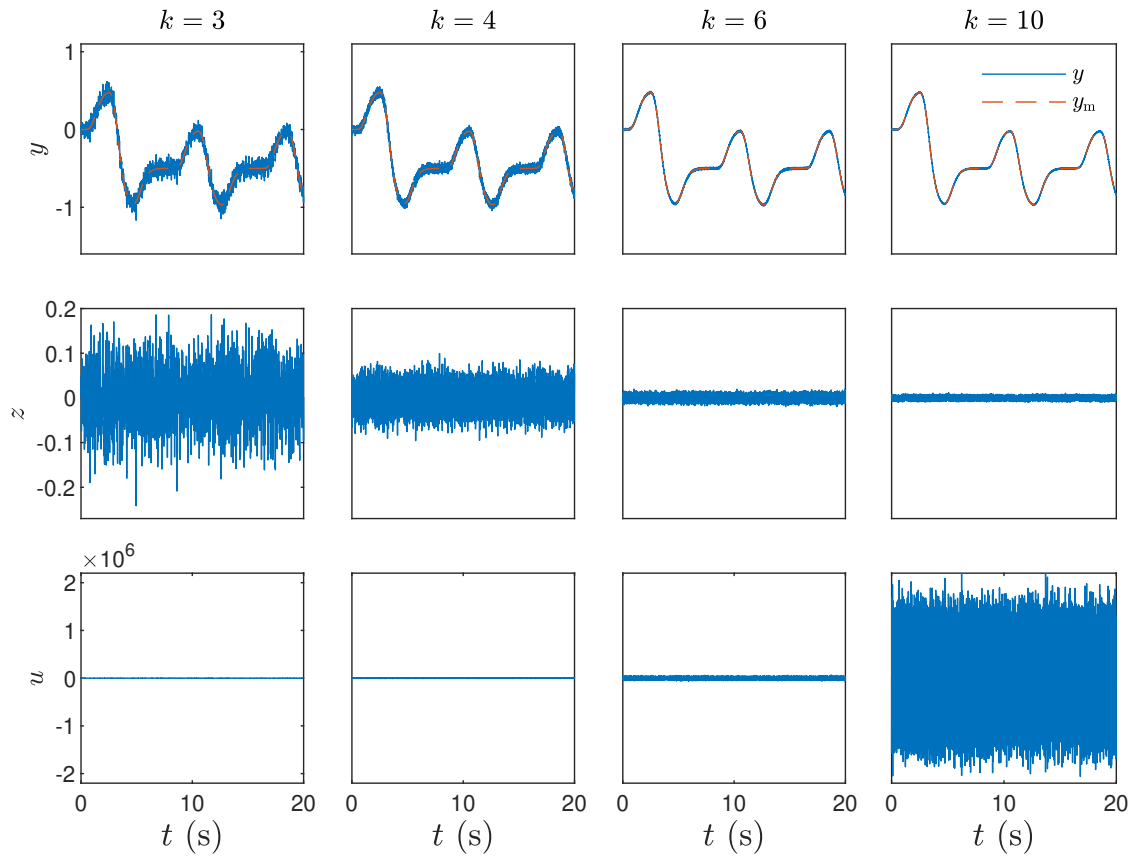


Figure 4.27: FDI control with  $k \in \{3, 4, 6, 10\}$  for the unstable mass-spring-damper system shown in Figure 4.14, with white-noise disturbance. The FDI controller (3.53)–(3.59), where  $k \in \{3, 4, 6, 10\}$ , is implemented in feedback with the mass-spring-damper system (4.25)–(4.27). In this case,  $d = 2$ . The performance  $z$  degrades slightly in comparison to the disturbance free case which is shown in Figure 4.23. By increasing  $k$  to 10, the average power of the performance  $z$  decreases.

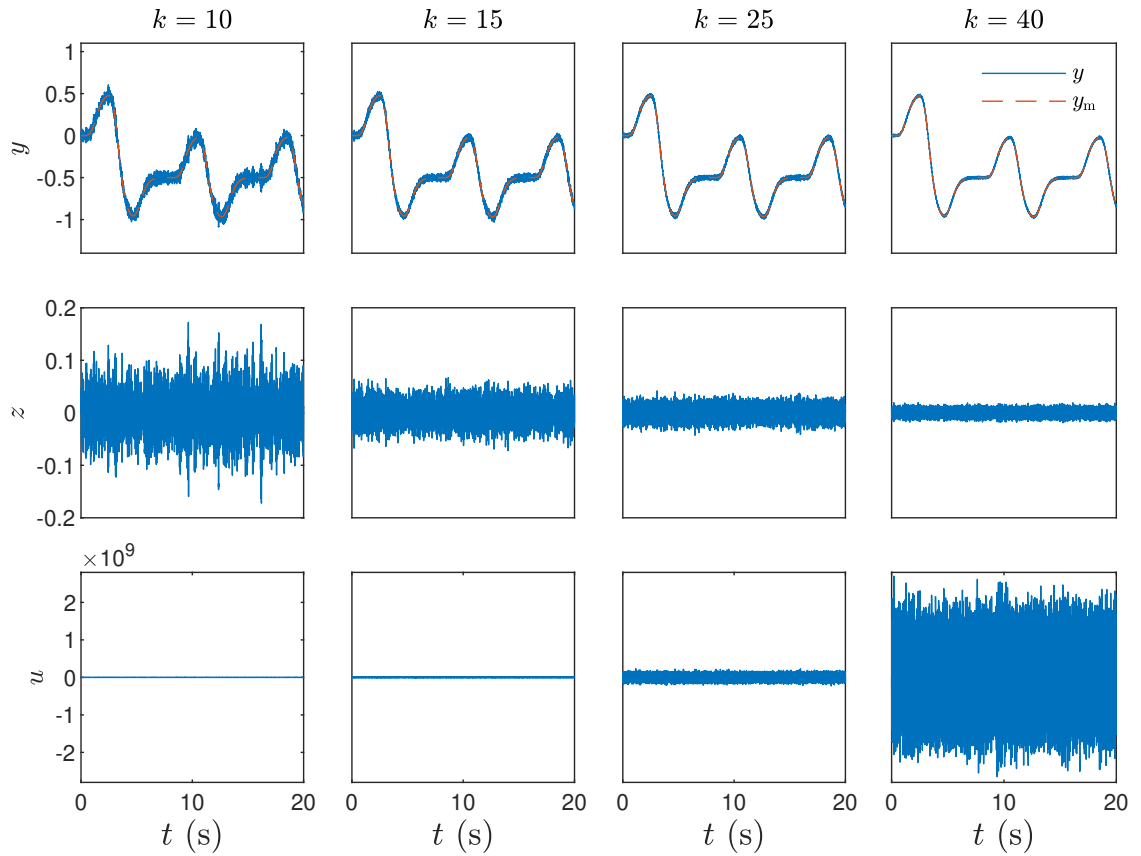


Figure 4.28: FDI control with  $k \in \{10, 15, 25, 40\}$  for the unstable mass-spring-damper system shown in Figure 4.14, with white-noise disturbance. The FDI controller (3.53)–(3.59), where  $k \in \{10, 15, 25, 40\}$ , is implemented in feedback with the mass-spring-damper system (4.25), (4.26), and (4.28). In this case,  $d = 3$ . The performance  $z$  degrades slightly in comparison to the disturbance free case which is shown in Figure 4.24. By increasing  $k$  to 40, the average power of the performance  $z$  decreases.

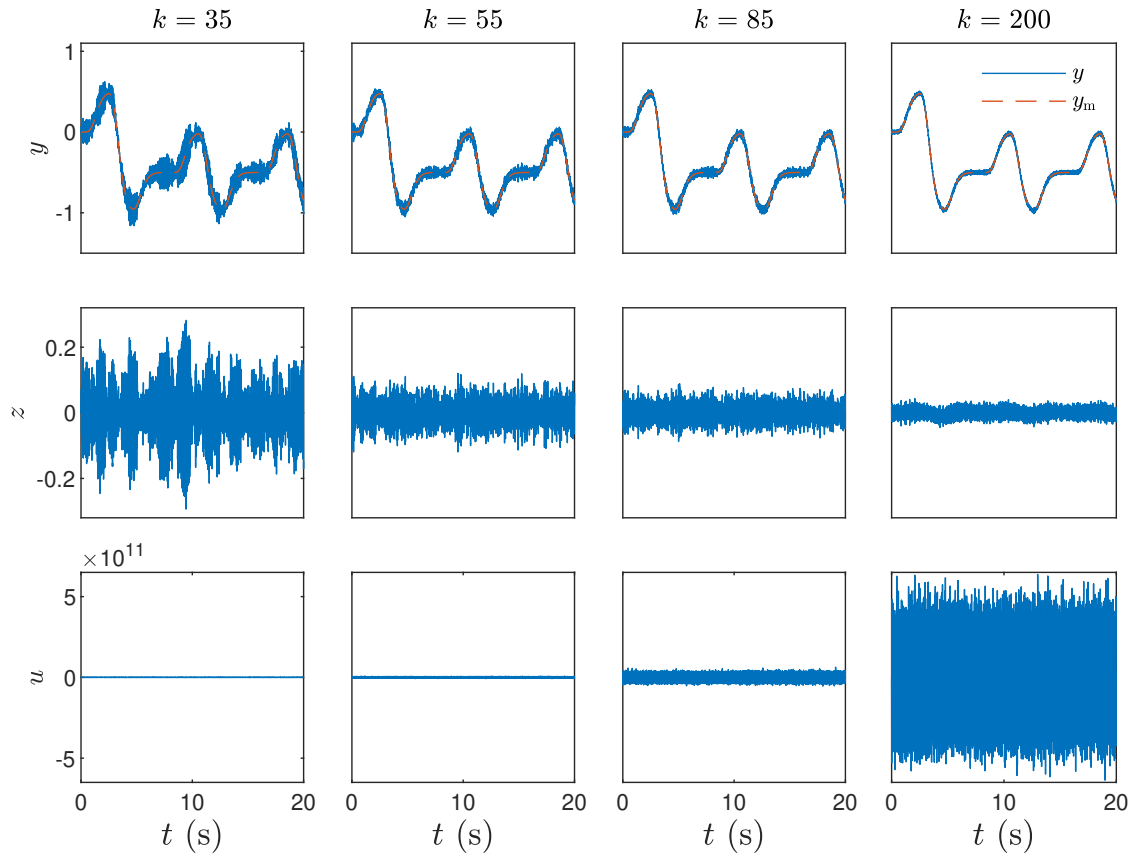


Figure 4.29: FDI control with  $k \in \{35, 55, 85, 200\}$  for the unstable mass-spring-damper system shown in Figure 4.14, with white-noise disturbance. The FDI controller (3.53)–(3.59), where  $k \in \{35, 55, 85, 200\}$ , is implemented in feedback with the mass-spring-damper system (4.25), (4.26), and (4.29). In this case,  $d = 4$ . The performance  $z$  degrades slightly in comparison to the disturbance free case which is shown in Figure 4.25. By increasing  $k$  to 200, the average power of the performance  $z$  decreases.



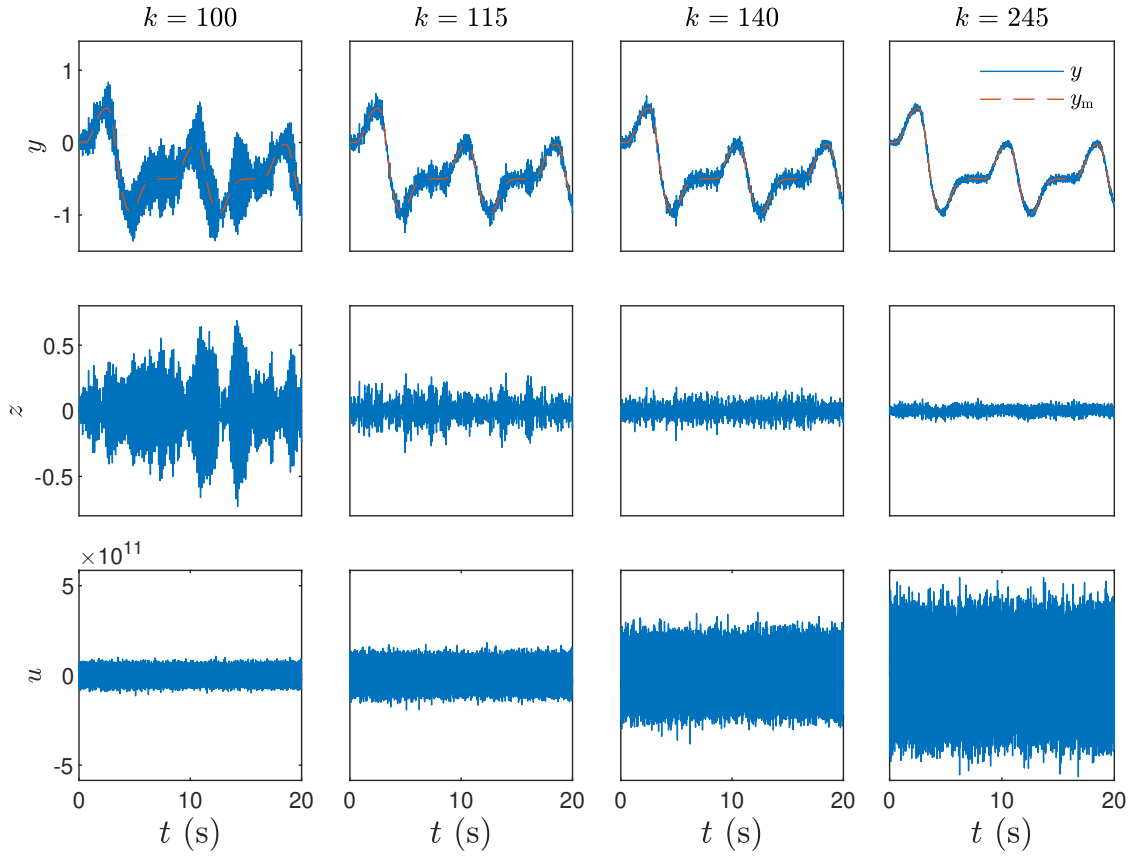


Figure 4.30: FDI control with  $k \in \{100, 115, 140, 245\}$  for the unstable mass-spring-damper system shown in Figure 4.14, with white-noise disturbance. The FDI controller (3.53)–(3.59), where  $k \in \{100, 115, 140, 245\}$ , is implemented in feedback with the mass-spring-damper system (4.25), (4.26), and (4.30). In this case,  $d = 5$ . The performance  $z$  degrades slightly in comparison to the disturbance free case which is shown in Figure 4.26. By increasing  $k$  to 245, the average power of the performance  $z$  decreases.

### 4.2.2 Serially Connected Mass-Spring-Damper System (MIMO)

Consider the serially connected mass-spring-damper system (4.20)–(4.24), where the masses are  $m_1 = m_2 = m_3 = m_4 = 1$  kg, the damping coefficients are  $c_1 = c_2 = c_3 = c_4 = 1$  kg/s, and the spring constants are  $k_1 = 2$  kg/s<sup>2</sup>,  $k_2 = 4$  kg/s<sup>2</sup>,  $k_3 = 1$  kg/s<sup>2</sup>, and  $k_4 = 3$  kg/s<sup>2</sup>. The mass-spring-damper system can be expressed as (3.1), (3.2), where  $x$  and  $w$  are given by (4.25), and  $A$  is given by (4.26).

We consider different choices of  $B$  and  $C$  (sensor and actuator placements). First, consider

$$B \triangleq \begin{bmatrix} 0_{4 \times 2} \\ \begin{bmatrix} 1 & 0 \\ 0 & 1 \\ 0 & 0 \\ 0 & 0 \end{bmatrix} \\ -M_0^{-1} \end{bmatrix}, \quad C \triangleq \begin{bmatrix} 1 & 0 & 0 & 0 & 0 & 0 & 0 & 0 \\ 0 & 1 & 0 & 0 & 0 & 0 & 0 & 0 \end{bmatrix}, \quad (4.33)$$

where the controls are the forces on the first and the second masses and the outputs are the positions of the first and the second masses. In this case,  $d = 2$  and the first nonzero Markov parameter is  $H_d = I_2$ . Also, (A3.1), (A3.2), and (A3.4) are satisfied. Next, consider

$$B \triangleq \begin{bmatrix} 0_{4 \times 2} \\ \begin{bmatrix} 1 & 0 \\ 0 & 0 \\ 0 & 0 \\ 0 & 1 \end{bmatrix} \\ -M_0^{-1} \end{bmatrix}, \quad C \triangleq \begin{bmatrix} 0 & 1 & 0 & 0 & 0 & 0 & 0 & 0 \\ 0 & 0 & 1 & 0 & 0 & 0 & 0 & 0 \end{bmatrix}, \quad (4.34)$$

where the controls are the forces on the first and the fourth masses and the outputs are the positions of the second and the third masses. In this case,  $d = 3$  and the first

nonzero Markov parameter is  $H_d = I_2$ . Also, (A3.1), (A3.2), and (A3.4) are satisfied.

The objective is to design the FDI controller (3.53)–(3.59) to control the mass-spring-damper system (3.1), (3.2), (4.21)–(4.25), and  $A$  is given by (4.26), where  $B$  and  $C$  could be either of the above choices. Note that the upper bound on the relative degree is  $\bar{d} = 3$ . We select the reference-model polynomials as

$$\alpha_m(\mathbf{p}) = (\mathbf{p} + 5)^3, \quad \beta_m(\mathbf{p}) = 125. \quad (4.35)$$

Next, let  $\rho = 4 > \bar{d}$ , and let

$$\eta_k(s) \triangleq s^4 + 6k^2s^3 + 8k^3s^2 + 6k^4s + 4k^5, \quad (4.36)$$

which satisfies (C3.1) and (C3.2). The initial conditions are  $x(0) = 0$  and  $x_c(0) = 0$ .

**Example 4.10.** *MIMO, disturbance free, serially connected mass-spring-damper system, with command following.* Consider the mass-spring-damper system (4.20) shown in Figure 4.14. The disturbances are identically 0 (i.e.,  $\psi_1 = \psi_2 = \psi_3 = \psi_4 = 0$ ). The reference-model command is  $r = \begin{bmatrix} r_1 & r_2 \end{bmatrix}^T$ , where  $r_1$  is a sequence of steps, passed through the filter  $G_r(s) = 10^3/(s + 10)^3$ , and  $r_2(t) = 0.5 \sin 2\pi t$ . The control objective is to force  $y$  to follow the output  $y_m$  of the reference model (3.5).

The FDI controller, where  $k \in \{15, 20, 30\}$ , is implemented in feedback with the mass-spring-damper system, where  $B$  and  $C$  are given by (4.33). Figure 4.31 shows the time history of  $y$ ,  $y_m$ ,  $z$ , and  $u$ . We notice that  $y$  follows  $y_m$  with a small but noticeable error. By increasing  $k$ , the average power of the performance  $z$  decreases.

Next, the FDI controller, where  $k \in \{45, 60, 80\}$ , is implemented in feedback with the mass-spring-damper system, where  $B$  and  $C$  are given by (4.34). Figure 4.32 shows the time history of  $y$ ,  $y_m$ ,  $z$ , and  $u$ . We notice that  $y$  follows  $y_m$  with a small but noticeable error. By increasing  $k$ , the average power of the performance  $z$

decreases.

△

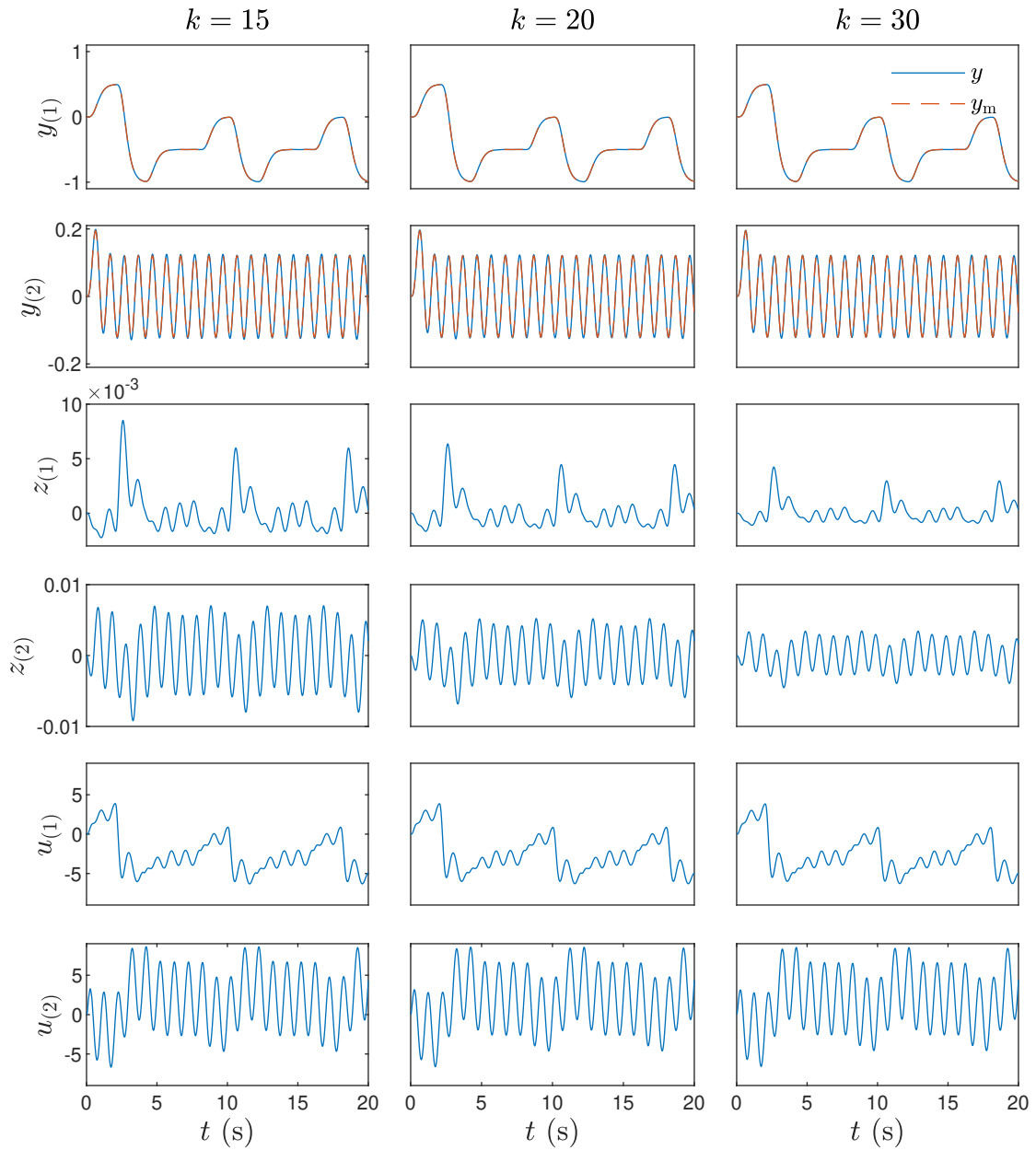


Figure 4.31: The FDI controller (3.53)–(3.59), where  $k \in \{15, 20, 30\}$ , is implemented in feedback with the mass-spring-damper system (3.1), (3.2), and (4.21)–(4.26).  $B$  and  $C$  are given by (4.33). In this case,  $d = 2$ . By increasing  $k$ , the performance  $z$  improves.

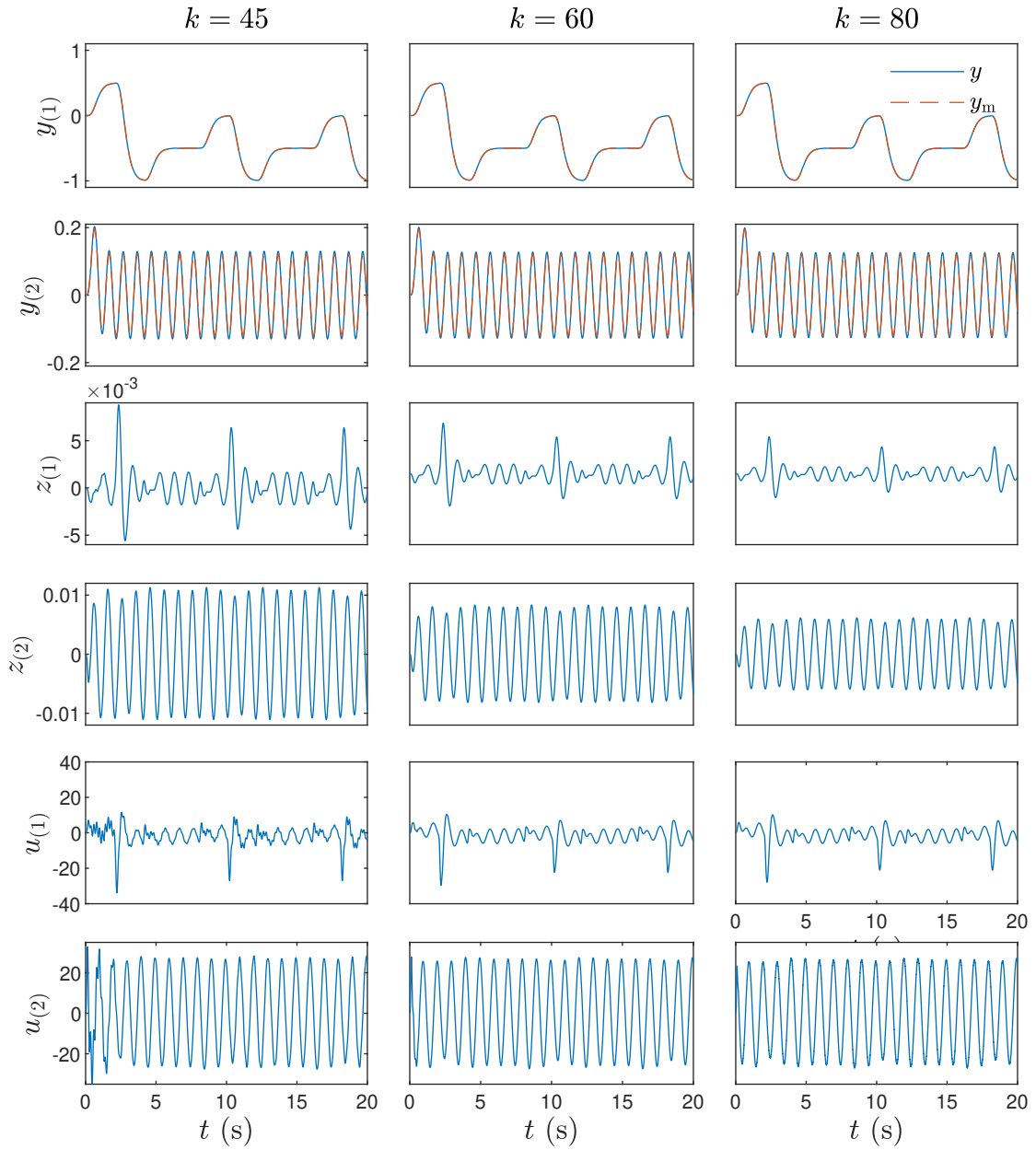


Figure 4.32: The FDI controller (3.53)–(3.59), where  $k \in \{45, 60, 80\}$ , is implemented in feedback with the mass-spring-damper system (3.1), (3.2), and (4.21)–(4.26).  $B$  and  $C$  are given by (4.34). In this case,  $d = 3$ . By increasing  $k$ , the performance  $z$  improves.

**Example 4.11.** *MIMO, serially connected mass-spring-damper system with command following and white-noise disturbance.* Consider the mass-spring-damper system (4.20) shown in Figure 4.14. The disturbances are  $\psi_1, \psi_2, \psi_3$ , and  $\psi_4$  are generated from independent zero-mean 20-variance Gaussian white-noise distributions. The reference-model command is  $r = \begin{bmatrix} r_1 & r_2 \end{bmatrix}^T$ , where  $r_1$  is a sequence of steps, passed through the filter  $G_r(s) = 10^3/(s + 10)^3$  and  $r_2(t) = 0.5 \sin 2\pi t$ . The control objective is to force  $y$  to follow the output  $y_m$  of the reference model (3.5).

The FDI controller, where  $k \in \{15, 20, 30, 50\}$ , is implemented in feedback with the MIMO mass-spring-damper system, where  $B$  and  $C$  are given by (4.33). Figure 4.33 shows the time history of  $y, y_m, z$ , and  $u$ . By comparing Figure 4.33 with Figure 4.31, we observe that the performance  $z$  degrades slightly in comparison to the disturbance free case. By increasing  $k$  to 50, the performance  $z$  improves.

Next, the FDI controller, and where  $k \in \{45, 60, 80, 250\}$ , is implemented in feedback with the MIMO system, where  $B$  and  $C$  are given by (4.34). Figure 4.34 shows the time history of  $y, y_m, z$ , and  $u$ . By comparing Figure 4.34 with Figure 4.32, we observe that the performance  $z$  degrades slightly in comparison to the disturbance free case. By increasing  $k$  to 250, the performance  $z$  improves.  $\triangle$

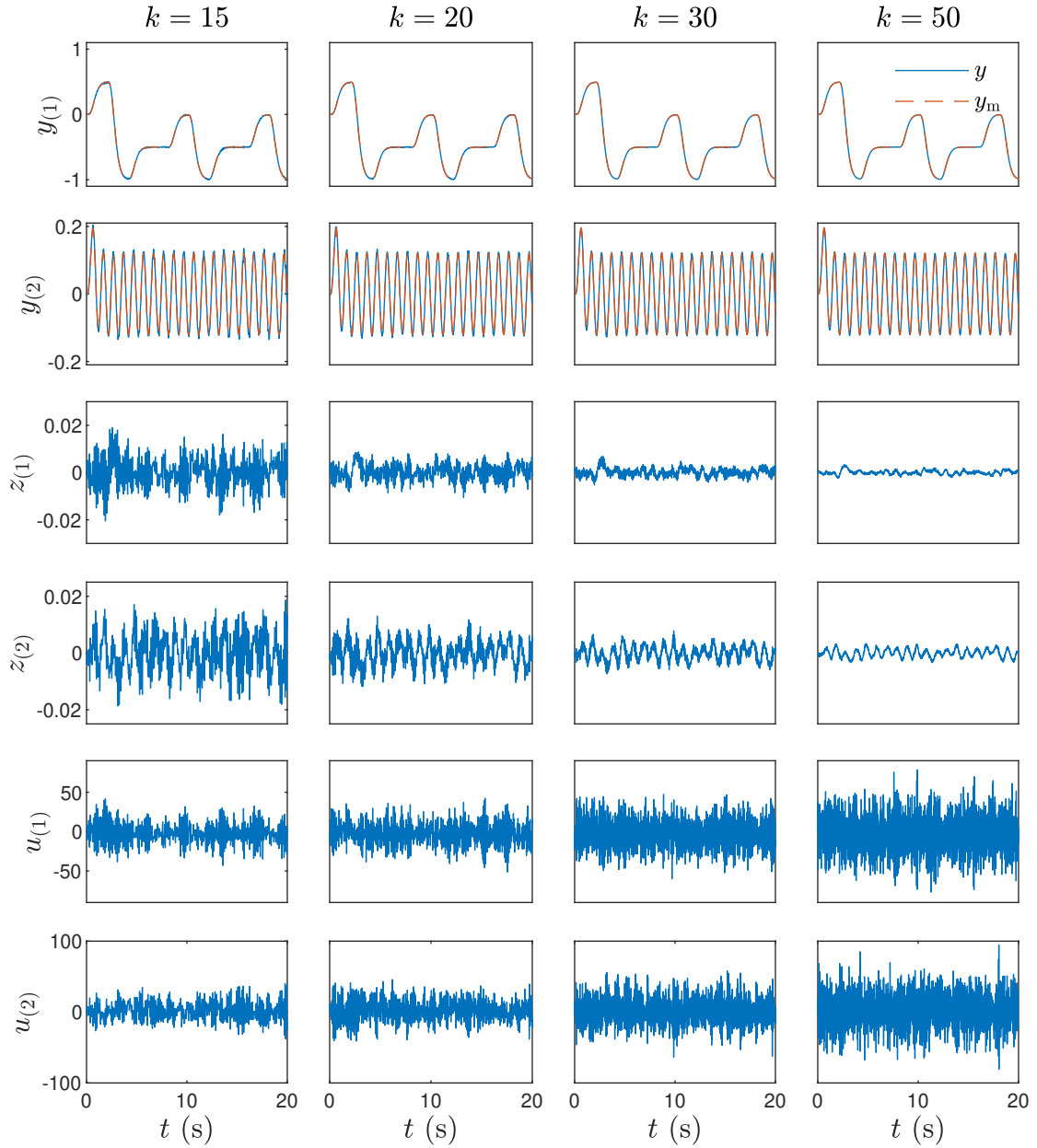


Figure 4.33: FDI control with  $k \in \{15, 20, 30, 50\}$  for the MIMO mass-spring-damper system with white-noise disturbance. The FDI controller (3.53)–(3.59), where  $k \in \{15, 20, 30, 50\}$ , is implemented in feedback with the mass-spring-damper system (3.1), (3.2), and (4.21)–(4.26).  $B$  and  $C$  are given by (4.33). In this case,  $d = 2$ . The performance  $z$  degrades slightly in comparison to the disturbance free case which is shown in Figure 4.31. By increasing  $k$  to 50, the performance  $z$  improves.

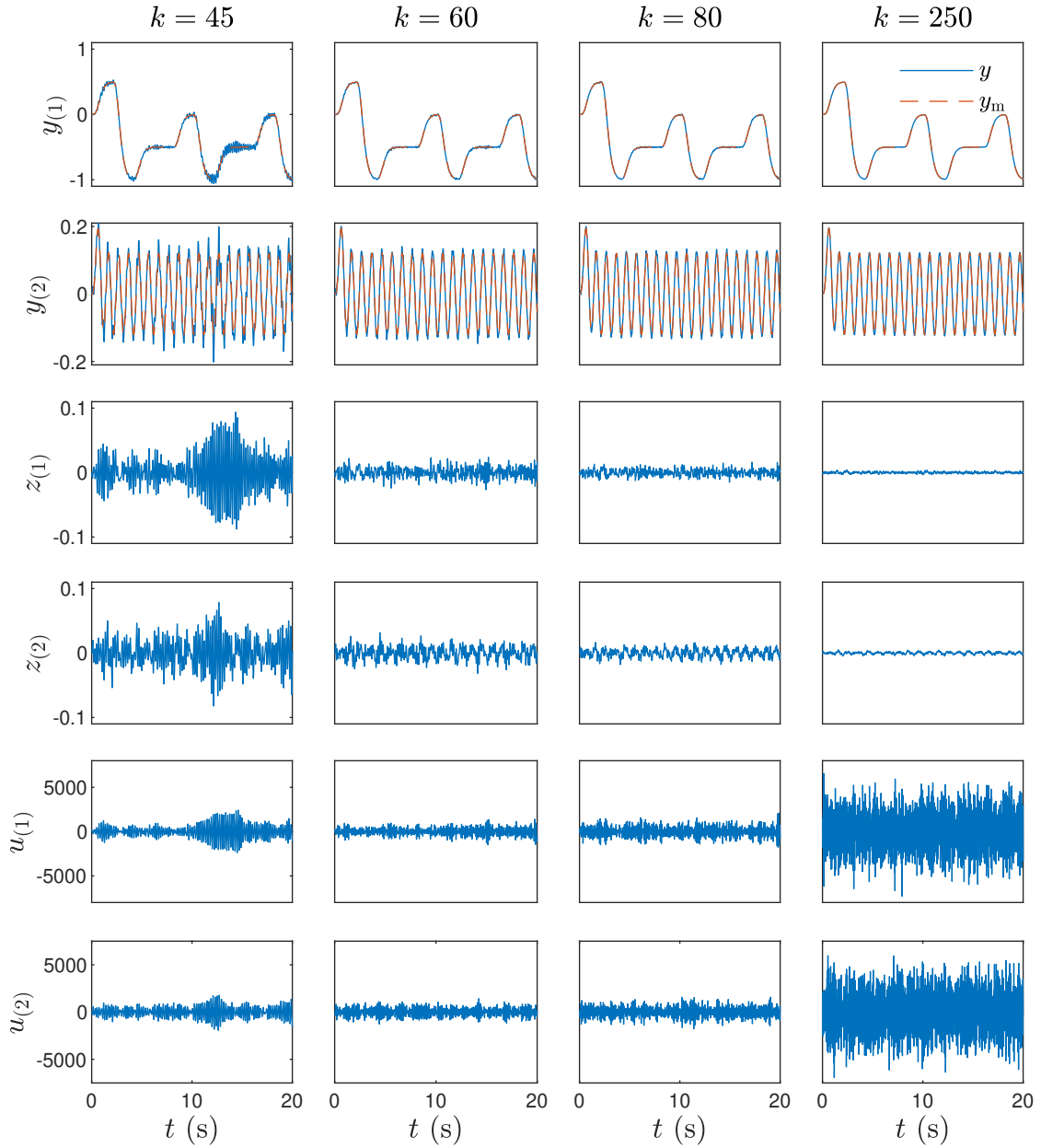


Figure 4.34: FDI control with  $k \in \{45, 60, 80, 250\}$  for the MIMO mass-spring-damper system with white-noise disturbance. The FDI controller (3.53)–(3.59), where  $k \in \{45, 60, 80, 250\}$ , is implemented in feedback with the mass-spring-damper system (3.1), (3.2), and (4.21)–(4.26).  $B$  and  $C$  are given by (4.34). In this case,  $d = 3$ . The performance  $z$  degrades slightly in comparison to the disturbance free case which is shown in Figure 4.32. By increasing  $k$  to 250, the performance  $z$  improves.



**Example 4.12.** *MIMO, unstable, disturbance free, serially connected mass-spring-damper system with command following.* Consider the mass-spring-damper system (4.20) shown in Figure 4.14, but the damping coefficient  $c_1 = -2$ . The resulting open-loop system is unstable. The disturbances are identically 0 (i.e.,  $\psi_1 = \psi_2 = \psi_3 = \psi_4 = 0$ ). The reference-model command is  $r = \begin{bmatrix} r_1 & r_2 \end{bmatrix}^T$ , where  $r_1$  is a sequence of steps, passed through the filter  $G_r(s) = 10^3/(s + 10)^3$ , and  $r_2(t) = 0.5 \sin 2\pi t$ . The control objective is to force  $y$  to follow the output  $y_m$  of the reference model (3.5).

The FDI controller, where  $k \in \{20, 30, 50\}$ , is implemented in feedback with the unstable mass-spring-damper system, where  $B$  and  $C$  are given by (4.33). Figure 4.35 shows the time history of  $y$ ,  $y_m$ ,  $z$ , and  $u$ . We notice that  $y$  follows  $y_m$  with a small but noticeable error. By increasing  $k$ , the average power of the performance  $z$  decreases.

Next, the FDI controller, and where  $k \in \{65, 80, 120\}$ , is implemented in feedback with the unstable mass-spring-damper system, where  $B$  and  $C$  are given by (4.34). Figure 4.36 shows the time history of  $y$ ,  $y_m$ ,  $z$ , and  $u$ . We notice that  $y$  follows reference model output  $y_m$  with a small but noticeable error. By increasing  $k$ , the average power of the performance  $z$  decreases. △

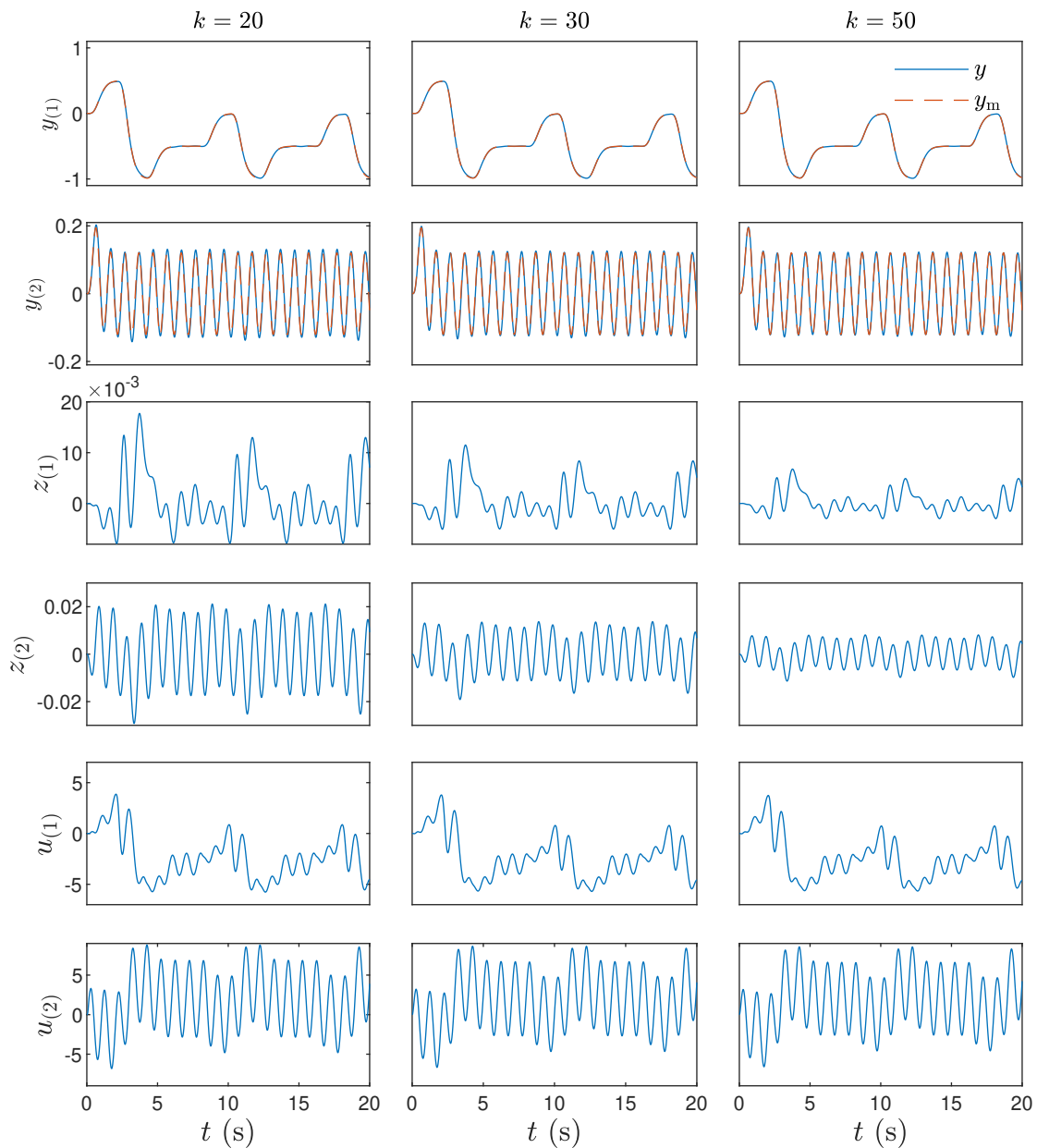


Figure 4.35: FDI control with  $k \in \{20, 30, 50\}$  for the unstable MIMO mass-spring-damper system (disturbance free). The FDI controller (3.53)–(3.59), where  $k \in \{20, 30, 50\}$ , is implemented in feedback with the mass-spring-damper system (3.1), (3.2), and (4.21)–(4.26).  $B$  and  $C$  are given by (4.33). In this case,  $d = 2$ . By increasing  $k$ , the performance  $z$  improves.

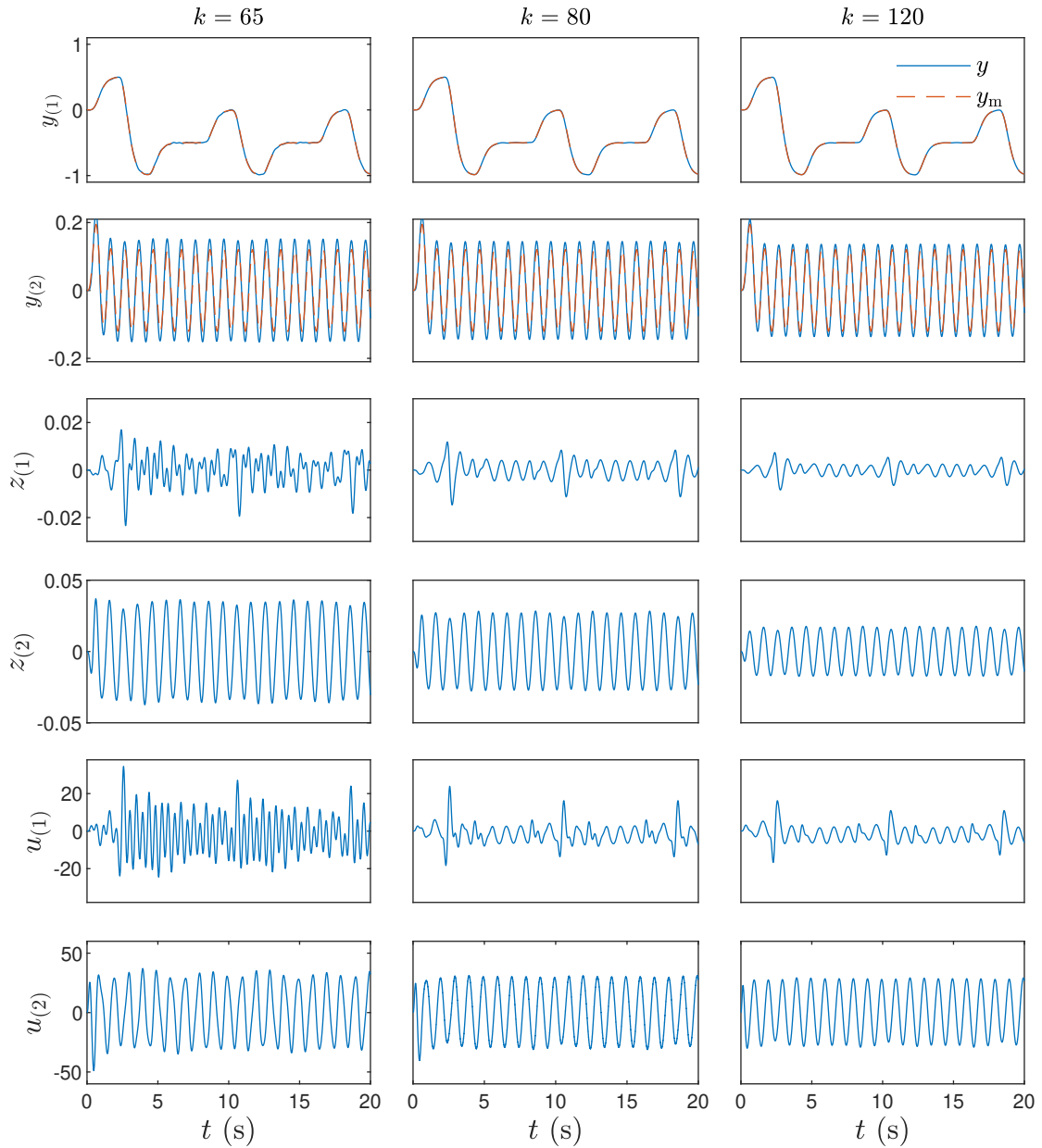


Figure 4.36: FDI control with  $k \in \{65, 80, 120\}$  for the unstable MIMO mass-spring-damper system (disturbance free). The FDI controller (3.53)–(3.59), where  $k \in \{65, 80, 120\}$ , is implemented in feedback with the mass-spring-damper system (3.1), (3.2), and (4.21)–(4.26).  $B$  and  $C$  are given by (4.34). In this case,  $d = 3$ . By increasing  $k$ , the performance  $z$  improves.

**Example 4.13.** *MIMO, unstable, serially connected mass-spring-damper system, with command following and white-noise disturbance.* Consider the mass-spring-damper system (4.20) shown in Figure 4.14, but the damping coefficient  $c_1 = -2$ . The resulting open-loop system is unstable. The disturbances  $\psi_1$ ,  $\psi_2$ ,  $\psi_3$ , and  $\psi_4$ , are generated from independent zero-mean 20-Newton-variance Gaussian white-noise distributions. The reference-model command is  $r = \begin{bmatrix} r_1 & r_2 \end{bmatrix}^T$ , where  $r_1$  is a sequence of steps passed through the filter  $G_r(s) = 10^3/(s + 10)^3$  and  $r_2(t) = 0.5 \sin 2\pi t$ . The control objective is to force  $y$  to follow the output  $y_m$  of the reference model (3.5).

The FDI controller, where  $k \in \{20, 30, 50, 80\}$ , is implemented in feedback with the MIMO mass-spring-damper system, where  $B$  and  $C$  are given by (4.33). Figure 4.37 shows the time history of  $y$ ,  $y_m$ ,  $z$ , and  $u$ . By comparing Figure 4.37 with Figure 4.35, we observe that the performance degrades slightly in comparison to disturbance free case. By increasing  $k$  to 80, the performance  $z$  improves.

Next, the FDI controller, and where  $k \in \{65, 80, 120, 300\}$ , is implemented in feedback with the MIMO mass-spring-damper system, where  $B$  and  $C$  are given by (4.34). Figure 4.38 shows the time history of  $y$ ,  $y_m$ ,  $z$ , and  $u$ . By comparing Figure 4.38 with Figure 4.36, we observe that the performance degrades slightly in comparison to disturbance free case. By increasing  $k$  to 300, the performance  $z$  improves.  $\triangle$

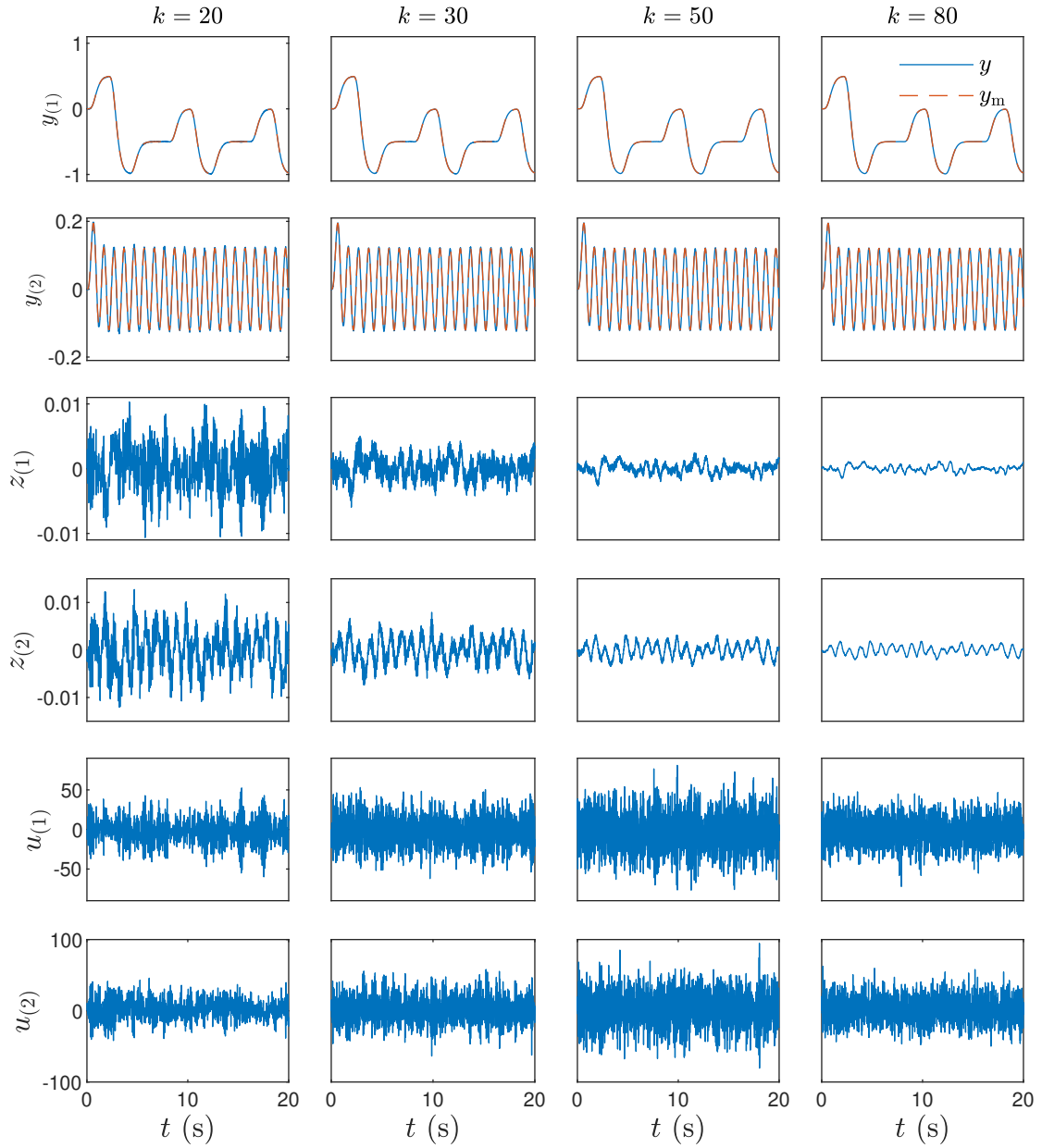


Figure 4.37: FDI control with  $k \in \{20, 30, 50, 80\}$  for the unstable MIMO mass-spring-damper system with white-noise disturbance. The FDI controller (3.53)–(3.59), where  $k \in \{20, 30, 50, 80\}$ , is implemented in feedback with the mass-spring-damper system (3.1), (3.2), and (4.21)–(4.26).  $B$  and  $C$  are given by (4.33). In this case,  $d = 2$ . By comparing with Figure 4.35, we observe that the performance  $z$  degrades slightly in comparison to the disturbance free case. By increasing  $k$  to 80, the performance  $z$  improves.

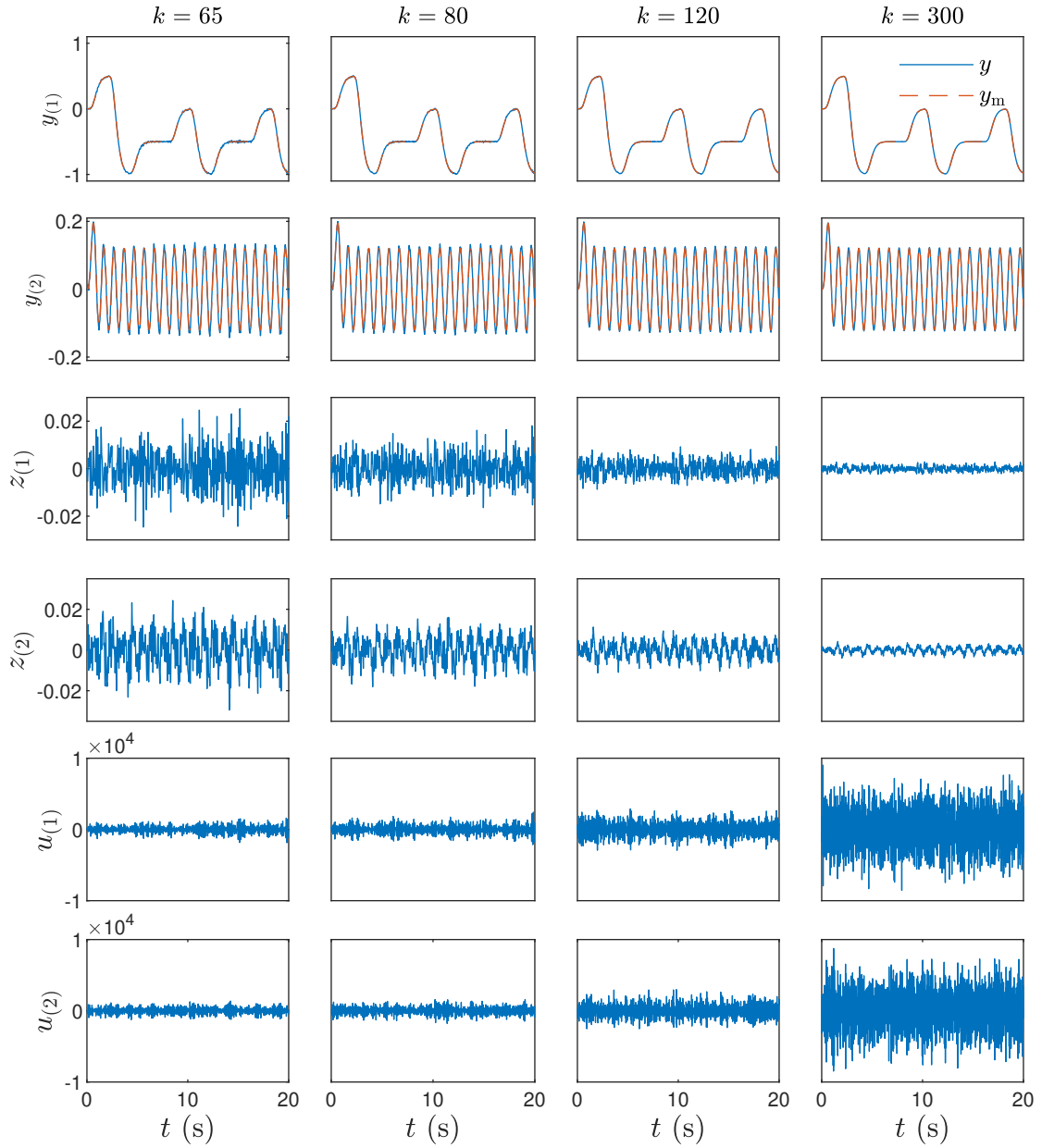


Figure 4.38: FDI control with  $k \in \{65, 80, 120, 300\}$  for the unstable MIMO mass-spring-damper system with white-noise disturbance. The FDI controller (3.53)–(3.59), where  $k \in \{65, 80, 120, 300\}$ , is implemented in feedback with the mass-spring-damper system (3.1), (3.2), and (4.21)–(4.26).  $B$  and  $C$  are given by (4.34). In this case,  $d = 3$ . By comparing with Figure 4.36, we observe that the performance  $z$  degrades slightly in comparison to the disturbance free case. By increasing  $k$  to 300, the performance  $z$  improves.

### 4.2.3 Two-Mass Servo System with Flexible Shaft

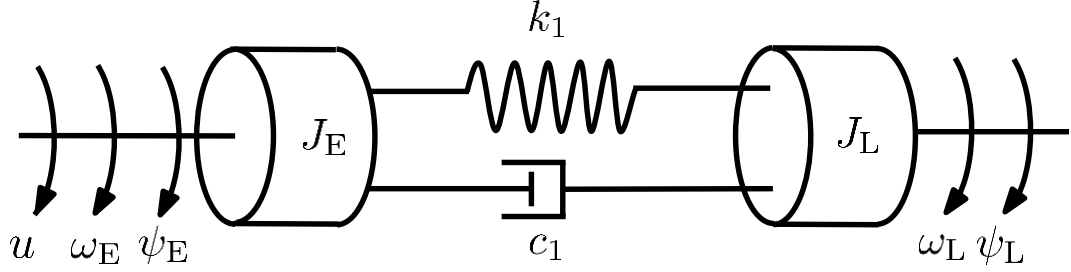


Figure 4.39: Two-mass servo system with flexible shaft.

Consider the two-mass servo system with flexible shaft shown in Figure 4.39, which has the equations of motion

$$\dot{\omega}_L(t) = -\frac{c_1}{J_L}\omega_L(t) + \frac{k_1}{J_L}\theta(t) + \frac{c_1}{J_L}\omega_E(t) + \frac{\psi_L(t)}{J_L}, \quad (4.37)$$

$$\dot{\theta}(t) = -\omega_L(t) + \omega_E(t), \quad (4.38)$$

$$\dot{\omega}_E(t) = \frac{c_1}{J_E}\omega_L(t) - \frac{k_1}{J_E}\theta(t) - \frac{c_1}{J_E}\omega_E(t) + \frac{\psi_E(t)}{J_E} + \frac{1}{J_E}u(t), \quad (4.39)$$

where  $\omega_L$  is the angular velocity of the load,  $\omega_E$  is the angular velocity of the electric drive, and  $\theta$  is the angle of twist between the electric drive and the load.  $c_1 = 0.1$  Nm/rad is the damping coefficient of the shaft.  $k_1 = 40$  Nms/rad is the stiffness of the shaft.  $J_L = 0.2$  kgm<sup>2</sup> is the moment of inertia of the load.  $J_E = 0.1$  kgm<sup>2</sup> is the moment of inertia of the electric drive. Note that  $\psi_L$  and  $\psi_E$  are the unknown-and-unmeasured disturbances acting on the load and the electric drive.  $u$  is the control. It follows that (4.37)–(4.39) can be expressed as (3.1), where

$$x(t) \triangleq \begin{bmatrix} \omega_L(t) \\ \theta(t) \\ \omega_E(t) \end{bmatrix}, \quad w(t) \triangleq \begin{bmatrix} \frac{\psi_L(t)}{J_L} \\ 0 \\ \frac{\psi_E(t)}{J_E} \end{bmatrix}, \quad (4.40)$$

$$A \triangleq \begin{bmatrix} \frac{-c_1}{J_L} & \frac{k_1}{J_L} & \frac{c_1}{J_L} \\ -1 & 0 & 1 \\ \frac{c_1}{J_E} & \frac{-k_1}{J_E} & \frac{-c_1}{J_E} \end{bmatrix}, \quad B \triangleq \begin{bmatrix} 0 \\ 0 \\ \frac{1}{J_E} \end{bmatrix}, \quad (4.41)$$

We consider different choices of  $C$  (i.e., sensor placements). First, consider

$$C \triangleq \begin{bmatrix} 0 & 0 & 1 \end{bmatrix}, \quad (4.42)$$

where  $\omega_E$  is measured at output. In this case,  $d = 1$ , and the first nonzero Markov parameter is  $H_d = 10$ . Also, (A3.1), (A3.2), and (A3.4) are satisfied. Next, consider

$$C \triangleq \begin{bmatrix} 1 & 0 & 0 \end{bmatrix}, \quad (4.43)$$

where,  $\omega_L$  is measured at output. In this case,  $d = 2$ , and the first nonzero Markov parameter is  $H_d = 10$ . Also, (A3.1), (A3.2), and (A3.4) are satisfied.

The objective is to design an FDI controller for the two-mass servo system with flexible shaft (3.1), (3.2), (4.40), and (4.41), and where  $C$  could be either of the above choices. Note that the upper bound on the relative degree is  $\bar{d} = 2$ . We select the reference-model polynomials as

$$\alpha_m(\mathbf{p}) = (\mathbf{p} + 5)^2, \quad \beta_m(\mathbf{p}) = 25. \quad (4.44)$$

Next, let  $\rho = 3 > \bar{d}$ , and let

$$\eta_k(s) \triangleq s^3 + 18ks^2 + 36k^2s + 18k^3. \quad (4.45)$$

**Example 4.14.** *Two-mass servo system with flexible shaft, command following, disturbance free.* Consider the two-mass flexible servo system 3.1), (3.2), (4.40), and (4.41). The disturbances are identically 0 (i.e.,  $\psi_L = \psi_E = 0$ ). The reference-



model command  $r$  is a sequence of steps, which are passed through the filter  $G_r(s) = 10^2/(s + 10)^2$ . The control objective is to force  $y$  to follow the output  $y_m$  of the reference model (3.5).

The FDI controller (3.53)–(3.59), where  $\eta_k$  is given by (4.45) and  $k \in \{5, 10, 20\}$ , is implemented in feedback with the two-mass flexible servo system, where  $C$  is given by (4.42). In this case,  $d = 1$ . Figure 4.40 shows the time history of  $y$ ,  $y_m$ ,  $z$ , and  $u$ . We notice that  $y$  follows  $y_m$  with a small but noticeable error. By increasing  $k$ , the performance  $z$  improves.

Next, the FDI controller (3.53)–(3.59), where  $\eta_k$  is given by (4.45) and  $k \in \{480, 650, 900\}$ , is implemented in feedback with the two-mass flexible servo system, where  $C$  is given by (4.43). In this case,  $d = 2$ . Figure 4.41 shows the time history of  $y$ ,  $y_m$ ,  $z$ , and  $u$ . We notice that  $y$  follows  $y_m$  with a small but noticeable error. By increasing  $k$ , the performance  $z$  improves. △

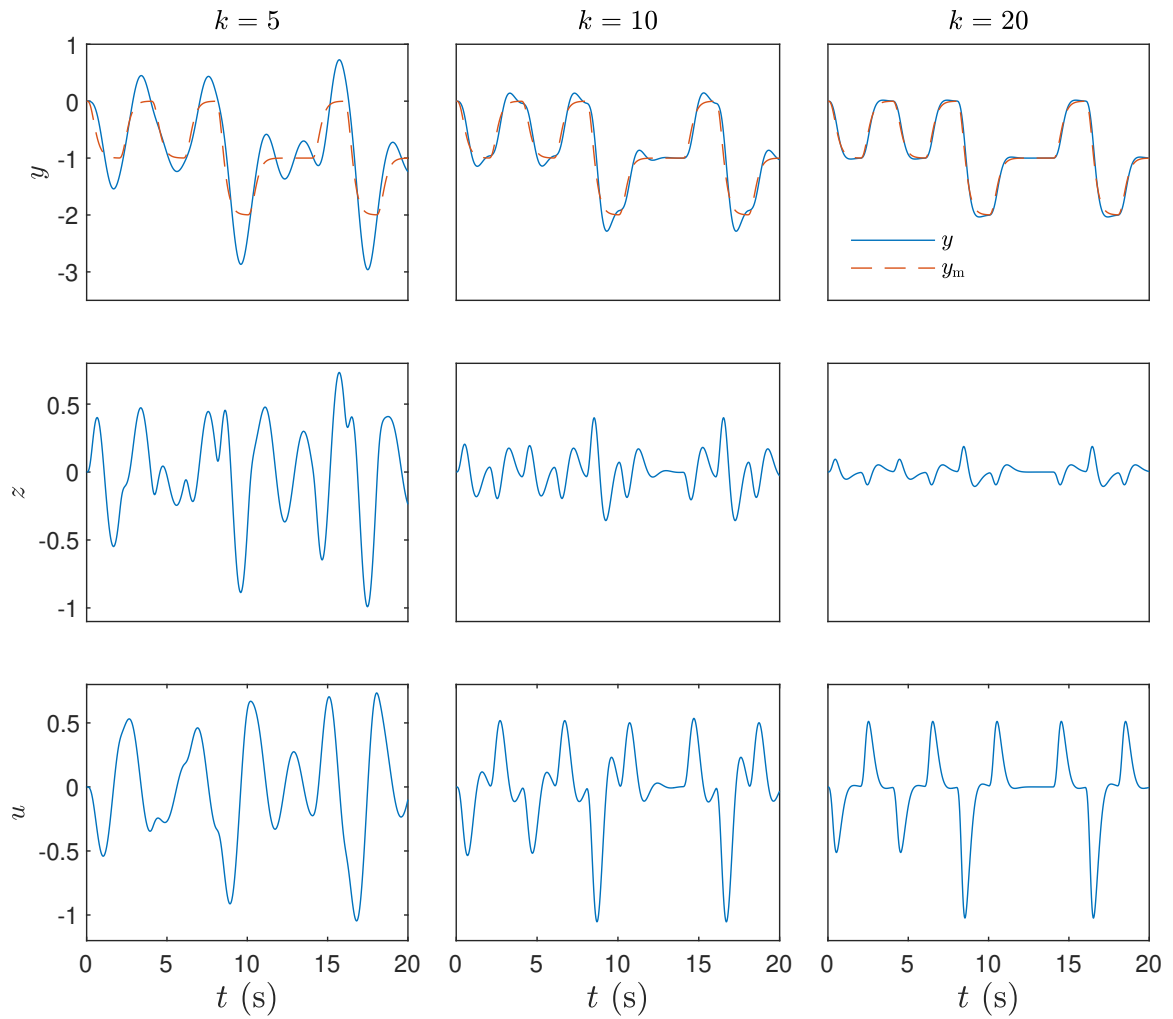


Figure 4.40: The FDI controller (3.53)–(3.59), where  $k \in \{5, 10, 20\}$ , is implemented in feedback with the two-mass servo system with flexible shaft (4.40)–(4.42). In this case,  $d = 1$ . The angular velocity of the electric drive  $\omega_E$  is measured at output. By increasing  $k$ , the performance  $z$  improves.

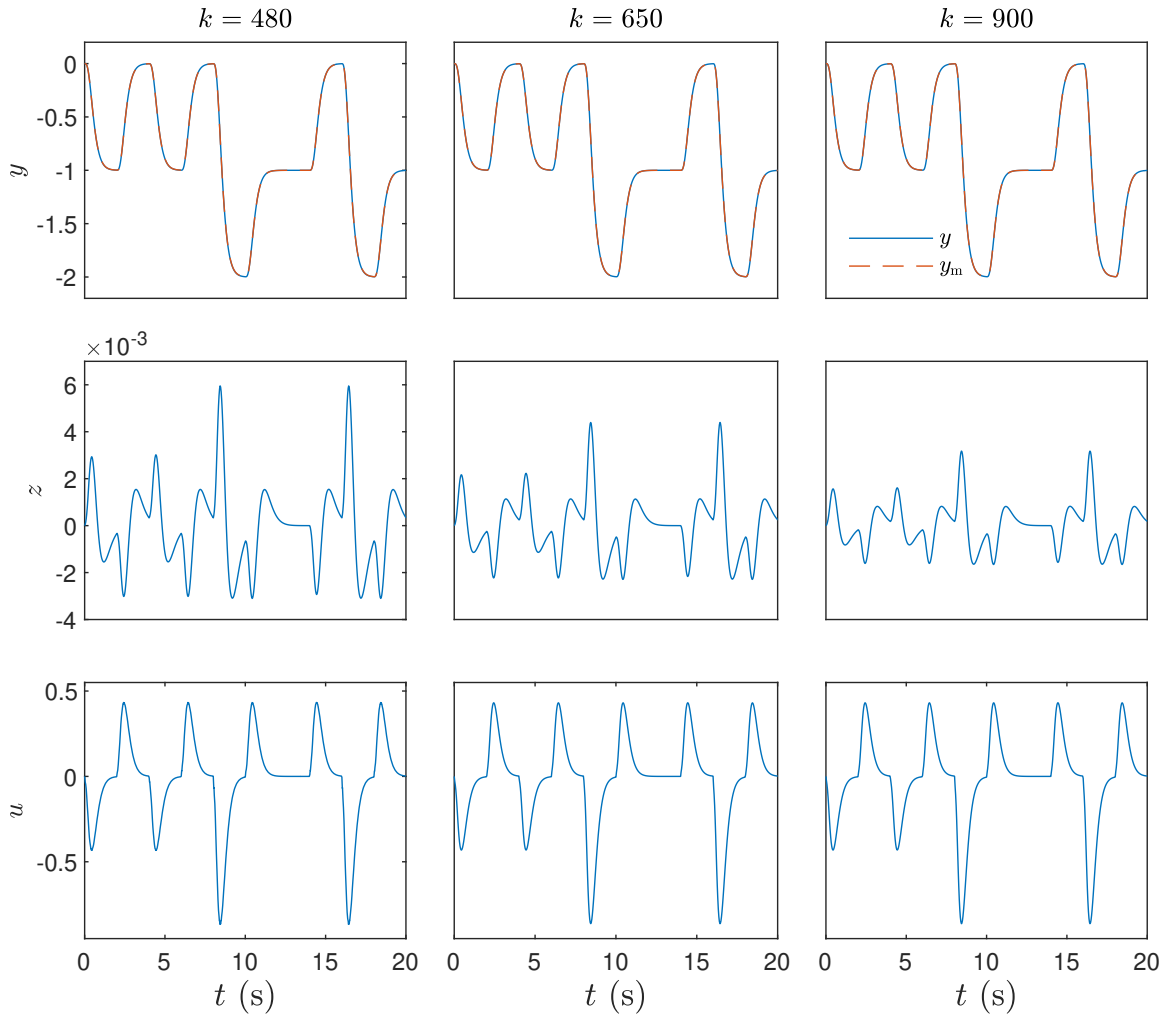


Figure 4.41: The FDI controller (3.53)–(3.59), where  $k \in \{480, 650, 900\}$ , is implemented in feedback with the two-mass servo system with flexible shaft (4.40), (4.41), and (4.43). In this case,  $d = 2$ . The angular velocity of the load  $\omega_L$  is measured at output. By increasing  $k$ , the performance  $z$  improves.

**Example 4.15.** *Two-mass servo system with flexible shaft, command following, white-noise disturbance.* Consider the two-mass flexible servo system (3.1), (3.2), (4.40), and (4.41). The disturbances are generated from independent zero-mean 20-variance Gaussian white-noise distributions. The reference-model command  $r$  is a sequence of steps, which are passed through the filter  $G_r(s) = 10^2/(s + 10)^2$ . The control objective is to force  $y$  to follow the output  $y_m$  of the reference model (3.5).

The FDI controller (3.53)–(3.59), where  $\eta_k$  is given by (4.45) and  $k \in \{5, 10, 20, 100\}$ , is implemented in feedback with the two-mass flexible servo system, where  $C$  is given by (4.42). In this case,  $d = 1$ . Figure 4.42 shows the time history of  $y$ ,  $y_m$ ,  $z$ , and  $u$ . By comparing Figure 4.42 with Figure 4.40, we observe that the performance  $z$  degrades slightly in comparison to disturbance free case. By increasing  $k$  to 100, the performance  $z$  improves.

Next, the FDI controller (3.53)–(3.59), where  $\eta_k$  is given by (4.45) and  $k \in \{480, 650, 900, 2500\}$ , is implemented in feedback with the two-mass flexible servo system, where  $C$  is given by (4.43). In this case,  $d = 2$ . Figure 4.43 shows the time history of  $y$ ,  $y_m$ ,  $z$ , and  $u$ . By comparing Figure 4.43 with Figure 4.41, we observe that the performance  $z$  degrades slightly in comparison to disturbance free case. By increasing  $k$  to 2500, the performance  $z$  improves.  $\triangle$

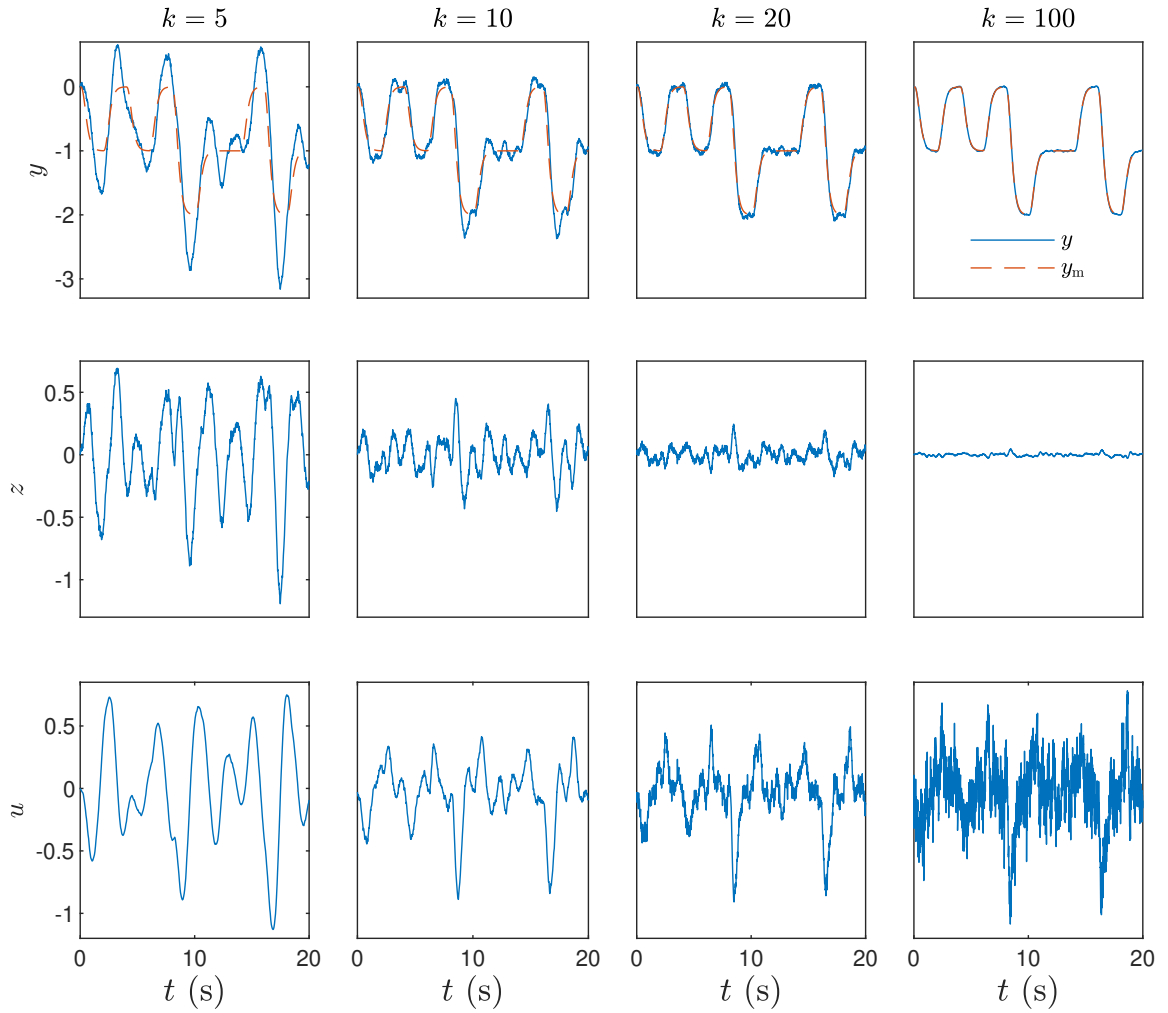


Figure 4.42: The FDI controller (3.53)–(3.59), where  $k \in \{5, 10, 20, 100\}$ , is implemented in feedback with the two-mass servo system with flexible shaft (4.40)–(4.42). In this case,  $d = 1$ . The angular velocity of the electric drive  $\omega_E$  is measured at output. The performance  $z$  decreases slightly in comparison to the disturbance free case as shown in Figure 4.40. By increasing  $k$  to 100, the performance  $z$  improves.

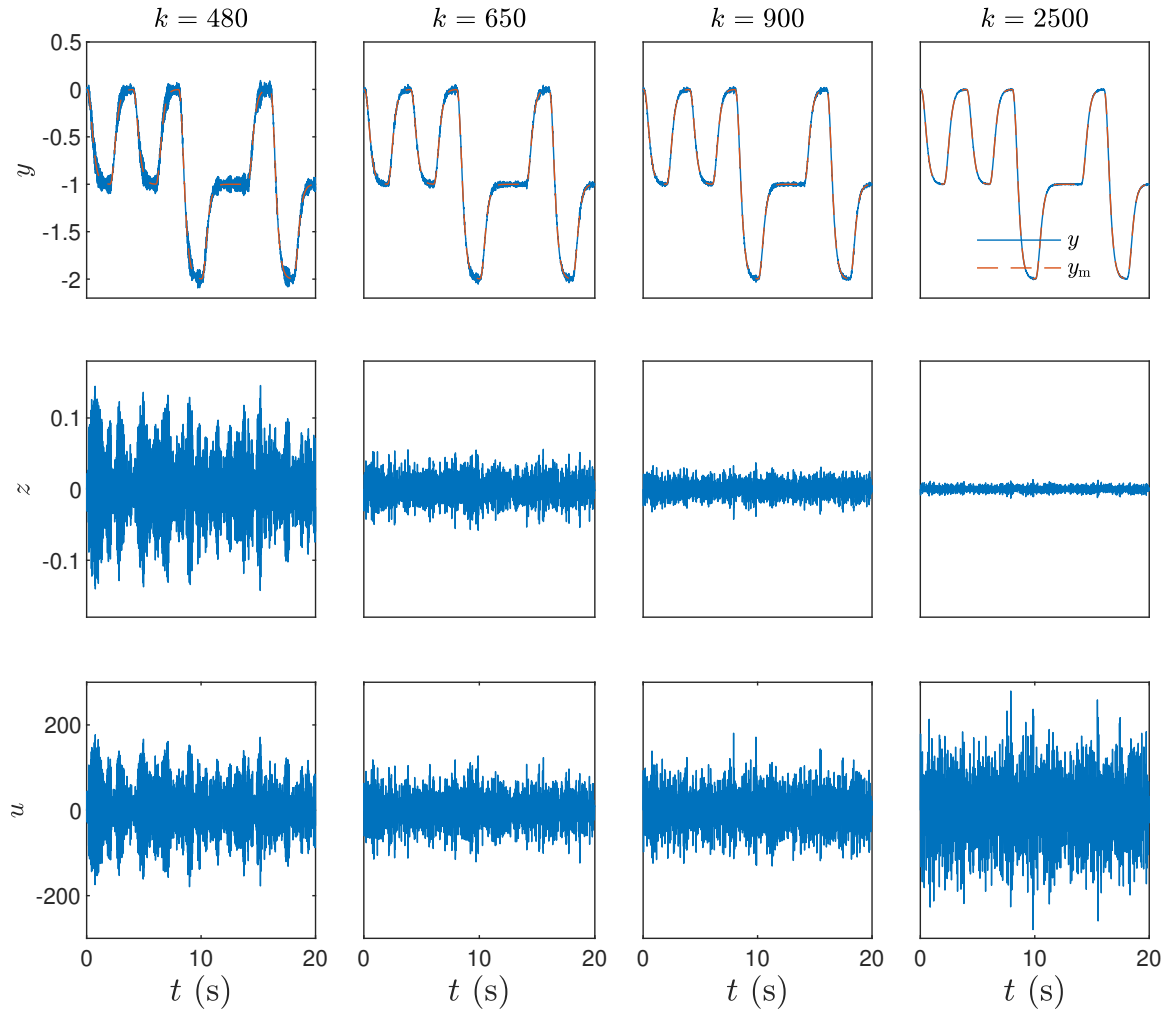


Figure 4.43: The FDI controller (3.53)–(3.59), where  $k \in \{480, 650, 900, 2500\}$ , is implemented in feedback with the two-mass servo system with flexible shaft (4.40), (4.41), and (4.43). In this case,  $d = 2$ . The angular velocity of the load  $\omega_L$  is measured at output. The performance  $z$  decreases slightly in comparison to the disturbance free case as shown in Figure 4.41. By increasing  $k$  to 2500, the performance  $z$  improves.

# Chapter 5

---

## Conclusions and Future Work

In this thesis, Chapter 2 reviewed the filtered dynamic inversion (FDI) controller presented in [26,27] and presented an example demonstrating that FDI is not necessarily robust to uncertainty in the relative degree. This provided the motivation of work in this thesis.

In Chapter 3, we extended the FDI control to accommodate unknown relative degree. This extended FDI control is a method for unknown linear time-invariant (LTI) systems that are multi-input multi-output (MIMO) and minimum phase with unknown-but-bounded relative degree. The FDI controller requires limited model information, specifically, knowledge of an upper bound on the relative degree and the first nonzero Markov parameter. This FDI controller is a single-parameter high-parameter-stabilizing controller that is robust to uncertainty in the relative degree. We show that the origin of the closed-loop system, consisting of the FDI controller for unknown relative degree connected in feedback with a single-input single-output (SISO) open-loop system, is an asymptotically stable equilibrium.

In Chapter 4, we presented numerical examples, where the FDI controller is implemented in feedback with mathematical and physical systems. We implemented a

single FDI controller for unknown relative degree in feedback with a single integrator, double integrator, and triple integrator. We then implemented an FDI controller for unknown relative degree in feedback with a MIMO system, where we consider different choices of input matrices and output matrices, which result in different relative degrees. We implemented an FDI controller for unknown relative degree in feedback with a serially connected mass-spring-damper system with different choices of sensor and actuator placements, which result in different relative degrees. Finally, we implemented an FDI controller in feedback with a two-mass servo system with a flexible shaft with different choices of sensor placements, which result in different relative degrees. The numerical examples demonstrated that the FDI controller for unknown relative degree is effective for stabilization, command following, and disturbance rejection with limited modeling information. We demonstrated that for a sufficiently large parameter, the average power of the closed-loop performance is arbitrarily small.

## 5.1 Future Work

First, we need to address the open questions in the thesis. We need to show that  $\eta_k$  given by (3.42), which satisfies (C3.1), also satisfies (C3.2). We need to characterize the performance of the closed-loop SISO system. We need to also characterize the stability and the performance of the closed-loop MIMO system.

Next, we consider the extensions that can be made to the FDI control for unknown relative degree. We can extend the FDI control for unknown relative degree to address uncertainty in the high-frequency gain, thus weakening (A3.4). We suggest that the FDI control method presented in this thesis can be extended to address stabilization, command following, and disturbance rejection for MIMO decentralized subsystems, which would be an extension of the FDI control presented in [27]. We can further extend the FDI controller for unknown relative degree presented in this



thesis to control nonlinear systems, which would be an extension of filtered feedback linearization presented in [30,31]. Note that for nonlinear systems, we would consider the vector relative degree and the dynamic-inversion matrix.

## Bibliography

- [1] J. Mullen, S. C. Bailey, and J. B. Hoagg, “Filtered dynamic inversion for altitude control of fixed-wing unmanned air vehicles,” *Aerospace Science and Technology*, vol. 54, pp. 241–252, 2016.
- [2] J. B. Hoagg, J. Chandrasekar, and D. S. Bernstein, “On the zeros, initial undershoot, and relative degree of collinear lumped-parameter structures,” *Journal of Dynamic Systems, Measurement, and Control*, vol. 129, no. 4, pp. 493–502, 2006.
- [3] M. Ben Hariz, F. Bouani, and M. Ksouri, “Robust controller for uncertain parameters systems,” *ISA Transactions*, vol. 51, no. 5, pp. 632–640, 2012.
- [4] H. Ambrose and Z. Qu, “Model reference robust control for MIMO systems,” *International Journal of Control*, vol. 68, no. 3, pp. 599–624, 1997.
- [5] H. Ayad, F. Mesquine, and M. A. Rami, “Robust control for uncertain linear systems with state and control constraints,” *IFAC Proceedings Volumes*, vol. 41, no. 2, pp. 1153–1158, 2008.
- [6] R. Sakthivel, S. Santra, K. Mathiyalagan, and A. Arunkumar, “Reliable robust control design for uncertain mechanical systems,” *Journal of Dynamic Systems, Measurement, and Control*, vol. 137, no. 2, 2015.

- [7] O. U. Rehman, I. R. Petersen, and H. Pota, “Nonlinear robust state feedback control system design for nonlinear uncertain systems,” *International Journal of Robust and Nonlinear Control*, vol. 27, no. 13, pp. 2234–2252, 2017.
- [8] A. A. Bobtsov and S. A. Holunin, “Adaptive control design of linear system with unknown parameters via output1,” *IFAC Proceedings Volumes*, vol. 37, no. 12, pp. 597–601, 2004.
- [9] X. Zou, J. Luo, and C. Cao, “Adaptive control for uncertain hysteretic systems,” *Journal of Dynamic Systems, Measurement, and Control*, vol. 136, no. 1, 2014.
- [10] W. M. Haddad and T. Hayakawa, “Direct adaptive control for non-linear uncertain systems with exogenous disturbances,” *International Journal of Adaptive Control and Signal Processing*, vol. 16, no. 2, pp. 151–172, 2002.
- [11] A. L. Fradkov, “Synthesis of an adaptive system for linear plant stabilization,” *Automat. Remote Control*, vol. 35, pp. 1960–1966, 1974.
- [12] C. I. Byrnes and J. C. Willems, “Adaptive stabilization of multivariable linear systems.” in *Proceedings of the IEEE Conference on Decision and Control*, 1984, pp. 1574–1577.
- [13] J. C. Willems and G. Byrnes, “Global adaptive stabilization in the absence of information on the sign of the high frequency gain,” in *Lecture Notes Control and Information Sciences*, vol. 62. New York: SpringerVerlag, 1984, pp. 49–57.
- [14] A. Ilchmann, *Non-Identifier-Based High-Gain Adaptive Control*. Berlin, Heidelberg: Springer-Verlag, 1993.
- [15] A. Ilchmann and E. Ryan, “Universal -tracking for nonlinearly-perturbed systems in the presence of noise,” *Automatica*, vol. 30, no. 2, pp. 337–346, 1994.

- [16] F. Allgöwer, J. Ashman, and A. Ilchmann, “High-gain adaptive -tracking for nonlinear systems,” *Automatica*, vol. 33, no. 5, pp. 881–888, 1997.
- [17] A. Ilchmann and E. P. Ryan, “On gain adaptation in adaptive control,” *IEEE Transactions on Automatic Control*, vol. 48, no. 5, pp. 895–899, 2003.
- [18] C. Zhao and D. Li, “Control design for the SISO system with the unknown order and the unknown relative degree,” *ISA Transactions*, vol. 53, no. 4, pp. 858–872, 2014.
- [19] D. Miller and E. Davison, “An adaptive controller which provides an arbitrarily good transient and steady-state response,” *IEEE Transactions on Automatic Control*, vol. 36, no. 1, pp. 68–81, 1991.
- [20] G. Tao and P. Ioannou, “Model reference adaptive control for plants with unknown relative degree,” *IEEE Transactions on Automatic Control*, vol. 38, no. 6, pp. 976–982, 1993.
- [21] R. G. Moctezuma, R. Lozano, and D. A. Suarez, “Model reference adaptive control with unknown relative degree,” in *Proceedings of 32nd IEEE Conference on Decision and Control*, 1993, pp. 1087–1092.
- [22] G. Bartolini, A. Ferrara, and A. Stotsky, “Stability and exponential stability of an adaptive control scheme for plants of any relative degree,” *IEEE Transactions on Automatic Control*, vol. 40, no. 1, pp. 100–104, 1995.
- [23] J. B. Hoagg and D. S. Bernstein, “Direct adaptive dynamic compensation for minimum phase systems with unknown relative degree,” *IEEE Transactions on Automatic Control*, vol. 52, no. 4, pp. 610–621, 2007.
- [24] J. B. Hoagg and D. S. Bernstein, “Direct adaptive command following and disturbance rejection for minimum phase systems with unknown relative degree,”

- International Journal of Adaptive Control and Signal Processing*, vol. 21, no. 1, pp. 49–75, 2007.
- [25] M. Wang, Y. Liu, and Y. Man, “Global outputfeedback stabilization for nonlinear systems with unknown relative degree,” *International Journal of Robust and Nonlinear Control*, vol. 28, no. 4, pp. 1425–1439, 2018.
- [26] J. B. Hoagg and T. M. Seigler, “Filtered-dynamic-inversion control for unknown minimum-phase systems with unknown-and-unmeasured disturbances,” *International Journal of Control*, vol. 86, no. 3, pp. 449–468, 2013.
- [27] J. B. Hoagg and T. M. Seigler, “Decentralized filtered dynamic inversion for uncertain minimum-phase systems,” *Automatica*, vol. 61, pp. 192–200, 2015.
- [28] T. M. Seigler and J. B. Hoagg, “Filtered dynamic inversion for vibration control of structures with uncertainty,” *Journal of Dynamic Systems, Measurement, and Control*, vol. 135, no. 4, 2013.
- [29] A. Ghasemi, J. B. Hoagg, and T. M. Seigler, “Decentralized vibration and shape control of structures with colocated sensors and actuators,” *Journal of Dynamic Systems, Measurement, and Control*, vol. 138, no. 3, 2016.
- [30] J. B. Hoagg and T. M. Seigler, “Filtered feedback linearization for nonlinear systems with unknown disturbance,” *Systems & Control Letters*, vol. 62, no. 8, pp. 613–625, 2013.
- [31] A. H. Ghasemi, J. B. Hoagg, and T. M. Seigler, “Decentralized filtered feedback linearization for uncertain nonlinear systems,” *International Journal of Robust and Nonlinear Control*, vol. 28, no. 4, pp. 1496–1506, 2018.

## Vita

Sumit Suryakant Kamat was born in Goa, India, in 1994. He received the B.Tech. degree in mechanical engineering from Sardar Vallabhbhai National Institute of Technology, Surat, India, in 2016. He started his M.S. studies in mechanical engineering at the University of Kentucky in 2016.